


## Article

# Desalination of Irrigation Water Using Metal Polymers

David D. J. Antia 

DCA Consultants Ltd. the Bungalow, Castleton Farm, Falkirk FK2 8SD, UK; dcacl@btconnect.com

**Abstract:** Rain-fed and irrigated agriculture associated with salinized soil and saline water supplies is characterized by low crop yields. Partial desalination of this saline water will increase crop yields. Recent studies have established that supported metal polymers can be used to produce partially desalinated irrigation water without producing a waste reject brine. This study assesses the ability of more than 90 different unsupported metal polymer formulations (containing one or more of Al, Ca, Fe, K, Mg, Mn, and Zn) to remove  $\text{Na}^+$  ions and  $\text{Cl}^-$  ions from saline water (seawater, brine, brackish water, and flowback water). The polymers were constructed using a simple sol-gel approach at ambient temperatures. The overall ion removal followed a first-order reaction. Removal selectivity between  $\text{Na}^+$  and  $\text{Cl}^-$  ions was a function of polymer formulation.  $\text{Mg@Al}$  polymers preferentially remove  $\text{Cl}^-$  ions, while  $\text{Fe@Ca}$  polymers tend to remove  $\text{Cl}^-$  and  $\text{Na}^+$  ions in more equal proportions. Ion removal can be rapid, with >50% removed within 1 h. These results were used to develop a process methodology, which will allow most seawater, brackish water, and saline flowback water to be desalinated to form usable irrigation water.

**Keywords:** catalysis; crop yield; irrigation; iron polymer; metal polymer; partial desalination; saline irrigation; zero valent iron; flowback water



**Citation:** Antia, D.D.J. Desalination of Irrigation Water Using Metal Polymers. *Water* **2022**, *14*, 3224. <https://doi.org/10.3390/w14203224>

Academic Editor: Andrea G. Capodaglio

Received: 25 September 2022

Accepted: 11 October 2022

Published: 13 October 2022

**Publisher's Note:** MDPI stays neutral with regard to jurisdictional claims in published maps and institutional affiliations.



**Copyright:** © 2022 by the author. Licensee MDPI, Basel, Switzerland. This article is an open access article distributed under the terms and conditions of the Creative Commons Attribution (CC BY) license (<https://creativecommons.org/licenses/by/4.0/>).

## 1. Introduction

The global arable land area is about 5 billion ha [1], of which 1.24 ha is arable cropland [1]. Irrigated cropland (about 270 million ha [2]) accounts for >70% of anthropogenic water usage [3–6], 90% of consumptive water usage [3,5], and 40% of global arable production [7,8]. About 20% of irrigated land (54 million ha) is irrigated with saline water [9]. About 1 billion ha globally of agricultural land is salinized [9]. About 34 million ha of salinized soil has become salinized as a direct result of irrigation [9].

Saline water and salinized soils reduce the potential crop yield, and the number of crop varieties that can be grown, when compared with freshwater irrigation [10–15]. The combination of irrigation water demand (which can be in the range 1000 to 10,000  $\text{m}^3 \text{ha}^{-1} \text{a}^{-1}$ ), low crop yield ( $\text{t ha}^{-1}$ ), and low crop value ( $\text{USD t}^{-1}$ ), ensure that most global agricultural units, growing staple crops (e.g., rice, wheat, barley, maize), will be unable to economically purchase desalinated water for a price of <USD 0.5  $\text{m}^3$ . Specialist horticultural concerns, growing high value fruit and vegetables with higher yields ( $\text{t ha}^{-1}$ ), lower irrigation requirements ( $\text{m}^3 \text{ha}^{-1} \text{a}^{-1}$ ), and higher product prices ( $\text{USD t}^{-1}$ ), may be able to economically sustain a purchased water cost of <USD 5  $\text{m}^3$ .

Conventional desalination routes using membrane technology, or thermal technology, typically produce a desalinated water product for a cost (which may be subsidised) within the range USD 0.5 to USD 5  $\text{m}^3$ . Consequently, this water has had limited commercial application for use as an irrigation water for most staple crops.

Unconventional desalination approaches have used a chemical approach to remove the NaCl. They have focused on using zero valent iron ( $\text{Fe}^0$ , ZVI) to remove the NaCl. Their advantages over traditional desalination are that: (i) they produce no waste brine, and all the feed water is converted to partially desalinated water; (ii) they can be operated at ambient temperatures and atmospheric pressure; and (iii) they can be operated using no external energy, or they can be operated with a lower energy requirement.

In this study, the term  $\text{Fe}^0$  is used *sensu stricto* to mean iron metal. The term ZVI is used *sensu lato*, to mean one or more of  $\text{Fe}^0$ ,  $\text{Fe}_x\text{O}_y$ ,  $\text{Fe}_x\text{O}_y\text{H}_z$  and associated metal polymers.

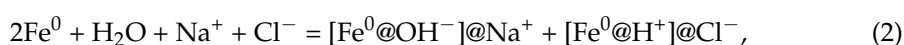
### 1.1. ZVI Desalination Process

The exact method used by ZVI to desalinate water is unknown. A number of hypotheses exist. The principal hypotheses are:

- Spanish Patent ES2598032B1 assumes that magnetic n- $\text{Fe}^0$  surfaces will become charged in water, due to the presence of  $\text{OH}^-$  ions and  $\text{H}^+$  ions. Functionalization may take the form:



This will result in:



This approach uses the  $\text{Fe}^0$  to increase water pH, and in doing so, creates a functionalized surface, which will remove  $\text{Na}^+$  and  $\text{Cl}^-$  ions.

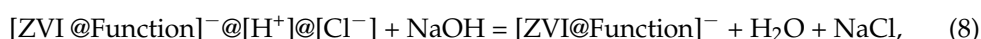
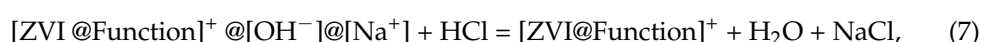
- US patent US8636906B2 assumes that the n-ZVI can be functionalized by the addition of cationic and anionic coatings to allow NaCl removal:



This then allows the recovered functionalized ZVI to be desalinated, i.e.,

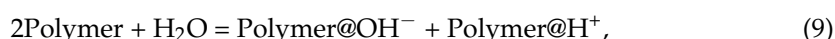


The functionalised ZVI can be reused. Regeneration in the next ZVI reuse cycle takes the form:



This approach treats the ZVI as an inert (magnetic) support, which is used to carry a cationic, or anionic, coated surface. In theory this should allow a single ZVI charge to be reused many hundreds of times.

These two models form the starting point for any ZVI desalination analysis. This study specifically explores whether non-magnetic Fe-polymers and other metal polymers, could be used to replace magnetic  $\text{Fe}^0$  and magnetic ZVI in the desalination process, within an alkali environment (pH = 7 to 13). Most metal polymers have cationic, and/or anionic surfaces and will form polar aggregates. The hypothesis being tested in this study is:



In saline water, this will result in:



Since functionalisation is a function of pH, it follows that the polymers, once recovered, may potentially be reactivated by placing them in fresh water, or a new saline water batch. This simplifies the process relative to Equations (5)–(8).

### 1.2. Past ZVI Approaches Used to Desalinate Water

Four ZVI desalination approaches have been used to desalinate water. They are:

- Adding ZVI, or  $\text{Fe}^0$ , to saline water to directly remove NaCl from the water [16]. This approach may have a desalination cost within the range USD 2 to USD 500  $\text{m}^{-3}$ . This approach results in the formation of  $\text{Fe}^0\text{:Fe(a,b,c)}$  polymers on the surfaces of the individual ZVI particles and entrained colloidal and flocculate  $\text{n-Fe(a,b,c)}$  polymers within the water. Ion removal is by direct reaction and incorporation within the polymers. The addition of ZVI to water, results in an increase in the pH of the water. The ZVI is normally only effective to treat a single volume of water with a concentration of 10 to 100  $\text{g Fe}^0 \text{ L}^{-1}$  water. The wide range in ZVI desalination cost is a function of particle size, ZVI source and the concentration of ZVI added to the water to achieve the required result. Micron sized particles may be purchasable (FOB) for between USD 500 and 5000  $\text{t}^{-1}$  depending on supplier, quantity, and quality. Nano sized particles may be purchasable (FOB) for between USD 10,000 and 1,000,000  $\text{t}^{-1}$  depending on supplier, quantity, and quality. FOB = free of board.
- Using ZVI to manufacture pellets, which, if added to water, removes NaCl from the water [16,17]. These pellets contain a high proportion of dead-end pores, and the ZVI surface, and pore surfaces are lined with  $\text{Fe}^0\text{:Fe(a,b,c)}$  polymers. These polymers remove  $\text{Na}^+$  and  $\text{Cl}^-$  ions from the open water body and deposit them into the dead-end pores contained with the pellets; the addition of pellets to water results in an increase in the pH of the water. The ZVI is normally only effective to treat a single volume of water with a concentration of 20 to 50  $\text{g Pellet L}^{-1}$  water. However, the pellets can be regenerated and reconstituted to allow reuse [17].
- Using ZVI to manufacture  $\text{Fe}^0$  supported polymers of the form  $\text{Fe}^0\text{:Fe(a,b,c)}$  and  $\text{Fe}^0\text{:Fe(a,b,c)@urea}$ , where the pH increase is effected by bubbling air through the water [18]. Cyclic pressure fluctuations in the water are used to promote adsorption and desorption from the polymer.  $\text{Na}^+$  and  $\text{Cl}^-$  ion removal rates decrease with time. Catalyst regeneration is achieved by replacing the partially desalinated water with a fresh saline water charge. A single polymer charge located on 400  $\text{g Fe}^0$  was demonstrated to process 70 batches of water (17  $\text{m}^3$ ) without loss of activity [18].
- Using  $\text{Fe}^{n+}$  ions to manufacture  $\text{SiO}_2$  supported polymers of the form  $\text{SiO}_2\text{@Fe(a,b,c)}$  and  $\text{SiO}_2\text{@Fe(a,b,c)@urea}$ , where the pH increase is effected by bubbling air through the water [19]. Cyclic pressure fluctuations in the water are used to promote adsorption and desorption from the polymer.  $\text{Na}^+$  and  $\text{Cl}^-$  ion removal rates decrease with time. Catalyst regeneration is achieved by replacing the partially desalinated water with a fresh saline water charge. A single polymer charge containing 10  $\text{g Fe}$  was demonstrated to process 50 batches of water (43  $\text{m}^3$ ) without loss of activity [19]. It was proposed that the polymer catalyses the formation of entrained polymer particles in the water using metal cations present in the feed water [19]. The water contained Fe, Ca, Mg and Al ions. It is currently unclear which metal (Fe, Ca, Mg, Al) based polymers, can remove  $\text{Na}^+$  or  $\text{Cl}^-$  ions.

This study considers whether the desalination polymers can be manufactured directly within the saline water, or added to the saline water to achieve a desalination. The metal cations considered for polymer formation are Fe, Ca, Mg, Mn, Zn, K, and Al. The associated anions considered are  $\text{SO}_4^{2-}$ ,  $\text{R-COO}^-$ ,  $\text{CO}_3^{2-}$ ,  $\text{OH}^-$ , and  $\text{O}^{2-}$ .

A detailed screening methodology, which will allow the expected impact of partial desalination on crop yield, for 70 different crop types, to be quickly assessed, is provided in references [18,19].

### 1.3. ZVI Water Remediation

ZVI ( $\text{Fe}^0$ , zero valent iron) water remediation (or water purification, or water desalination) involves the removal from water of one or more contaminants (e.g.,  $\text{Na}^+$  ions and  $\text{Cl}^-$  ions). This is achieved using one or more of the following processes [20]:

- (i) Redox modification of the Eh and pH of the water to force a change in the equilibrium reactant quotient associated with a pollutant, to convert a pollutant into a benign product;
- (ii) Direct reaction with the pollutant to either form an iron complex or a benign product
- (iii) Physical adsorption, or chemical adsorption, of the pollutant;
- (iv) Catalysis to convert a pollutant into a benign product;
- (v) Adsorption by, or interaction with, iron polymers (flocclulants).

These processes allow ZVI to be used to decontaminate (e.g., US Patents US7887709B2; US20170334755A1; Korean Patent KR20090127385A), dechlorinate (e.g., US Patents US5,611,936; US5,616,253; US5,758,389; US5,803,174), desalinate (e.g., US Patent US8636906B2; Spanish Patent ES2598032B1; UK Patent GB2520775A), denitrify (e.g., US Patent US8,057,682; US10,081,007), and remediate aquifers, soils, biosolids (sewage sludge (e.g., US Patents US8,758,616, US8,758,617)), impoundments, reservoirs, ponds, wells, riparian water, overland flow, irrigation water, flowback water, ground water, mine water, municipal (potable and waste) water, foul (sewage) water, grey water, emergency relief water, household (potable and waste) water, livestock feed water, agricultural wastewater, irrigation water, industrial wastewater, feed water to reverse osmosis desalination plants, and reject brine from desalination plants [20]. These nano-materials can also be used to process water to produce heavy water, hydrogen, and hydrocarbons [20]. The ZVI can be used as the primary remediation agent, or can be used as part of a managed suite of remediation processes [20].

The behaviour of ZVI in water is enigmatic. It behaves as a “smart material” and can undertake a multitude of functions simultaneously [21]. Changes in external stimuli, such as Eh, pH, temperature, pressure, light, and chemical compounds, result in a specific charge of ZVI interacting differently with a specific water charge. Smart material characteristics are difficult to easily resolve, and this has led to conflicting interpretations of the ZVI mode of operation. These conflicting interpretations are reviewed elsewhere [22–27].

In this study, the assumption is made that the  $\text{Fe}^0$  corrodes to form a  $\text{Fe}^0:\text{Fe}(a,b,c)$  polymer coating to the  $\text{Fe}^0$  particle [18,20]. Under this model,  $\text{Fe}(a,b,c)$  polymers that leave the  $\text{Fe}^0$  surface to become entrained in the water body are replaced with fresh polymer produced by the corrosion of the residual  $\text{Fe}^0$  [20]. Therefore, it is possible that desalination will occur if the polymers are created using a sol-gel approach, directly within the saline feed water. This study considers whether metal polymers (which can be either placed on a support to form a desalination pellet, or used as entrained particles within the water) can be used to achieve a rapid water desalination.

The polymers considered in this study are summarized in Figure 1. More than 90 different polymers are considered. In order to increase accessibility, the detailed analyses and results are summarized in the Appendices A and B and Supplementary Information File. The text first considers the methodology and terminology used in this study. The study then considers the  $\text{Fe}@\text{C}$  (Figure 1) polymers, before providing an analysis of the sol-gel polymers. The approach used first ascertains what happens when  $n\text{-Fe}^0$  is placed in water. These results are then compared with the sol-gel polymer results.

The combined results are then used to construct a model for ZVI desalination and construct probability distributions for desalination as a function of polymer type and reaction time. These distributions are used to estimate the expected increase in crop yield associated with polymer use for irrigation.

The polymers and product water are further processed to create an overall reaction process, which would allow most saline groundwater, seawater, and saline impoundment water associated with the resource industries to be used for irrigation.



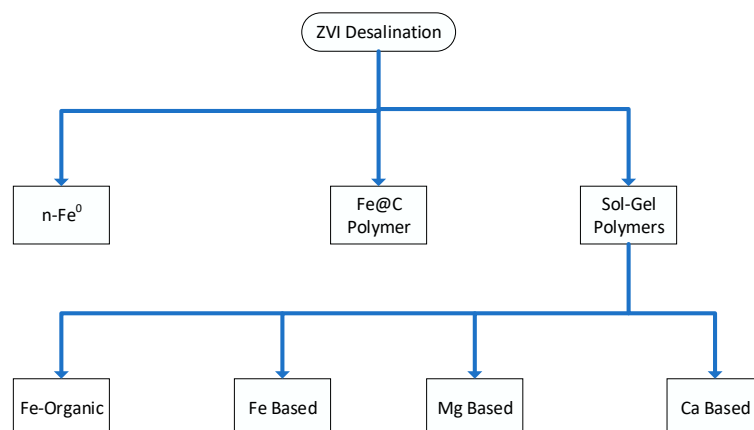


**Figure 1.** ZVI desalination approaches considered in this study.

## 2. Technology, Methodology, Materials and Equipment Used

### 2.1. Data, Data Terminology and Data Interpretation

The data generated by this study are provided in the Supplementary Information File, Figures S1–S24; Tables S1 and S2; and in Appendix A, Sections Appendices A.1–A.10, Figures A1–A6, Appendix B, Tables 4, A1–A3 and A5–A10.

#### 2.1.1. Statistical Methodology Used

The measured data were collated and processed, in accordance with the methodology defined by the British Standards Institute [28]. Regression trend lines and associated statistics were calculated in MS Excel 2019. The Monte Carlo analyses were undertaken in MS Excel using the @Rand() random number generator function to generate values between 0 and 1. The polynomial equations, linear equations and power equations were generated using the Trendline function in MS Excel.

The coefficient of determination,  $R^2$ , is the square of the Pearson Correlation Coefficient (PCC). By definition,  $R^2$  falls within the range 1 and 0, and PCC falls between +1 and −1 [29,30]. The following interpretations are made [29,30]:

- PCC = 0.9 to 1.0 ( $R^2$  = 0.81 to 1.00): Interpretation = very strong correlation
- PCC = 0.7 to 0.89 ( $R^2$  = 0.49 to 0.79): Interpretation = strong correlation
- PCC = 0.4 to 0.69 ( $R^2$  = 0.16 to 0.47): Interpretation = moderate correlation
- PCC = 0.1 to 0.39 ( $R^2$  = 0.01 to 0.15): Interpretation = weak correlation
- PCC = 0.0 to 0.10 ( $R^2$  = 0.00 to 0.01): Interpretation = negligible correlation

#### 2.1.2. Polymer Terminology

The relationship indicator [:] is used here to signify chemical bonding [17,18]. The relationship indicator [@] is used here to signify physical bonding [17,18]. Polymers can take one of a number of forms. In this study, the following terminology approach is used [17,18,31–34]. M = metal. M(a) = mono-nuclear hydroxyl complexes, e.g.,  $\text{Fe}^{3+}$ ,  $\text{Fe}(\text{OH})^{2+}$ ,  $\text{Fe}(\text{OH})_2^+$ ,  $\text{Fe}(\text{OH})_3$  (molecule),  $\text{Fe}(\text{OH})_4^-$  ( $\text{Fe}_2(\text{OH})_2^{4+}$  and  $\text{Fe}_3(\text{OH})_4^{5+}$ ), some small polymers, and instantaneous reaction products. M(b) = polynuclear hydroxyl complexes, with medium and high molecular mass, e.g.,  $\text{Fe}(\text{OH})_2^{4+}$ ;  $\text{Fe}(\text{O}_2\text{H}_6)^{3+}$ ;  $\text{Fe}_3(\text{OH})_4^{5+}$ ;  $\text{Fe}_5(\text{OH})_9^{6+}$ , etc. M(c) = larger polymer or colloidal species, which include inert macro-molecular coagulation, of the form  $\text{M}(\text{OH})_x$  and  $\text{MOOH}$ . In practice most polymers are a mixture of M(a) + M(b) + M(c). The target polymer is M(a) and M(b), but can include  $\text{SO}_x$ ,  $\text{CO}_x$ ,  $\text{C}_x\text{H}_y$ , and  $\text{C}_x\text{H}_y\text{O}_z$  species.

The entrained polymers may act as Janus particles and show motility [20]. They grow by both aggregation and by snowball accretion [20], e.g., Figure A1. Individual aggregates tend to be polar and initially coalesce to form net-like structures and linear chains within the water [20]. The initial aggregation is commonly as nano-sized (or micron sized) hollow

spheres surrounding a fluid core (which can be water, or hydrogen) [20]. This structuring provides the initial aggregates with buoyancy and motility within the water [20].

Polymers containing Ca will generally take the form Ca(a) but may aggregate to form micron-sized framboids protected by calcium carbonate shell at the water-polymer interface (e.g., Figure A6). The calcium carbonate may form as one or more of: amorphous calcium carbonate (ACC), calcium carbonate hexahydrate, calcium carbonate monohydrate (hydrated forms), vaterite, aragonite and calcite. The calcium carbonate forms from the interaction of  $\text{Ca}(\text{OH})_2$  with one or more of  $\text{CO}_2$ ,  $\text{H}_x\text{CO}_3^{(x-2)}$ , and  $\text{C}_x\text{H}_y\text{O}_z$ .

## 2.2. Chemicals

The powders,  $\text{SiO}_2$  granules (1–10 mm), and Ca-montmorillonite granules (0.5–5 mm) used in the experiments were purchased from a variety of commercial industrial and agricultural sources. The halite used, was a natural geological product, and contained, varying concentrations of: hydrated NaCl,  $\text{CaCl}_2$ , KCl,  $\text{CaSO}_4$ ,  $\text{CaCO}_3$ ,  $\text{MgSO}_4$ ,  $\text{MgCO}_3$ ,  $\text{FeOOH}$ ,  $\text{Fe}(\text{OH})_x$  and  $\text{Fe}_x\text{O}_y$ . The halite granules (0.5–5 mm) were purchased from Wickes Ltd., Perth, UK.

The zero valent metals ( $\text{m-Fe}^0$ ,  $\text{m-Al}^0$ ,  $\text{m-Cu}^0$ ) were purchased from MB Fiberglass. Newtownabbey, UK. Powders had a particle size within the range 0.002 to 0.08 mm.

The water used in the test trials is either natural seawater extracted from the North Sea, at Blackness Castle, Blackness, Scotland, UK, or artificial saline water constructed by mixing natural halite (containing NaCl,  $\text{CaCl}_2$ ,  $\text{CaCO}_3$ ,  $\text{MgCO}_3$ ,  $\text{CaSO}_4$ ,  $\text{MgSO}_4$ ,  $\text{Fe}(\text{OOH})$ , and clays) with fresh water.

## 2.3. Construction of Entrained Polymers

The entrained polymers were constructed using the sol-gel method (e.g., [35–38]) at ambient temperatures (5 to 20 °C). Three approaches were adopted:

- Manufacture of the polymer, with concentration and extraction, prior to placement in water;
- Manufacture of the polymer, in proximity with a support (active carbon), prior to placement of the support in water;
- Manufacture of the polymer, in the target saline water body.

These approaches are summarized in Figure 2. In this study, the sol-gel method used is defined in UK Patent GB 2520775A. Unless otherwise stated the reactor contained 2.3 L of saline water. The reactor was operated as a sealed, static flow, diffusion reactor at ambient temperatures. Each reactor contained an air-water contact.

In this study (Figure 2),  $\text{MO}_x$  was selected from CaO, ZnO,  $\text{Al}_2\text{O}_3$  and  $\text{MnO}_2$ ;  $\text{MHCO}_3$  was selected from  $\text{KHCO}_3$ ;  $\text{MCO}_3$  was selected from  $\text{K}_2\text{CO}_3$ ,  $\text{CaCO}_3$  and  $\text{MgCO}_3$ ;  $\text{MSO}_4$  was selected from  $\text{FeSO}_4$ ,  $\text{MgSO}_4$  and  $\text{Al}_2(\text{SO}_4)_3$ ;  $\text{M}(\text{OH})_x$  was selected from  $\text{Al}(\text{OH})_3$ .  $\text{C}_x\text{H}_y\text{O}_z$  selected from  $\text{HCOOH}$ ,  $\text{CH}_3\text{COOH}$ ,  $\text{C}_4\text{H}_6\text{O}_5$ ,  $\text{C}_4\text{H}_6\text{O}_6$ ,  $\text{C}_6\text{H}_8\text{O}_7$ ,  $\text{C}_7\text{H}_6\text{O}_5$  + various polyphenols. Mixing temperature = 0 to 20 °C; Stirring duration = 30–60 s.

### 2.3.1. Characterisation

Chemical characterisation of the polymers produced by this sol-gel method is outside the scope of this study. This is an exploratory, scoping study, which is designed to determine if: (i) a sol-gel colloidal precipitate will form when specific ions are added to saline water; and (ii) if the gel will remove  $\text{Na}^+$  ions and/or  $\text{Cl}^-$  ions. This study is not designed to determine, for a specific sol ingredient combination, the ideal recipe required to maximise  $\text{Na}^+$  ion and  $\text{Cl}^-$  ion removal, or the impact on ion removal of altering polymer concentrations, water temperature, water salinity, pressure, pH, Eh, and the concentration of other ions in the water. The study is not designed to specifically identify how the  $\text{Na}^+$  and  $\text{Cl}^-$  ions are removed, or the chemistry of the products associated with  $\text{Na}^+$  and  $\text{Cl}^-$  removal.

The results from this study are designed to give an indication of the range of salinity outcomes as a function of reaction time and sol-gel compositions for a wide range of

feed water salinities. The commercial objective of this sol-gel approach was to indicate whether it would be possible to create a low cost, desalination solution, which could allow small and medium sized agricultural units to reduce the salinity of saline water without producing a reject (waste) brine, and without requiring an external energy source to achieve the desalination.

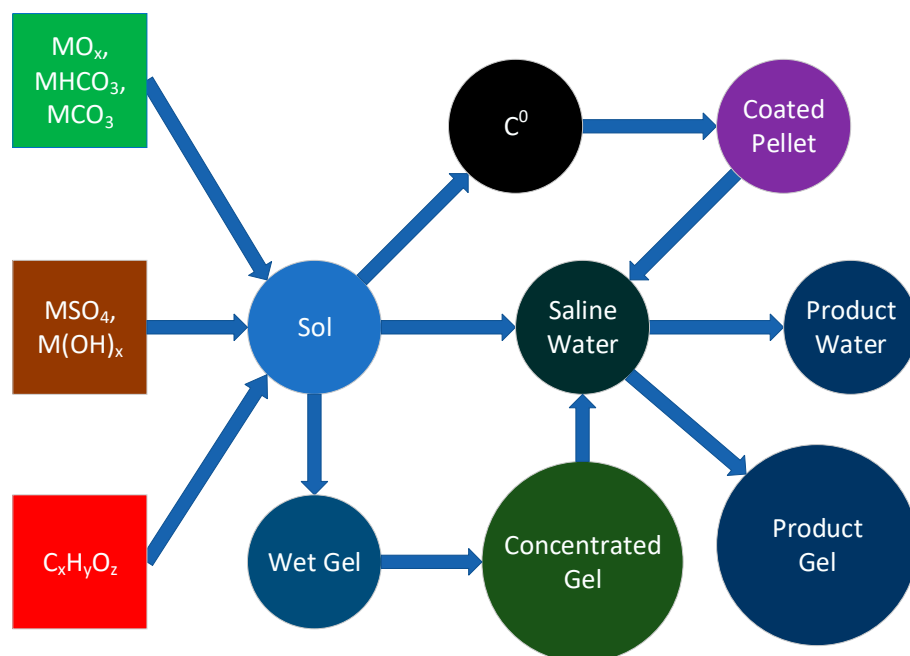


**Figure 2.** Summary of the Sol-Gel Approach used in this study.

### 2.3.2. Instant Desalination

A large number of different polymer compositions were trialed in order to establish which compositions, if any, were likely to operate with a high almost instantaneous ion removal. The manufacturing approach used was to mix the ingredients at ambient temperatures (0 to 20 °C) to produce an instantaneous precipitate. An example is illustrated in Figure 3, where the solutions are mixed in fresh water to produce a wet gel which is then concentrated prior to placement into saline water. More commonly, in this study, the sol-gel ingredients were directly mixed within the saline water.



**Figure 3.** Example of n-Fe(b)@gallic acid polymer manufacture. Left container: dissolved gallic acid-polyphenol mixture (derived from black tea). Middle container: dissolved FeSO<sub>4</sub>. Right container (black color): entrained n-Fe(b)@gallic acid polymer (gel) in water, manufactured by adding the gallic acid to the dissolved FeSO<sub>4</sub>. The containers are resting on 10 cm wide wooden boards.

The working model at the onset of this study was that NaCl acts as an electrolyte, so Cl<sup>−</sup> ions, and possibly Na<sup>+</sup> ions, may facilitate colloid formation, and in doing so may be removed as part of the process.

The product water, containing newly formed colloid gel, gravity separates into a (product concentrated gel (Figure A1)), and a product water body, which is largely free of precipitates.

The process shown in Figure 3 may produce, in addition to an entrained n-Fe(b)@gallic acid polymer (gel), some n-Fe<sup>0</sup>, e.g., Canadian patent CA2728987C; US patents US8,057,682B;

US20110110723A1; US9,375,684B; Chinese patents CN104857934B; CN105458283B; CN105750562A; CN106180755A; CN109967023A; UK Patent GB 2520775A.

#### 2.4. Measurement Equipment

The instruments used were:

- ORP (oxidation reduction potential) meter (HM Digital) calibrated at ORP = 200 mV; Measured ORP (oxidation reduction potential) values are converted to Eh, mV as:  $Eh, mV = -65.667pH + 744.67 + ORP (mV)$ , using a quinhydrone calibration at pH = 4 and pH = 7.
- pH meter (HM Digital) calibrated at pH = 4.01; 7.0; 10.0.
- EC (electrical conductivity) meter (HM Digital meter calibrated at  $EC = 1.431 mScm^{-1}$ ).
- $Cl^{-}$  ISE (Ion Selective Electrode); Bante  $Cl^{-}$  ISE, EDT Flow Plus Combination  $Cl^{-}$  ISE; Cole Parmer  $Cl^{-}$  ISE attached to a Bante 931 Ion meter. Calibration was undertaken using 0.001, 0.01, 0.1, 1.0 M NaCl calibration solutions.
- $Na^{+}$  ISE (Ion Selective Electrode); Bante Na ISE, Sciquip Na ISE, Cole Parmer Na ISE attached to a Bante 931 Ion meter. Calibration was undertaken using 0.001, 0.01, 0.1, 1.0 M NaCl calibration solutions.
- Temperature measurements, were made using a temperature probe, attached to a Bante 931 Ion meter.

#### 2.5. Salinity Units

Most agricultural holdings measure salinity using EC, where the units are in  $mScm^{-1}$  or  $dScm^{-1}$ . The user instructions accompanying most EC meters advise that salinity ( $g L^{-1}$ ) is determined as  $F \times EC$ , where  $F = 0.5$  or  $0.55$ . Most chemical data books indicate that  $F$  increases with salinity from an initial value of around 0.6 in pure saline water. Most saline water is composite, and the EC is used to measure the aggregate impact of a multitude of organic and inorganic ions. A regression plot of ion concentration versus EC will (in water containing low organic concentrations) be linear.  $F$  will normally vary between 0.7 and 1.0. The value of  $F$  will be unique to a particular type of feed water. A complication is that EC will rise when sol-gel ingredients are added to the saline water. Therefore, in this study, ISEs are used as the main measure of salinity.

### 3. m-Fe:n-Fe(b)@n- $C^0$ Polymer

$Cu^0$  shelled desalination pellets have previously been constructed containing a m- $Fe^0$ :n-Fe(b)@n- $C^0$  desalination catalyst polymer [16,17]. The manufacturing approach is complex. Two manufacturing approaches have been adopted:

- Approach A: Manufacture of the n- $C^0$ , n-Fe(b) and m- $Fe^0$ :n-Fe(b)@n- $C^0$  desalination catalyst polymer in a bubble column diffusion reactor containing ZVI. This described in detail in reference [17].
- Approach B: Manufacture by passing a gas containing entrained n- $C^0$  into a bubble column diffusion reactor containing ZVI. The manufacturing approach for this desalination pellet type may be published at a future date.

Both approaches produce a desalination catalyst containing a m- $Fe^0$ :n-Fe(b)@n- $C^0$  desalination catalyst polymer. Desalination using these catalysts can be described using a zero-order reaction [17,39–41], where:

$$(C_{t=n}) = -k_{obs}t_r + (C_{t=0}), \quad (11)$$

This contrasts with the polymers produced in this study (Supplementary Information Figures S1–S24) where desalination can be defined using a first-order reaction [39–41]:

$$\ln(C_{t=n}) = -k_{obs}t_r + \ln(C_{t=0}), \quad (12)$$

$C_{t=n}$  = product water ion concentration;  $C_{t=0}$  = initial feed water ion concentration;  $t_r$  = reaction time;  $k_{obs}$  = observed rate constant. An example of a desalination profile associated with Approach B, desalination pellet, is provided in Figure 4. This figure illustrates three key features associated with a supported metal polymer desalination catalyst:

- An initial period ( $T_{p1}$ ) where no desalination occurs, or desalination occurs at a slow rate;
- An active period ( $T_{p2}$ ) where desalination occurs at a higher rate;
- An inactive period ( $T_{p3}$ ) where desalination either ceases, proceeds at a slower rate, or a slow rate of resalination occurs.
- Salinity removal during the desalination period (Figure 4) follows a zero-order reaction (Equation (11)).

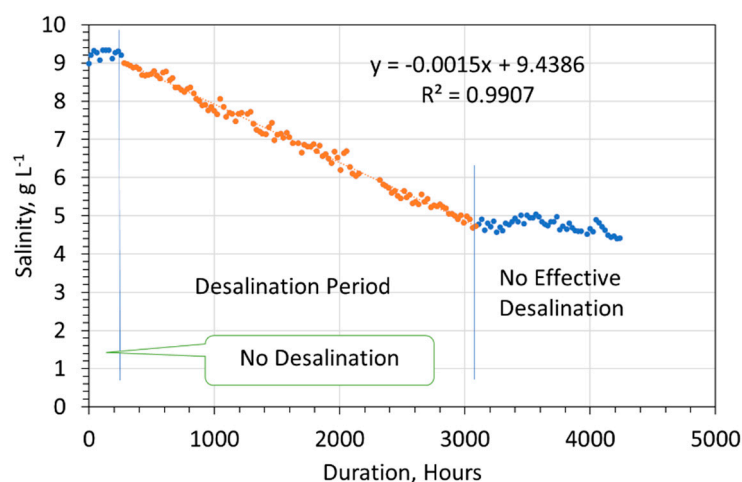


**Figure 4.** Desalination associated with  $m\text{-Fe}^0\text{:n-Fe(b)@n-C}^0$  polymer formed (Approach B) by manufacturing the  $n\text{-C}^0$  in a Halite Reactor prior to passing it into a bubble column diffusion reactor containing ZVI. Reactor size = 1 L. Pellet weight 75 g  $m\text{-Fe}^0\text{:n-Fe(b)@n-C}^0$  polymer  $\text{L}^{-1}$ . The blue and orange coloring is used to distinguish the different stages during desalination.

These three features are a common attribute of most desalination polymers.  $T_{p1}$  is commonly absent when Approach A pellets are operated [17].

#### 4. Results Associated with Sol-Gel Polymer Formation

More than 87 metal-organic and metal-inorganic sol-gel formulations were evaluated. The results are provided, for ease of access, in Appendix A, Sections Appendices A.1–A.10, Appendix B (Tables 4, A1–A3 and A5–A10) and Supplementary Information, Figures S1–S24, Tables S1 and S2. The ingredients used to manufacture each polymer (when not supplied in the Appendix B text and tables) are provided in the captions to Supplementary Information Figures S1–S24.

The majority of the examples in Appendices A and B are for entrained polymers manufactured within the saline feed water. A small number of examples placed the polymer on an active carbon support prior to use.

Most, but not all, formulations demonstrated ion removal. Some but not all formulations that demonstrated ion removal showed a pattern of ion removal that could be described by a first-order reaction (Supplementary Information Figures S1–S24). In most but not all examples, ion removal could be described using a power relationship (Table A5) where:

$$-k_{obs} t_r = \ln(C_{t=n}/C_{t=0}) = [a][c][b], \quad (13)$$

where  $[a]$ ,  $[b]$  = regression constants;  $[c]$  = reaction time in hours. The ability of a polymer to form is a function of the various ion components already present in the water. For example, the trials in Appendix A have demonstrated that if the water already contains  $\text{FeSO}_4$  (e.g.,

a typical base metal mine waste water), then the addition of an organic acid, or CaO, or carbonate, will be expected to result in polymer formation. Competing ions within the water may decrease, or increase, the ability of a specific polymer to remove  $\text{Na}^+$  ions, or  $\text{Cl}^-$  ions.

The regression constants [a] and [b] were determined (Table A5) for the 87 formulations described in Tables 4 and A1–A3. This information was used to determine the expected value of  $(C_{t=n}/C_{t=0})$  for each of the 87 formulations, for values of  $t_r = 0.1$  h, 1 h, 5 h, 10 h, 20 h, 30 h and 50 h (Supplementary Information Tables S1 and S2). These data were then sorted (ranked) for each value of  $t_r$  from lowest to highest, and a rank number ( $R_N$ ) was assigned to each value. The total number of ranked values,  $R_T$ , was <87, as not all formulations showed a change in  $\ln(C_{t=n}/C_{t=0})$ , which could be defined by a power function. The probability of a smaller value of  $(C_{t=n}/C_{t=0})$  was assessed for each ranked value as:

$$\text{Probability} = R_N / (R_T + 1), \quad (14)$$

The resultant probability distributions are provided in Figure 5. They confirm that  $\text{Na}^+$  ions are  $\text{Cl}^-$  ions are removed by separate processes, and that an initial rapid ion removal is followed by a slower subsequent ion removal. The relatively high, almost instant ion removal, which is associated with colloidal polymer formation, indicates that it may be possible to add the polymer ingredients to saline water in a flow line immediately prior to use. These observations indicate that polymer formation could be used as a desalination solution for applications where partially desalinated water is required.

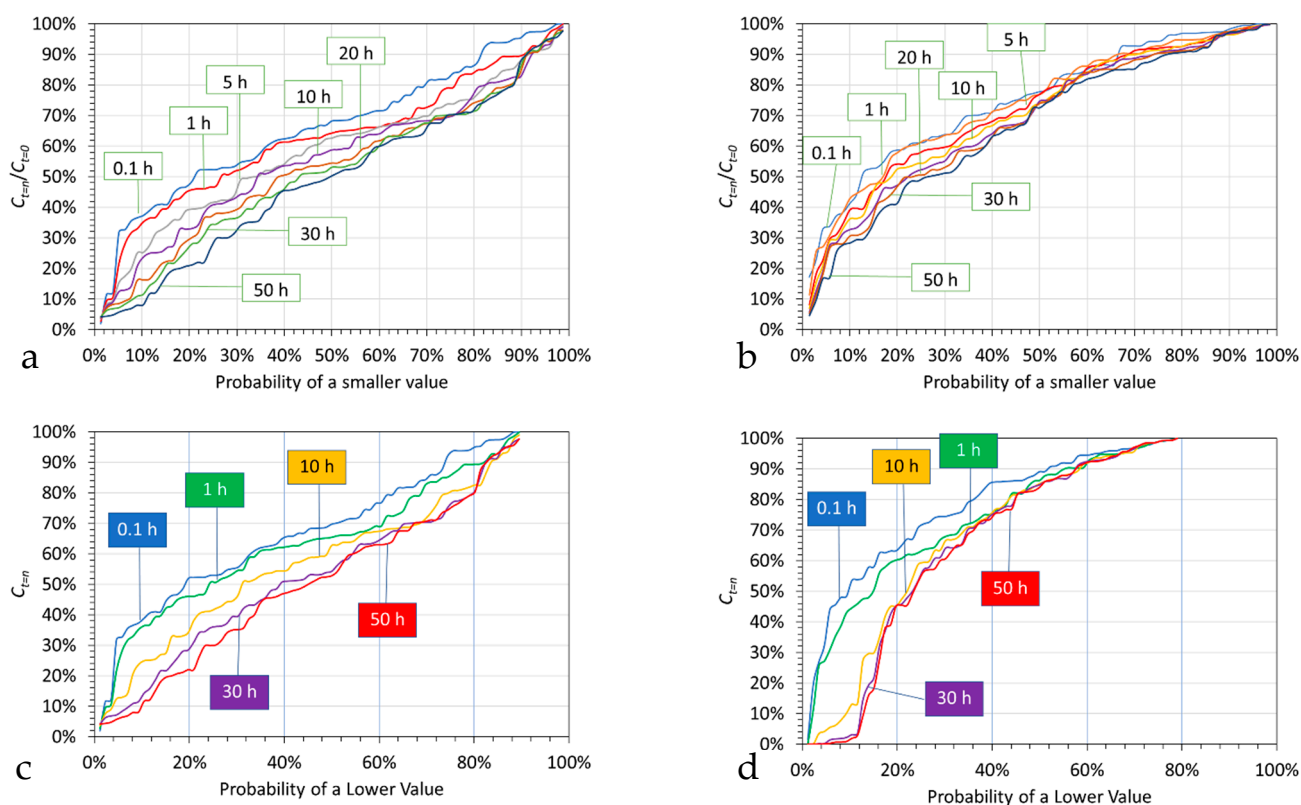


**Figure 5.** Probability of a smaller value versus  $C_{t=n}/C_{t=0}$  as a function of reaction time, hours. (a), Chloride ion (only results showing chloride removal considered). (b), Sodium ion (only results showing sodium ion removal considered). (c), Chloride ion (all results considered). (d), Sodium ion (all results considered). Data: Supplementary Information, Tables S1 and S2.

Colloids produced solely from  $\text{Fe}^{n+}$  ions tend to have a particle size of <0.1 micron, while those also containing Ca and/or Al ions will tend to be >1 micron [42].



## 5. Discussion

This study has established that simple entrained Fe(b)@X and M(a,b,c)@X polymer catalysts can remove both Na<sup>+</sup> and Cl<sup>−</sup> ions from water. The ion removal reactions appear to follow a first-order reaction (Supplementary Information, Figures S1–S24). If it is assumed that the observed remediation (water desalination) rate constant,  $k_{obs}$ , is a function of polymer surface area ( $a_s$ , m<sup>2</sup> g<sup>−1</sup>) and the polymer concentration in the water ( $P_w$ , g L<sup>−1</sup>), then it is reasonable to assume that the observed rate constant,  $k_{obs}$ , is determined as:

$$k_{obs} = k_{ins} a_s P_w, \quad (15)$$

or

$$k_{obs} = k_{ins} a [a_s]^c b [P_w]^d, \quad (16)$$

$k_{ins}$  = normalised rate constant, where:  $a_s = 1$  and  $P_w = 1$ ; [a], [b], [c], and [d] are constants. The assumption is that reducing polymer particle size will increase the polymer particle surface area per unit weight (m<sup>2</sup> g<sup>−1</sup>), and this increase in surface area will increase the number of reactive sites (s g<sup>−1</sup>). This concept was not tested in this study, but identifies an area for future research.

### 5.1. Colloid Growth

Crystal growth normally falls into two time-segregated intervals. An initial period of homogenous nucleation, followed by a period of heterogenous nucleation. This is then followed by a period of agglomeration and aggregation. The period of heterogenous nucleation will occur after the polymer concentration has exceeded a critical level. The initial polymers form small fluid filled spheres (Figure 6a). These colloids then aggregate over time to form macro-colloids (Figure 6b–d).

This same pattern of colloidal polymer formation also occurs when n-Fe<sup>0</sup> is used to desalinate water [20]. In this instance, the following can occur:

- Placement of n-Fe<sup>0</sup> in saline water is accompanied by a near instant drop in salinity, which is associated with the formation of fluid filled micron sized spheres of n-Fe<sup>0</sup>/n-Fe(a,b) (Figure 7a–c). This instantaneous salinity change may form the underlying basis for the near instant n-ZVI desalination observed in US Patent US8636906B2; French Patent FR2983191A1; and Spanish Patent ES2,598,032, and in reference [43]. The magnitude of the near instantaneous salinity reduction may increase with increasing water salinity [43]:
  - Fe<sup>0</sup> particles of 44–80 microns, when placed in saline water, initially release Fe<sup>n+</sup> ions into the water. This is then followed by a zero-order salinity decline until a critical salinity is achieved. At this point salinity decline follows a zero-order reaction at a slower rate [44].
  - Fe<sup>0</sup> particles of 44–80 microns, when placed in saline water, in the presence of Cu<sup>0</sup> and Al<sup>0</sup>, initially release Fe<sup>n+</sup> ions into the water. Salinity decline then follows a zero-order reaction [44]. In this example the zero-order salinity decline is associated with the removal of Fe<sup>n+</sup> ions as n-Fe(a,b,c) polymers. The combination of Fe<sup>0</sup>, Cu<sup>0</sup> and Al<sup>0</sup> ions slows the zero-order reaction rate when compared with Fe<sup>0</sup> [44].
  - A near instant decline in salinity is commonly associated with an initial high rate of Fe<sup>0</sup> dissolution to form Fe<sup>n+</sup> ions [45].
- A general (first-order) decline in salinity occurs as the fluid filled spheres aggregate and coalesce (Figure 7a–c);
  - Coated 50 nm Fe<sup>0</sup> commonly shows a second-order reaction rate, in low salinity water, when an initial instant salinity decline is absent [44].
- Cessation of the salinity decline is accompanied by the restructuring of the aggregated colloids to form amorphous flocculates (Figure 7c–f).

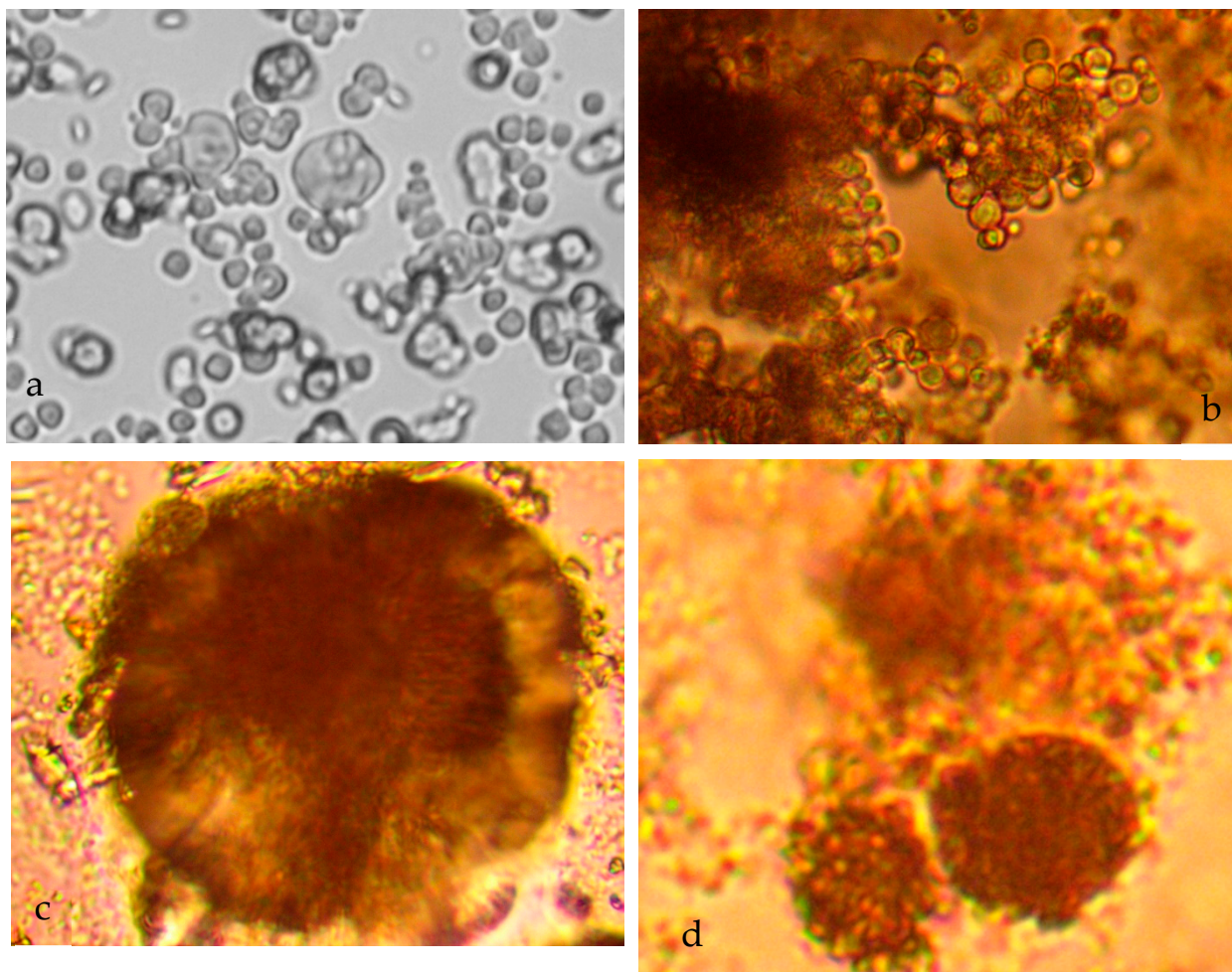


**Figure 6.** Initial colloids: (a), Fe@Ca@Zn polymer (Supplementary Information, Figure S2a). Field of view = 0.065 mm; Doughnut shapes are an optical illusion due to the fluid filled core of the colloid spheres. (b), Initial fluid filled colloids accumulating to form an amorphous colloidal mass: Example A1a. Field of view = 0.128 mm; (c), Fe(b)@Ca(a)@Mn(a)@Mg(a)@HCOOH polymer; 0.09 mm diameter colloid aggregate sphere constructed from coalesced colloids. Field of view = 0.11 mm. (d), Example A2b. Spheres aggregating to form a larger particle; Field of view = 0.047 mm.

The observations provided in this study, and the earlier studies indicate that  $n\text{-(m-)}\text{Fe}^0$  acts as a source of  $\text{Fe}^{n+}$  ions. These ions form Fe(a,b,c) polymers, which result in the removal of salinity. Under this model, the initial instantaneous drop in salinity will be maximized by both using uncoated, directly reduced,  $\text{Fe}^0$  particles, and minimizing the size of the  $\text{Fe}^0$  particles (Equation (6)). These two features will maximize the rate of  $\text{Fe}^0$  corrosion to form ions for a specific charge ( $\text{g L}^{-1}$ ) of  $\text{Fe}^0$ .

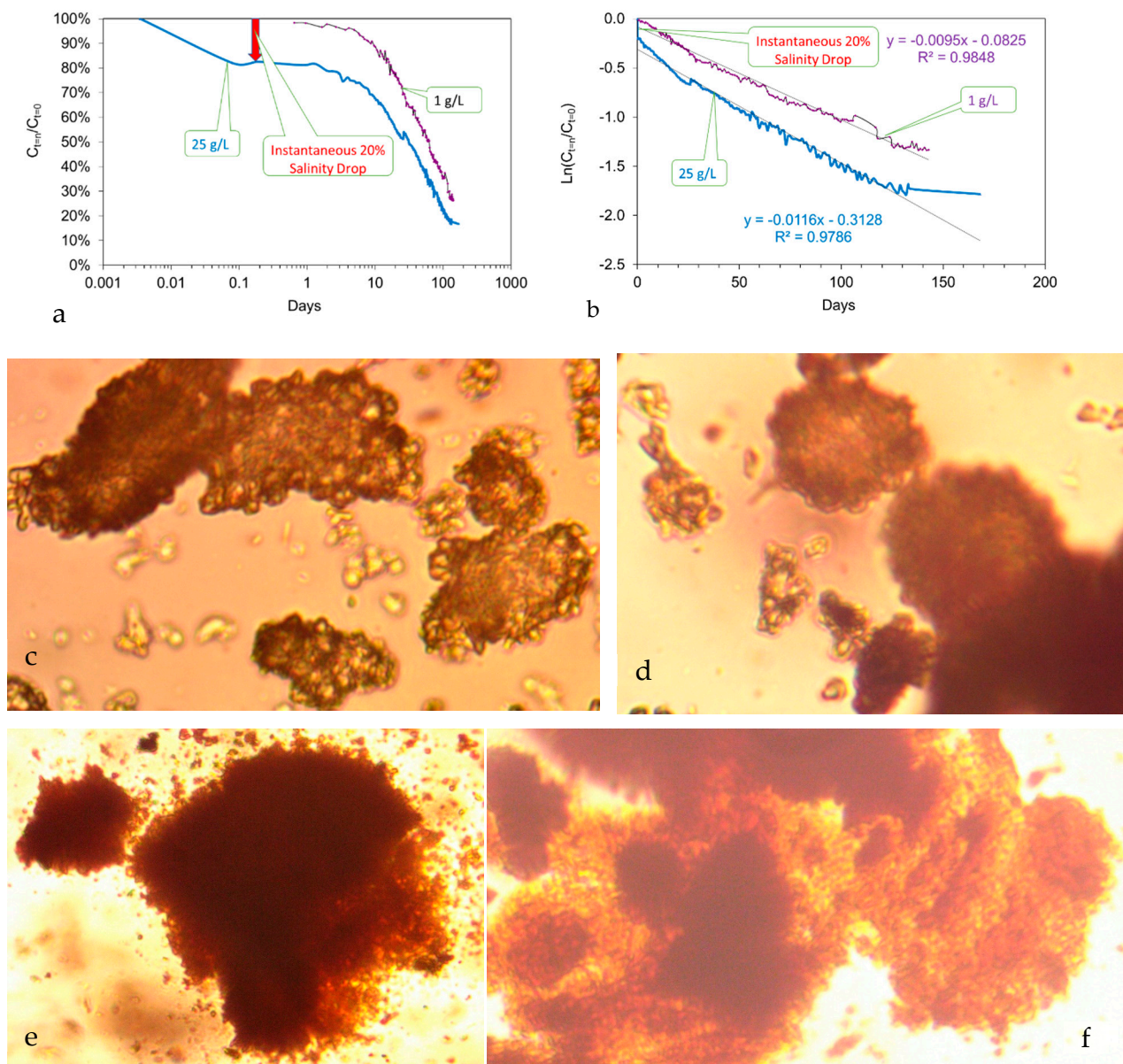


**Figure 7.** Example impact of changing  $P_w$  (for  $P_w = 25$  g n-Fe<sup>0</sup>/L and 1 g n-Fe<sup>0</sup>/L on water salinity as a function of time;  $a_s = 20$  m<sup>2</sup> g<sup>-1</sup>; (particle size 50 nm) coating: Fe<sub>3</sub>O<sub>4</sub>; (a),  $[C_{t=n}/C_{t=0}]$  versus reaction time, days; (b),  $\ln[C_{t=n}/C_{t=0}]$  versus reaction time, days; temperature = <298 K; pressure = atmospheric (0.1 MPa);  $C_{t=0}$  = initial water salinity = 13.4 g/L.  $C_{t=n}$  = water salinity at time  $t = n$ ; static water body; 1 L volume. The desalination reaction is a first-order reaction, after the initial 10 days, and terminates after about 130 days; field of view = 0.17 mm; (c), colloid formation (0.01–0.1 mm) from the aggregation of fluid filled spheres, where n-Fe<sup>0</sup> surrounds a fluid core; (d), aggregation of the initial colloid aggregates to form amorphous colloids. Field of view = 0.123 mm. (e), Aggregation of the initial colloid aggregates to form amorphous colloids. Field of view = 0.18 mm. (f), Aggregation of the initial colloid aggregates and fluid filled spheres, to form amorphous colloids. Field of view = 0.14 mm.

#### 5.1.1. Colloid Growth Kinetics

The growth rate aggregation kinetics of colloids follows a power relationship, where particle coagulation is a function of  $[M_p - R_p^h]$ , where  $M_p$  = colloid mass,  $R_p$  = radius of gyration and  $h$  = the mass fractal dimension where  $1 < h < 3$  [46]. Aggregate size increases



with increases in interaction energy. This is accompanied by an increase in the number of particles associated with each aggregate, e.g.,:

$$n_c = k_f n_0 t, \quad (17)$$

$n_c$  = number of colloidal particles at time  $t = n$ ;  $n_0$  = number of colloidal particles at time  $t = 0$ ;  $k_f$  = flocculation rate constant. The proportion of remaining colloid particles,  $n_r$ , at time  $t=n$  is

$$n_r = 1 - n_c/n_0, \quad (18)$$

A reverse reaction will have the formulation:

$$n_{t=n} = k_{fd} n_c t, \quad (19)$$

$k_{fd}$  = reverse colloid formation reaction rate constant. If there is a forward formation colloid reaction, and a reverse reaction, which reacts in its destruction then the expected concentration of colloid ingredients will be a function of  $k_f$  and  $k_{fd}$ . Figure 8a demonstrates that if  $k_{fd} = 0$ , then  $n_{t=n}$  will reduce to a base value of <10%. In this example, the initial decline can be modelled on a plot of  $n_{t=n}$  versus time as a straight line, indicating that the reaction could be zero-order. Increasing  $k_{fd}$  to >0 results (Figure 8b) in a relatively high equilibrium base value of  $n_{t=n}$ , combined with a reduced time range over which the ion removal reaction switches from a general decline to a stable level.

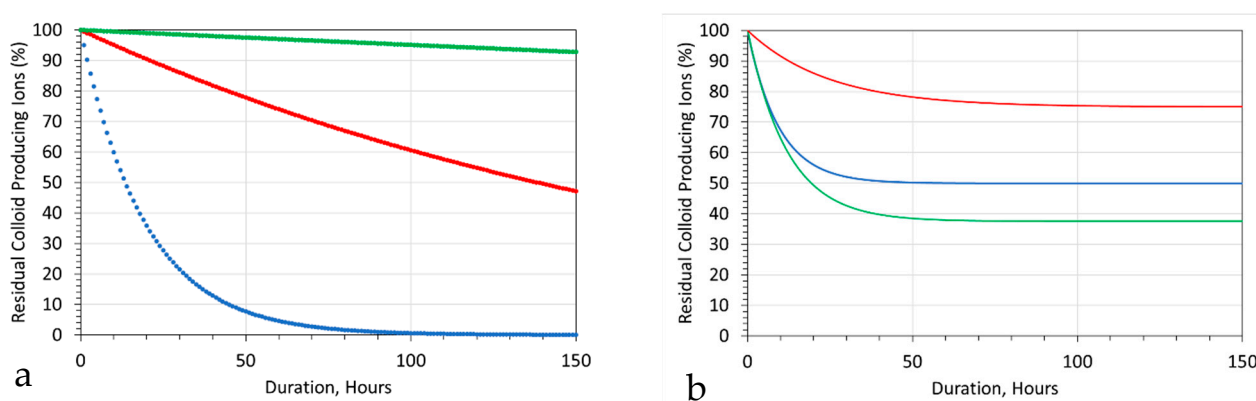


**Figure 8.** Colloid formation. (a), Residual colloid producing ions versus time. Assumptions:  $k_{fd} = 0$ ; Blue markers:  $k_f = 0.05$ ; Red markers:  $k_f = 0.005$ ; Green markers:  $k_f = 0.0005$ . (b), Residual colloid producing ions versus time. Assumptions:  $k_f = 0.05$ ; blue markers:  $k_{fd} = 0.05$ ; green markers:  $k_{fd} = 0.01$ ; red markers:  $k_{fd} = 0.03$ .

The observed ion decline patterns (Supplementary Information, Figures S1–S24), could be interpreted as a function of Equations (18) and (19).

### 5.1.2. Probability Analysis

Each colloidal sphere can be visualized as an aggregation of monomers, where the development of fluid filled porosity during the growth process increases the growing sphere volume. Individual colloidal spheres are polar. This allows individual colloidal spheres to aggregate to form chains and net-like structures, e.g., Figure 9.

Different colloid formulations produce different colloid sizes, different aggregation patterns and different rates of chloride and sodium removal. Colloid size does not appear to markedly affect the ability of some polymers to remove  $\text{Na}^+$  and  $\text{Cl}^-$  ions (Figure 10).

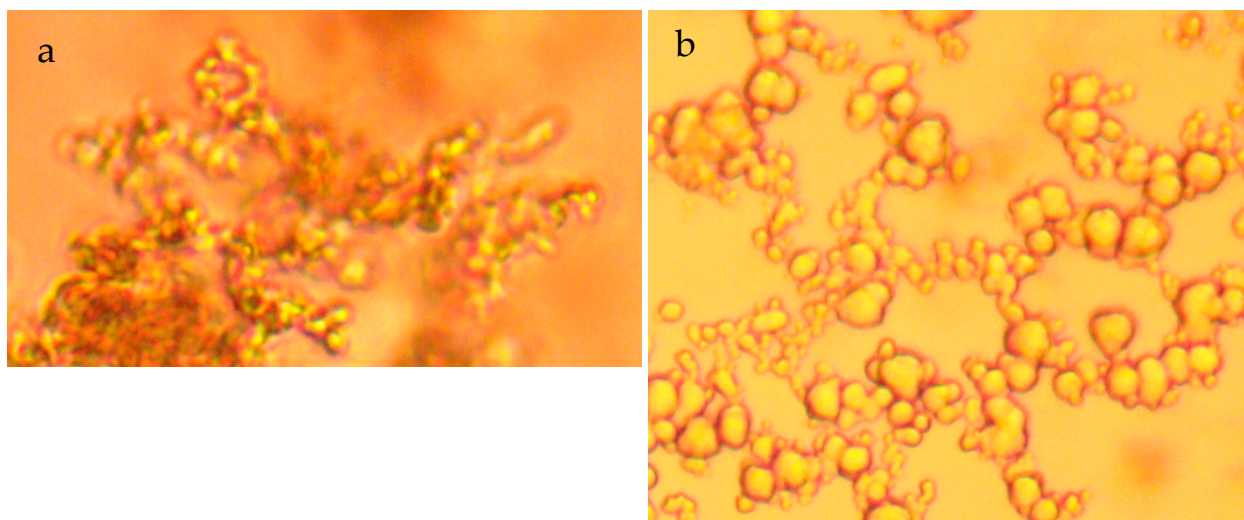


**Figure 9.** Polar colloidal spheres aggregating to form chains and net-like structures. (a), Fe@Ca@Mn@HCOOH polymer. Field of view = 0.07 mm; (b), Ca@urea polymer; field of view = 0.093 mm.

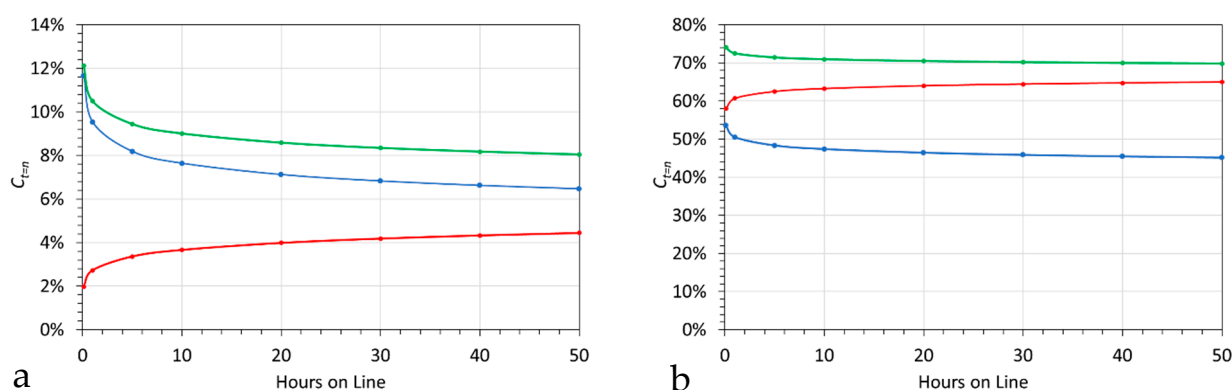


**Figure 10.** Removal of ions Fe@Ca@Mn@HCOOH polymer; (a), chloride; (b), sodium; red line = + tartaric acid; blue line = + malic acid; green line = + citric acid.

The ideal colloid composition has not been determined in this study. Some colloid formulations have minimal, or no ion removal associated with them. Others appear to be highly effective at removing one or more of  $\text{Cl}^-$  and  $\text{Na}^+$  ions.

While the analyses have indicated that the outcomes can be described using a first-order reaction (Supplementary Information File, Figures S1–S24), it has been previously established [17] that the detailed process could include a pseudo-zero-order reaction where an initial fast first-order reaction was followed by a slower product desorption reaction. This analysis demonstrated (Figure 5):

- An initial almost instant ion removal, in the majority of trials;
- An effective cessation of  $\text{Cl}^-$  ion removal after 10 to 30 h;
- An effective cessation of  $\text{Na}^+$  ion removal after 1 to 10 h;
- An expectation at the 50% probability level, after 0.1 h of 10%  $\text{Na}^+$  ion removal and 30%  $\text{Cl}^-$  ion removal.

### 5.1.3. Probability Outcomes as a Function of Polymer Type

The data set was subdivided into a number of groupings based on polymer composition. An outcome probability distribution was created for each polymer type using the data in Tables 4, A1–A3 and A5. Their results indicated:

- Mg@Al polymer (Figure 11a,b):  $\text{Cl}^-$  ions are removed preferentially relative to  $\text{Na}^+$  ions. The median expectation is, after 0.1 h, 32%  $\text{Cl}^-$  ion removal and 6%  $\text{Na}^+$  ion removal. Effective ion removal ceases after 10 to 30 h.
- Fe@Mg@Al polymer (Figure 11c,d):  $\text{Cl}^-$  ions are removed preferentially relative to  $\text{Na}^+$  ions. The median expectation is, after 0.1 h, 37%  $\text{Cl}^-$  ion removal and 5%  $\text{Na}^+$  ion removal. Effective ion removal ceases after 1 h.
- Fe@Ca@Zn polymer (Figure 11e,f):  $\text{Cl}^-$  ions are removed preferentially relative to  $\text{Na}^+$  ions. The median expectation is, after 0.1 h, 33%  $\text{Cl}^-$  ion removal and 17%  $\text{Na}^+$  ion removal. Effective ion removal ceases after 50 h.
- Fe@Ca polymer (Figure 11g,h):  $\text{Cl}^-$  ions are removed preferentially relative to  $\text{Na}^+$  ions. The median expectation is, after 0.1 h, 29%  $\text{Cl}^-$  ion removal and 25%  $\text{Na}^+$  ion removal. Effective ion removal ceases after 50 h.
- Ca polymer (Figure 11i,j):  $\text{Cl}^-$  ions are removed preferentially relative to  $\text{Na}^+$  ions. The median expectation is, after 0.1 h, 29%  $\text{Cl}^-$  ion removal and 3%  $\text{Na}^+$  ion removal. Effective ion removal ceases after 0.1 to 10 h.

This analysis indicates that an almost instant removal of 20% to 30% of  $\text{Na}^+$  ions and  $\text{Cl}^-$  ions may be achievable by adding polymer to water. Fe@Ca polymers appear to provide a larger instant desalination than either Ca polymers, or Mg@Al polymers.

Fe(c).  $\text{Fe}^0$  cannot normally form under these redox conditions.

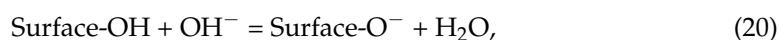
#### 5.1.4. Formation of $\text{Fe}^0$

It is established that under appropriate redox (Eh:pH) conditions,  $\text{Fe}^{n+}$  and  $\text{Cu}^{n+}$  ions will form zero valent metals ( $\text{Fe}^0$ ,  $\text{Cu}^0$ ) [47]. The aqueous environment has recently been classified into three redox zones based on the equilibrium stable hydrogen species [21]. They are Stability Zone 0, where the stable hydrogen species is  $\text{H}^+$ ; Stability Zone 1, where the stable hydrogen species is  $\text{H}_2$ ; and Stability Zone 2, where the stable hydrogen species is  $\text{H}^-$ .  $\text{Fe}^0$  can only form in Stability Zone 1, or Stability Zone 2 [47].  $\text{Cu}^0$  can form in Stability Zones 0, 1 and 2 [47].

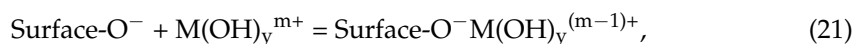
All the trials in this study were operated in Stability Zone 0. In this environment the stable Fe oxidation number is 3. Consequently, the stable Fe polymers are Fe(a) and Fe(b).

#### 5.2. Dilution

A recent study [19] hypothesised that supported  $\text{SiO}_2\text{@Fe(a,b,c)@urea}$  polymers catalysed the formation of M(a,b,c) polymers, where the active surface sites react with  $\text{OH}^-$  ions to form negatively charged surfaces, e.g.,



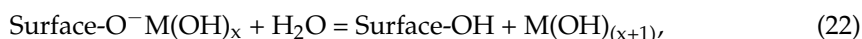
Polymer growth takes the form:



This creates a situation where the polymer surfaces contain negatively charged ( $\text{Surface-O}^-$ ), positively charged ( $\text{Surface-O}^- \text{M(OH)}_y^{n+}$ ), and neutral ( $\text{Surface-O}^- \text{M(OH)}_y$ ), surface sites. Over time, the proportion of charged sites reduces as a new polymer-water equilibrium develops.

Sulphate, bicarbonate and carbonate ions may be removed from the water by the colloids to form carbonate, or sulphate, outer shells, to the colloidal networks.

Addition of water to either the partially desalinated water (containing entrained polymers) or the concentrated settled polymer precipitates (extracted from the partially desalinated water) would be expected to regenerate the catalyst by creating new surface-OH sites as [19]:





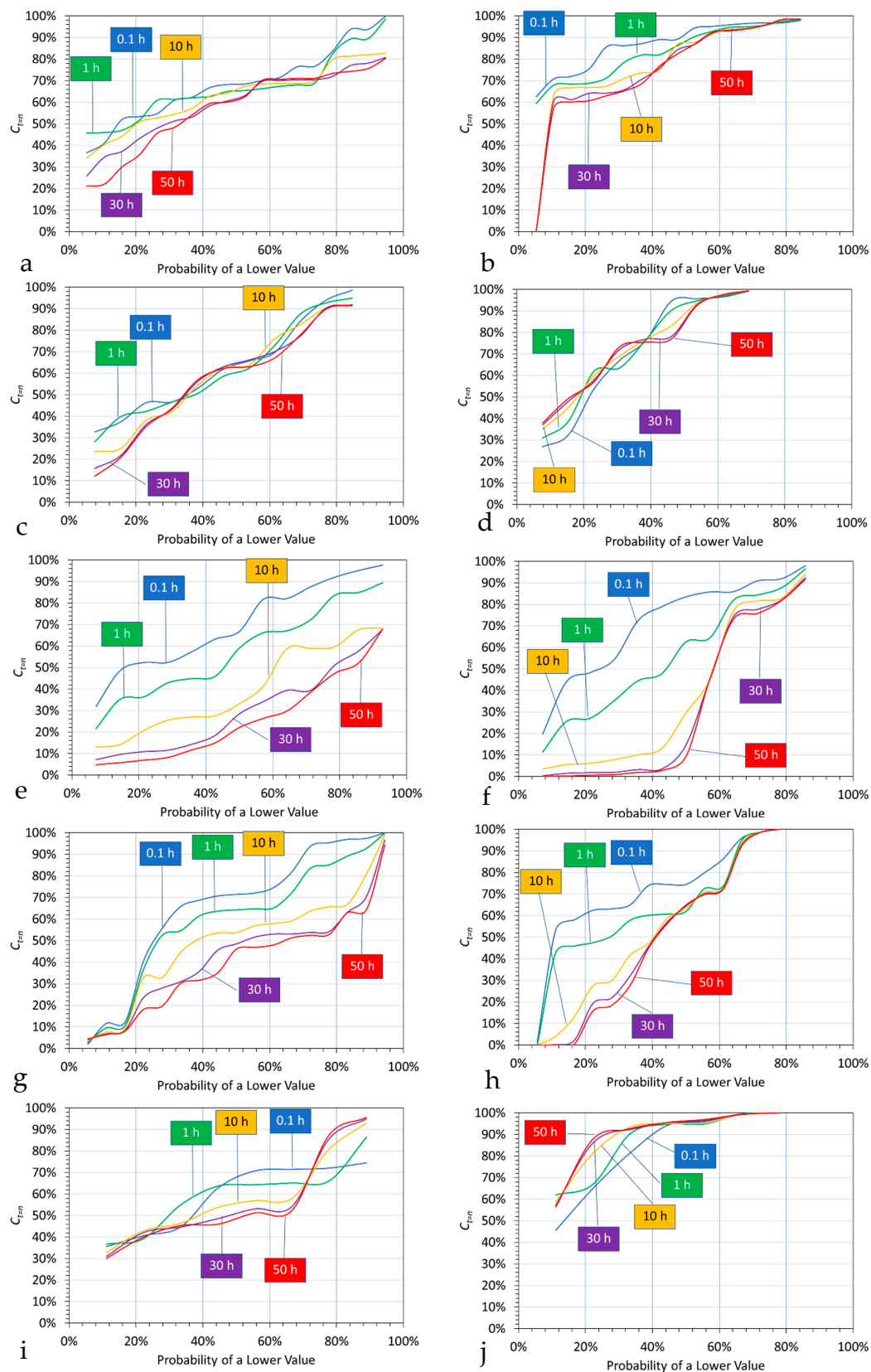


**Figure 11.** Probability of a lower value versus proportion of an ion removed; h = hours. (a), Mg@Al polymer: chloride; (b), Mg@Al polymer: sodium; (c), Fe@Mg@Al polymer: chloride; (d), Fe@Mg@Al polymer: sodium; (e), Fe@Ca@Zn polymer: chloride; (f), Fe@Ca@Zn polymer: sodium; (g), Fe@Ca polymer: chloride; (h), Fe@Ca polymer: sodium; (i), Ca polymer: chloride; (j), Ca polymer: sodium.

This regeneration concept should apply irrespective of the initial composition of the metal polymer, when the blocked site structure is  $\text{Surface-O}^-\text{M}(\text{OH})_x$ . If the blocked site structure is a carbonate, or sulphate, then regeneration will require acidification of the polymer to release the carbonate or sulphate.

This concept was tested by elutriation, where the desalinated water was split into a concentrate ( $P_{C1}$ ) containing particulate polymer colloids, and a water body ( $P_{C2}$ ), which was largely free of particulate colloids.

#### 5.2.1. Fe(a,b,c)@Ca@HCOOH Dilution Trials

Nine 15 L, Fe(a,b,c)@Ca@HCOOH polymer trials processing seawater, which showed no effective desalination over a 24 h period, were separated, and the water body ( $P_{C2}$ ) was put into storage for 4 months at a temperature of between 4 and 16 °C. At the end of that period the water bodies were reanalysed. Six of the water bodies showed no effective  $\text{Cl}^-$  ion removal (Table A6). Eight of the water bodies demonstrated  $\text{Na}^+$  ion removal (Table A6). Over the 24 h following dilution with a ratio of 1 part water body to 5 parts fresh water, both  $\text{Na}^+$  and  $\text{Cl}^-$  ion removal occurred (Table A7). The ion removal was regressed as a power function (Table A8). This analysis indicated that if a polymer formulation fails to initially desalinate the saline water, the polymer catalyst may become activated following dilution of the saline water with fresh water. This observation is consistent with the polymer regeneration model outlined in reference [19].

#### 5.2.2. Dilution Trials: Extracted Product Polymer Slurry Water

The extracted product polymer slurry concentrate water ( $P_{C1}$ ) from 20 (2.3 L) polymer trials was left standing for >700 h at ambient temperatures (Table A9) prior to dilution. Following dilution, the residual entrained polymers were reactivated, resulting in additional ion removal (Table A10). Dilution resulted in an increase in average  $\text{Cl}^-$  ion removal from 28.80% to 45.67%, and an increase in average  $\text{Na}^+$  ion removal from 19.77% to 44.77% (Figure 12, Tables A9 and A10). This observation is consistent with the polymer regeneration model outlined in reference [19].

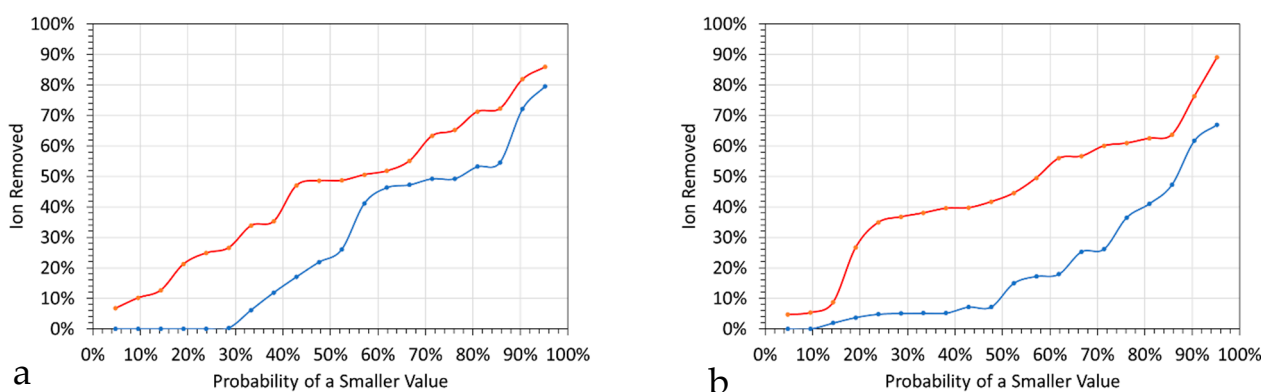


**Figure 12.** Probability of a smaller value versus percentage of the ion in the feed water which is removed. (a),  $\text{Cl}^-$  ion; (b),  $\text{Na}^+$  ion. Blue = undiluted product water >700 h following addition of the polymer and >650 h following separation from the bulk of the settled polymer. Red = diluted product water following >700 storage prior to dilution.

## 6. Applications

Each polymer ingredient costs around USD 200 to USD 3000  $\text{t}^{-1}$ . At a cost of USD 1000  $\text{t}^{-1}$ , an ingredient concentration of 1  $\text{g L}^{-1}$ , represents a treatment cost of USD 1  $\text{m}^{-3}$ . Many of the potential polymer ingredients, used in this study, are already used as fertilisers, or nutrients, or soil improvers, or for other crop management purposes. Therefore, if the polymers are manufactured in situ on the agricultural unit, there may be associated cost savings.

### 6.1. Irrigation

This study has demonstrated that saline water can be:

- Rapidly partially desalinated with a reasonable expectation of a flow line desalination of 10 to 30%;
- Placed in storage for 1 to 50 h to allow polymer formation and a slower partial desalination, with a reasonable expectation of a desalination of 15 to 50%;
- Placed in storage for >1000 h with an expectation of a higher level of desalination.

Crop yields are a function of variety, soil quality, location, weather, agricultural practice, soil salinity, irrigation (and natural) water availability and irrigation water salinity. Under ideal conditions, soil salinity increases with irrigation salinity, and vice versa. Crop yield will decrease with increasing soil salinity and increasing irrigation water salinity. The appropriate relationships between salinity and crop yield are described elsewhere [11,16,17,19].

#### 6.1.1. Example Assessment of the Impact of Desalination on Crop Yield

An example relationship between wheat crop yield and irrigation water salinity is provided in Figure 13a. Integrating the probability distribution for NaCl removal (Figure 4, Table A5) with an initial feed water salinity of  $3.5 \text{ g L}^{-1}$  results in a probability distribution for the product water following polymer formation (Figure 13b,c). The irrigation water salinity is a function of the length of time between adding the polymer ingredients to the water and its application as irrigation water (Figure 13b,c).

Integrating the expected yield curve for the crop (Figure 13a) with the expected irrigation water salinity following desalination (Figure 13b), produces an expected crop yield matrix, where the limit boundaries vary with  $t_r$ , [c] (Figure 13d–f). In this example, without desalination of the irrigation water, the median outcome expectation was  $2.5 \text{ t ha}^{-1}$  (Figure 13a,d–f). This median expectation increased to  $4.5 \text{ t ha}^{-1}$  for [c] = 0.1 h;  $4.9 \text{ t ha}^{-1}$  for [c] = 5 h; and  $5.5 \text{ t ha}^{-1}$  for [c] = 50 h. This example indicates that there is a median expectation of being able to increase the crop yield from  $2.5 \text{ t ha}^{-1}$  to between 4.5 and  $5.5 \text{ t ha}^{-1}$ . At a crop price of  $\text{USD } 300 \text{ t}^{-1}$ , the desalination has the potential to add between  $\text{USD } 600$  and  $900 \text{ ha}^{-1}$  to the wheat crop gross sales. However, the economic viability of achieving this increase is dependent on the cost of the partially desalinated water being less than this gross sales value increase.

Crop prices ( $\text{USD t}^{-1}$ ) are highly variable. They vary both with time, and with geographic region. In September 2022 world wheat prices averaged around  $\text{USD } 330 \text{ t}^{-1}$  but varied during the day within the range  $\text{USD } 180$  to  $440 \text{ t}^{-1}$ . Commodity prices for the polymer ingredients, transport costs and energy costs are similarly variable, on both a geographic, or regional basis, and on a time basis. Therefore, the economic viability of this desalination process for crop irrigation can only be assessed on a regional or local basis.

#### 6.1.2. Leaf and Stem Foliage

It was discovered that if live Blueberry leaves were placed in the saline water containing  $\text{Fe}^{n+}$  ions, that they actively adsorbed NaCl through the stomata. The recovery of the leaves following desalination established that NaCl crystals will form in the stomata as the leaves are dried (Figure 14a) and within its internal vein network (Figure 14b). The vegetable material, if placed in the water will act as dead-end pores and repositories for the removed NaCl. This raises the possibility that placement of live foliage in saline water combined with the addition of  $\text{FeSO}_4$ , with a plant extract, can result in the partial desalination of the water body.

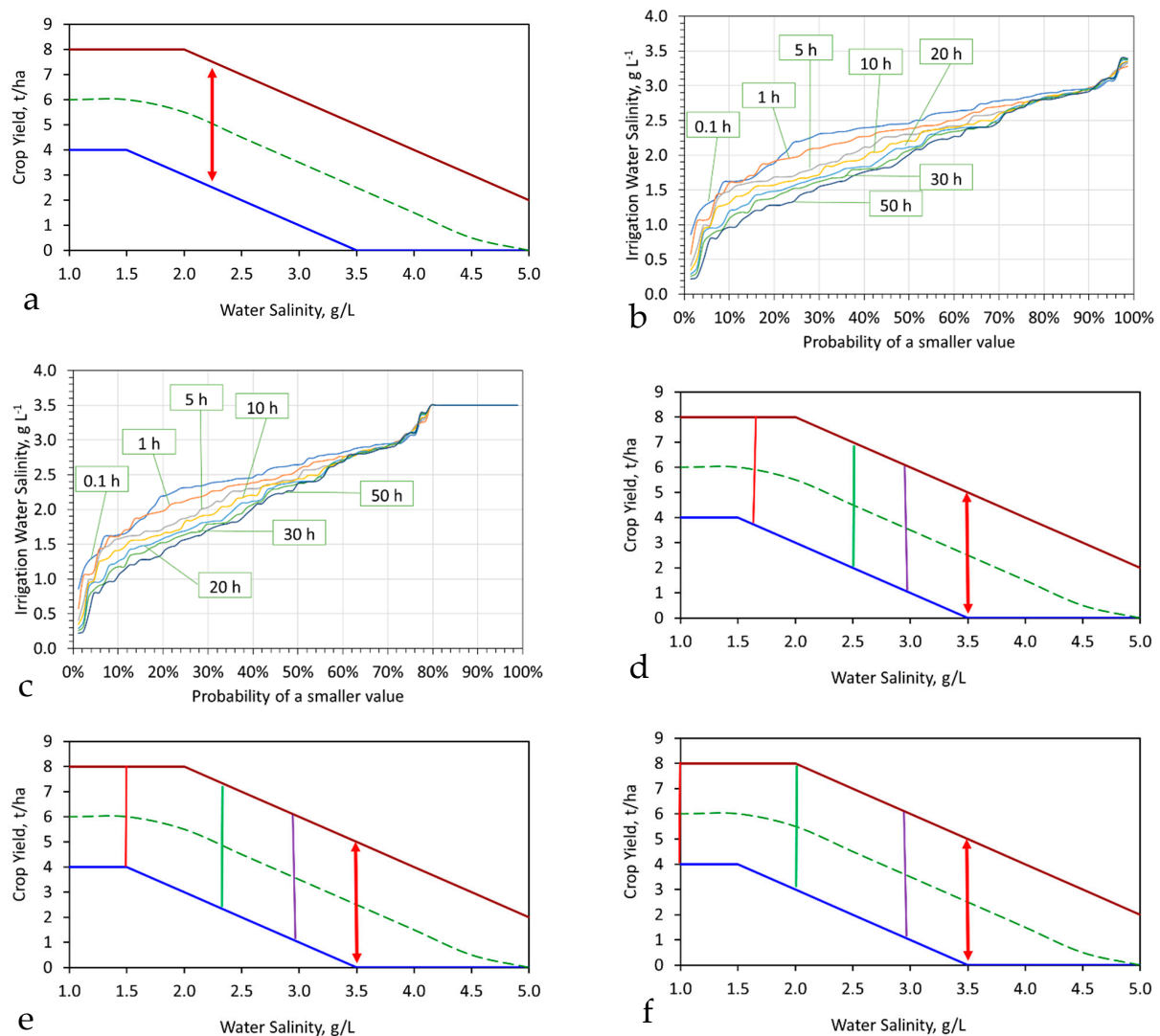


**Figure 13.** Impact of desalination on crop yield. (a), Expected relationship: green dotted line = median expectation; blue solid line = 90% probability of a higher yield; brown solid line = 90% probability of a lower yield. Red arrow = outcome range. (b), Expected irrigation water salinity distribution as a function of  $t_r$ , and [b], if the feed water salinity is  $3.5 \text{ g L}^{-1}$  and addition of the polymer to the water always results in desalination.  $h$  = hours. Data source: Figure 5, Table A5. (c), Expected irrigation water salinity distribution as a function of  $t_r$ , and [c], if the feed water salinity is  $3.5 \text{ g L}^{-1}$  and addition of the polymer to the water only results in desalination in 80% of water batches or volumes. Data source: Figure 5, Table A5. (d), Expected outcome range following desalination.  $t_r$ , [c] = 0.1 h, addition of the polymer always results in desalination. Red arrow is outcome range without desalination. Vertical purple line = 90% probability of a lower water salinity; Vertical green line = 50% probability of a lower water salinity; Vertical red line = 10% probability of a lower water salinity. (e), Expected outcome range following desalination.  $t_r$ , [c] = 5 h, addition of the polymer always results in desalination. Red arrow is outcome range without desalination. Vertical purple line = 90% probability of a lower water salinity; Vertical green line = 50% probability of a lower water salinity; Vertical red line = 10% probability of a lower water salinity. (f), Expected outcome range following desalination.  $t_r$ , [c] = 50 h, addition of the polymer always results in desalination. Red arrow is outcome range without desalination. Vertical purple line = 90% probability of a lower water salinity; vertical green line = 50% probability of a lower water salinity; vertical red line = 10% probability of a lower water salinity.

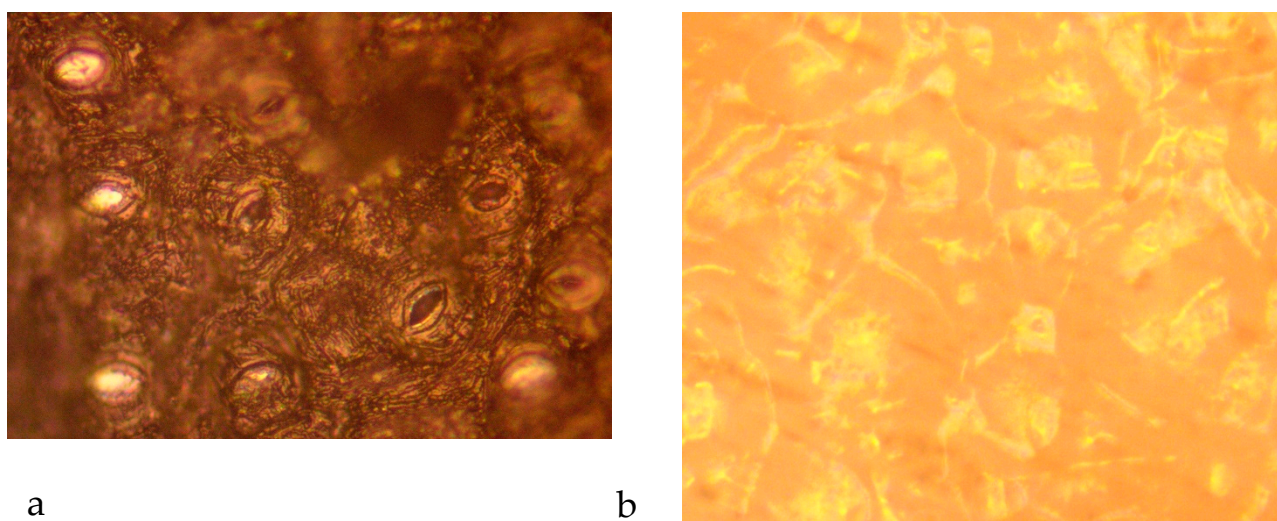


**Figure 14.** Blueberry leaves (Bluecrop) recovered from partially desalinated seawater containing Fe@blue crop polymer. (a), View of the stomata showing NaCl in the stomatal cavities (white) and NaCl present under the cuticle, reflected light; Field of view = 1.1 mm; (b), view of the leaf showing NaCl precipitated within the leaf structure under the cuticle; reflected light, field of view = 0.25 mm.

#### 6.1.3. Ion Removal

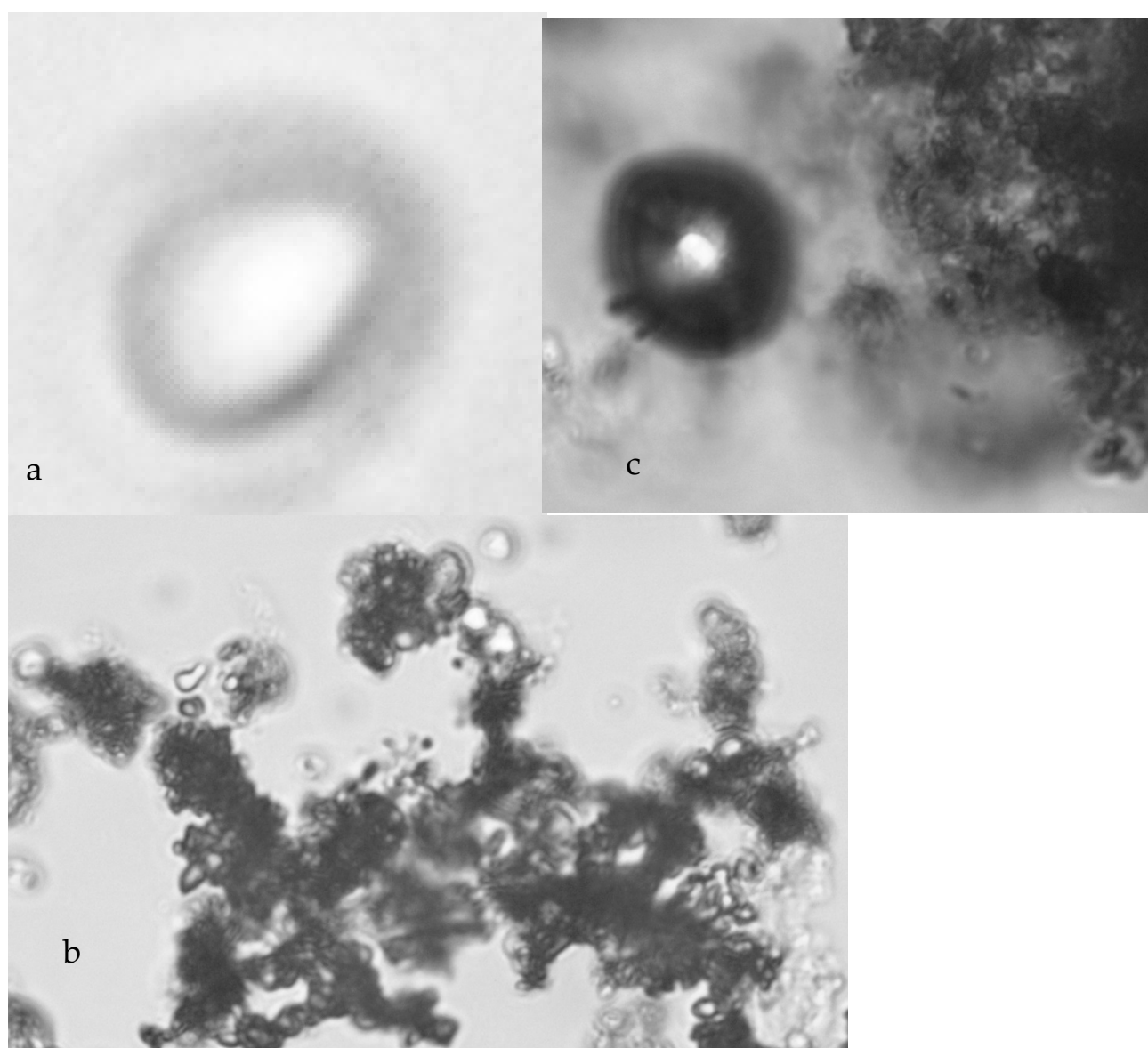
The entrained polymers first coalesce to form small fluid filled spheres (Figure 15a). These spheres then aggregate to form colloidal structures with a cellular appearance (Figure 15b). This mode of cellular formation has been observed when  $n\text{-Fe}^0$  is first placed in water. The fluid within the cells associated with  $n\text{-Fe}^0$  is initially  $\text{H}_2$ , but is subsequently replaced by water as the cell's loose buoyancy. Occasional polymer spheres filled with hydrogen have been observed (Figure 15c). Their presence may indicate that some  $n\text{-Fe}^0$  can be produced during the polymer's manufacturing process.

Figure 16 indicates the general life cycle of a polymer sphere, which is created using  $n\text{-Fe}^0$  or as an entrained metal polymer. Stage 1 is associated with the initial removal of  $\text{Na}^+$  and  $\text{Cl}^-$  ions; Stage 2 is associated with the faster longer-term removal of  $\text{Na}^+$  and  $\text{Cl}^-$  ions. Stage 3 is associated with the observed effective termination of ion removal and in some instances resalination of the water. This model assumes that the polymer adsorbs  $\text{Na}^+$  ions and  $\text{Cl}^-$  ions from the water, and then discharges them into the fluid core within the polymer sphere. Ion removal associated with each of these three distinct stages form distinct first-order reaction patterns as demonstrated in Figures 4 and 6 and Supplementary Information Figures S3–S7.

The polymer formation stages shown in Figures 15 and 16a are:

- Stage 0:  $n\text{-ZVI}$ —formation of a sol-gel nano-particle polymer;
- Stage 1—aggregation of the polymer particles to form a sphere encapsulating a fluid core;
- Stage 2—Expansion of the fluid core volume, with thinning of the polymer rim;
- Stage 3—Dissociation of the polymer rim from the fluid core resulting in collapse of the spheres to form an amorphous flocculate. The fluid core may disassociate into the surrounding water body or remain trapped within an amorphous flocculate body.





**Figure 15.** Polymer spheres produced as Fe(a,b,c)@blue crop polyphenol. (a), Initial fluid filled polymer sphere. Transmitted light. Field of view = 0.730 microns; (b), network of aggregated polymer spheres. Transmitted light. Field of view = 0.12 mm; (c), polymer sphere filled with hydrogen. Transmitted light. Field of view = 0.095 mm.

The ideal desalination polymer either maximises the duration of Stage 2 to maximise ion removal while minimising the adverse effects of Stage 3, or maximises the ion removal associated with Stage 1. The analyses in Supplementary Information Figures S8–S24 have focussed on maximising the short-term removal of  $\text{Na}^+$  and  $\text{Cl}^-$  ions. The maximisation of the short-term removal of these ions requires the polymer spheres to aggregate to form colloidal, or flocculate, bodies constructed from polymer spheres (Figures 9 and 15). The general stages in polymer colloid formation and aggregation observed in this study are summarised in Figure 16a,b. The stages of polymer colloid formation and aggregation shown in Figure 16b are summarised as follows:

- Stage 1—Formation of a polymer sphere (Figure 16b). The measured sizes associated with these initial pre-aggregation colloidal spheres varies with polymer type. Example sizes associated with the initial pre-aggregation colloidal spheres is provided in Table 1.



- Stage 2—Aggregation of the floating polymer spheres to form small floating clusters or chains or networks of chains;
- Stage 3—Aggregation of the small polymer clusters to form larger floating clusters;
- Stage 4—Aggregation of the larger clusters to form settled aggregated, highly porous clusters;
- Stage 5—Breakdown of the polymer spheres to form an amorphous high porosity polymer colloid or flocculate. A proportion of these pores will be dead end pores which will allow fluid and ion sequestration. Some polymer sequences will move from Stage 3 to Stage 5 without an intervening Stage 4.

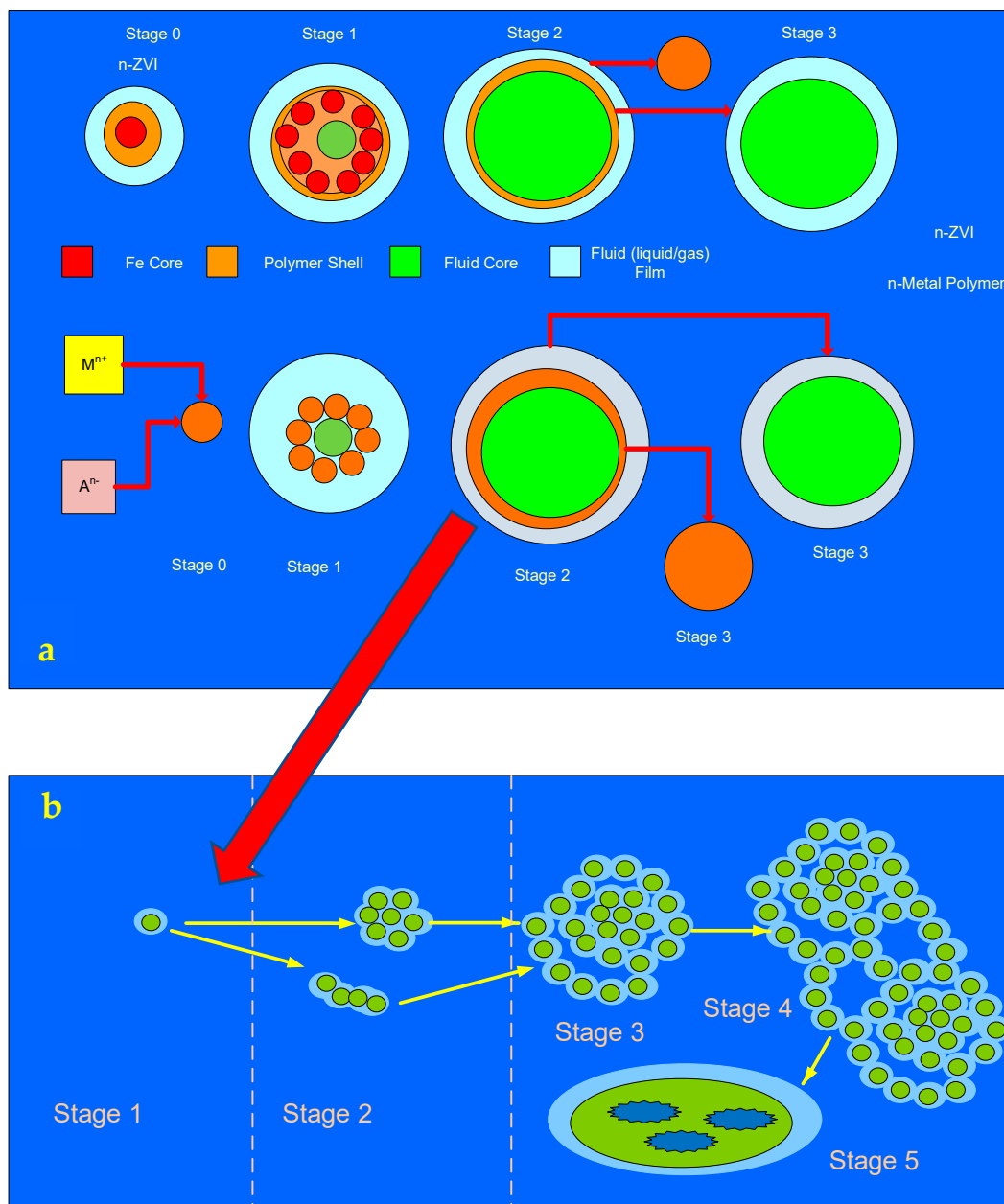


**Figure 16.** Colloidal aggregate formation. (a), Stages in the formation of polymer spheres.  $M^{n+}$  = metal cation;  $A^{n-}$  = Anion. (b), Stages in the formation of polymer flocculates and colloidal particles. Red arrow provides the link between polymer sphere formation and colloidal aggregate formation.

**Table 1.** Example measured pre-aggregation colloidal sphere sizes (microns) associated with the colloids illustrated or analysed in Figures 6, 7, 9 and 10. Number of measurements for each set of data = 50 to 80.

	Mean	Standard Deviation	1st Quartile	Median	3rd Quartile	Figures
n-Fe <sup>0</sup>	2.09	0.80	1.60	2.00	2.40	Figure 7c
Fe@Ca@Zn polymer	2.01	0.52	1.67	2.00	2.33	Figure 6a
Fe@Ca@Zn polymer	4.11	1.26	3.12	4.20	4.77	Figure 6b
Fe(b)@Ca(a)@Mn(a)@Mg(a)@HCOOH polymer	1.48	0.35	1.23	1.47	1.67	Figure 6c
Fe(b)@Ca(a)@Mn(a)@Mg(a)@HCOOH polymer	0.89	0.24	0.70	0.85	0.98	Figure 6d
Fe@Ca@Mn@HCOOH polymer	1.11	0.32	0.90	1.06	1.34	Figure 9a
Fe@Ca@Mn@HCOOH@Tartaric Acid polymer	3.61	1.05	2.95	3.62	4.16	Figure 10
Fe@Ca@Mn@HCOOH@Malic Acid polymer	1.54	0.52	1.18	1.44	1.70	Figure 10
Fe@Ca@Mn@HCOOH@Citric Acid polymer	1.72	0.49	1.40	1.67	1.94	Figure 10
Ca@urea polymer	3.05	1.28	2.03	3.07	3.60	Figure 9b

### 6.2. Impact on Standard Irrigation Water Quality Indices

The most widely used criteria used to characterise irrigation water (apart from electrical conductivity (EC) is the sodium adsorption ratio (SAR) [48].

$$\text{SAR} = \text{Na} / ((\text{Ca} + \text{Mg}) / 2)^{0.5}, \quad (23)$$

Na = sodium concentration, milliequivalent per Litre (meq L<sup>-1</sup>). Ca = calcium concentration, meq L<sup>-1</sup>; Mg = Magnesium concentration, meq L<sup>-1</sup>; 1 meq L<sup>-1</sup> = (1 mmol L<sup>-1</sup> (molecular weight, g)).

An average seawater composition contains Na = 469 meq L<sup>-1</sup>; Ca = 10.3 meq L<sup>-1</sup>; Mg = 52.8 meq L<sup>-1</sup>, and has a SAR value of 83.5. Decreasing the Na value by 50%, without altering the Ca and Mg concentrations decreases SAR by 50% to 41.75. Doubling the Ca and Mg concentrations would further reduce the SAR value to 29.5. Decreasing SAR decreases the tendency for Na to replace Ca and Mg ions, which are adsorbed into clays and organic matter within the soil.

The FAO guideline is that if the SAR value is less than [3.1429 EC–1.2857] [11,48] then the relative rate of water infiltration into the soil is unaffected by salinity. The majority of the polymer examples in this study add meq Ca L<sup>-1</sup> and Mg L<sup>-1</sup> to the feed water. These changes have the effect of increasing the rate of SAR reduction, as Na<sup>+</sup> ion concentrations decrease.

The analysis of the SAR values associated with the 87 polymer examples (Table A1) indicates (Figure 17) that there is a 50% probability that a polymer will reduce the SAR value by between 30 and 35%.

### 6.3. Treatment of Flowback Water to Form Irrigation Water

One of the earliest identified potential markets for ZVI desalination was the treatment of flowback water, associated with shale gas and shale oil wells [44]. The purpose of treating flowback water is to reduce its ion concentrations sufficiently, to allow disposal as either irrigation water, or riparian water, or ground water, or alternatively, allow its reuse as frac water [49].

A typical TDS (total dissolved solids) range for flowback water is within the range 4 to 130 g L<sup>-1</sup> [49,50]. This is within the range analysed in this study (Tables 4, A1–A3 and A5–A10). While this study has not tested the effectiveness of the polymers on flowback water, their potential for changing the composition of flowback water can be illustrated by integrating the polymer desalination results from this study with the published compositions of flowback water [49,51]. Example flowback water compositions are provided in Table 2, using data extracted from references [49,51]. The Australian examples have higher

salinities, higher Ca values, higher Mg values, higher K values, and lower SAR values than the USA examples.

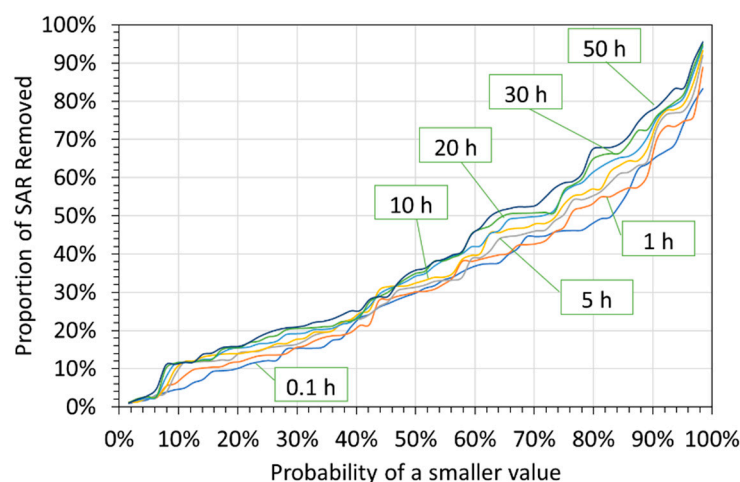


**Figure 17.** Proportion of SAR removed versus probability of a smaller value, for  $[c] = 0.1$  h, 1 h, 5 h, 10 h, 20 h, 30 h and 50 h. Assumptions: initial Ca =  $10.3 \text{ meq L}^{-1}$ ; initial Mg =  $52.8 \text{ meq L}^{-1}$ .

**Table 2.** Example flowback water compositions from shale gas wells in Australia (Northern Territory (Wells 1 and 2)) and USA (Marcellus Shale (Wells 3 to 11)). All measurements are in  $\text{g L}^{-1}$ .

Well	Ca	K	Mg	Na	Cl	HCO <sub>3</sub>	SO <sub>4</sub>	NaCl	SAR
1	1.4200	0.2420	0.3430	6.9600	14.9000	0.3900	0.1000	21.86	60.65
2	22.7000	3.9200	4.8100	40.3000	117.0000	0.0610	0.0400	157.30	89.42
3	0.1717	0.0215	0.0153	4.3850	6.5240	1.3030	0.0749	10.91	121.43
4	0.1979	0.0239	0.0207	4.8580	7.8860	0.8535	0.0640	12.74	123.92
5	0.1633	0.0327	0.0262	4.6590	7.6400	1.0360	0.0656	12.30	125.94
6	0.2292	0.0490	0.0345	5.7990	9.4350	0.6951	0.0426	15.23	133.19
7	0.2566	0.0547	0.0384	6.0950	10.3590	0.5367	0.0389	16.45	132.38
8	0.1851	0.0278	0.0268	5.7170	8.8060	0.7464	0.0144	14.52	146.67
9	0.2265	0.0302	0.0268	6.1280	10.0360	0.6744	0.0211	16.16	144.72
10	0.2431	0.0265	0.0343	6.1870	9.9270	0.5841	0.0316	16.11	138.85
11	0.2669	0.0302	0.0381	6.9340	11.6500	0.5793	0.0087	18.58	148.35

#### Assessment of Expected Water Salinity following Desalination

The probability distributions for  $(C_{t=n}/C_{t=0})$  (Figure 4) can be reduced to a series of polynomial expressions (Figure 18a,b). These expressions can be used to determine the expected salinity distributions for the flowback water following polymer treatment. An example Monte Carlo integration of the equations in Figure 18a,b with the flowback water salinity in Well 1 (Table 2) is provided in Table 3 and Figure 18c,d. This analysis indicates that there is a reasonable expectation that the mean NaCl removal will be between 30% and 45% and that  $\text{Cl}^-$  ions are removed preferentially relative to  $\text{Na}^+$  ions. This analysis indicates what might be possible without focussed selectivity.

Switching to a Fe@Ca@Zn polymer (Figure 11) or Fe@Ca polymer (Figure 11) creates the possibility of a significantly higher rapid desalination. The polynomial outcome equations versus probability for a Fe@Ca@Zn polymer are provided in Figure 18e,f for  $t = 0.1$  h and  $t = 50$  h. The integration of these equations with the flowback water composition for Well 1 (Table 2) creates an outcome probability distribution (Figure 18, which is summarised in Table 4. This analysis (Table 4) indicates that after 50 h of treatment, it is possible to reduce the average water salinity by 63% to  $7.92 \text{ g L}^{-1}$  (median 68%,  $6.98 \text{ g L}^{-1}$ ).

**Table 3.** Modelled removal of Na<sup>+</sup> and Cl<sup>−</sup> ions for Well 1 (Table 1) after 0.1 h and 50 h using a metal polymer (Figure 18).

	0.1 h Cl <sup>−</sup>	Na <sup>+</sup>	NaCl	50 h Cl <sup>−</sup>	Na <sup>+</sup>	NaCl
Feed	14.9	6.96	21.86	14.9	6.96	21.86
Product						
Mean	9.87	5.23	15.10	7.20	4.65	11.85
Standard Deviation	3.37	1.50	3.67	4.05	1.51	4.39
1st Quartile	8.08	4.37	13.00	3.71	3.80	8.33
Median	9.78	5.42	15.34	7.54	4.63	11.99
3rd Quartile	12.59	6.59	17.83	10.17	5.93	15.03
Removed						
Mean	33.7%	24.9%	30.9%	51.7%	33.1%	45.8%
1st Quartile	45.8%	37.3%	40.5%	75.1%	45.4%	61.9%
Median	34.4%	22.2%	29.8%	49.4%	33.5%	45.1%
3rd Quartile	15.5%	5.3%	18.4%	31.8%	14.8%	31.3%

**Table 4.** Modelled removal of Na<sup>+</sup> and Cl<sup>−</sup> ions for Well 1 (Table 1) after 0.1 h and 50 h using a Fe@Ca@Zn polymer (Figure 18).

	0.1 h Cl <sup>−</sup>	Na <sup>+</sup>	NaCl	50 h Cl <sup>−</sup>	Na <sup>+</sup>	NaCl
Feed	14.9	6.96	21.86	14.9	6.96	21.86
Product						
Mean	10.27	4.97	15.24	4.05	3.88	7.92
Standard Deviation	3.35	1.89	3.89	3.47	11.09	11.59
1st Quartile	7.99	3.96	12.91	1.04	0.71	3.89
Median	10.21	5.68	15.11	2.95	3.05	6.98
3rd Quartile	13.73	6.45	18.55	6.07	5.85	10.03
Removed						
Mean	31.1%	28.6%	30.3%	72.9%	44.3%	63.8%
1st Quartile	46.4%	43.1%	40.9%	93.0%	89.8%	82.2%
Median	31.5%	18.4%	30.9%	80.2%	56.2%	68.1%
3rd Quartile	7.8%	7.4%	15.1%	59.3%	16.0%	54.1%

These product water salinities are too high for use as irrigation water for most crops [11]. However, dilution of the desalinated flowback water with fresh water will allow usage for irrigation.

The trial results in Table A7 indicate that dilution using one part desalinated water to five parts freshwater results in reactivation of the polymer, coupled with additional ion removal (Figure 18). Integrating the polynomial outcome equations for polymer reactivation following dilution with the expected water salinity following dilution creates a product water distribution following dilution (Figure 18). This integration demonstrates that, following dilution with polymer reactivation (Figure 18), the resultant irrigation water salinity would be suitable to irrigate most staple crops and grasslands, and may be suitable for some vegetables [11].

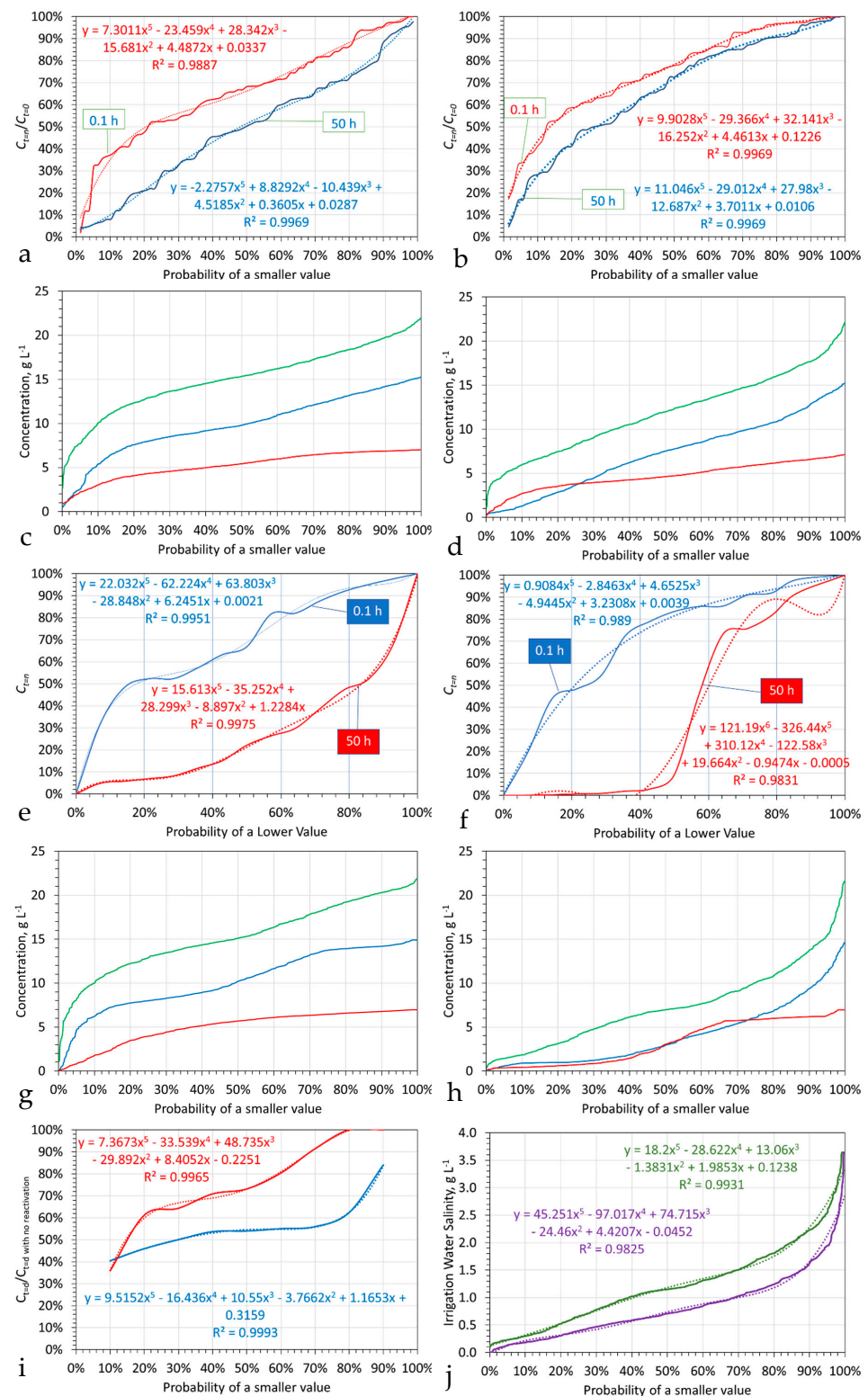


**Figure 18.** Desalination assessment: *Generic Observed Ion Removal*: Probability of a smaller value versus  $C_{t=n}/C_{t=0}$  versus probability for  $t = 0.1$  h (red) and  $t = 50$  h (blue) with the associated polynomial equations, and (a), chloride; (b), sodium; *Monte Carlo Modelling*: Modelled concentration ( $g L^{-1}$ ) versus probability for the flowback water in Trial 1 (Table 1) following metal polymer treatment. (c),  $t = 0.1$  h; (d),  $t = 50$  h; Red = sodium; Blue = chloride; Green = NaCl. Number of Monte-

Carlo Analysis Iterations = 1000; *Specific Polymer Ion Removal*:  $C_{t=n}/C_{t=0}$  versus probability for  $t = 0.1$  h (red) and  $t = 50$  h (blue) with the associated polynomial equations for the Fe@Ca@Zn polymers: Y-axis is labelled  $C_{t=n}$  when  $C_{t=0}$  is 100%. (e), chloride; (f), sodium; *Monte Carlo Modelling*: Modelled concentration ( $\text{g L}^{-1}$ ) versus probability for the flowback water in Trial 1 (Table 2) following Fe@Ca@Zn metal polymer treatment; (g),  $t = 0.1$  h; (h),  $t = 50$  h; (i), Expected additional ion removal associated with a dilution after 50 h of 1 part desalinated water and 5 parts freshwater; (j), Irrigation water salinity following a 1 part desalinated water + 5 parts freshwater dilution, where green = expected irrigation water salinity if no polymer reactivation occurs following dilution (mean =  $1.23 \text{ g L}^{-1}$ ; standard deviation = 0.74; 1st quartile =  $0.66 \text{ g L}^{-1}$ ; median =  $1.15 \text{ g L}^{-1}$ ; 3rd quartile =  $1.67 \text{ g L}^{-1}$ ); purple = expected irrigation water salinity following polymer reactivation following dilution; (mean =  $0.83 \text{ g L}^{-1}$ ; standard deviation = 0.60; 1st quartile =  $0.39 \text{ g L}^{-1}$ ; median =  $0.71 \text{ g L}^{-1}$ ; 3rd quartile =  $1.12 \text{ g L}^{-1}$ );  $C_{t=d}$  = observed ion concentration in the diluted water/ion concentration in the diluted water if polymer reactivation does not occur.  $C_{t=d}$  is measured 24 h after dilution. Red = sodium; Blue = chloride; Green = NaCl. Number of Monte-Carlo Analysis Iterations = 1000.

## 7. Novelty

This study has expanded the understanding of entrained colloidal aggregate formation in saline water to produce a unified formational model, which appears to operate across a wide range of metal polymer compositions (Figure 16).

This model suggests that the polymers are polar and are able to abstract both anions and cations from the water. The traditional view has been that metal polymers adsorb ions from water on both their surfaces and in their intralayer porosity, when they form as layered double hydroxides (LDH) or layered hydroxide salts (LHS). This traditional view restricts the molar removal from water of adsorbed ions to a fraction of the mole weight of the polymer.

This study has discovered that something quite different can occur. Consistently, as demonstrated in Figure 4, the median expectation is that about 50% of  $\text{Cl}^-$  and  $\text{Na}^+$  ions will be removed. The removal reaction is demonstrated to be first-order (Supplementary Figures S1–S24). This implies that the time taken to reduce the initial ion concentration by 50%, (half life)  $t_{50}$ , is:

$$t_{50} = 0.693/k_{\text{obs}}, \quad (24)$$

The observed half-life is recorded in Figures 4 and 11, for a variety of polymers. An analysis of the amount of NaCl removed  $\text{g}^{-1}$  polymer ingredients indicated that the average removal using sub-optimised polymer compositions and loadings was about  $3.75 \text{ g NaCl g}^{-1}$  polymer ingredients. This suggests that the polymers act as catalysts for NaCl removal and are not solely adsorbents. The widespread observation that the initial structural unit is a fluid filled sphere (Figure 16) suggests that the fluid filled spheres could act as a sink and store for the removed  $\text{Na}^+$  ions and  $\text{Cl}^-$  ions.

If the polymers had been solely adsorbents, dilution with lower pH water would be expected to release adsorbed  $\text{Na}^+$  and  $\text{Cl}^-$  ions into the water. This did not happen; instead, the polymers continued to remove  $\text{Na}^+$  and  $\text{Cl}^-$  ions. This implies that the polymers act as catalysts for the ion removal.

The study has demonstrated that the polymers will also remove  $\text{Fe}^{n+}$ ,  $\text{Ca}^{2+}$ ,  $\text{Mg}^{2+}$ ,  $\text{Zn}^{2+}$ ,  $\text{Mn}^{n+}$ ,  $\text{Al}^{n+}$  cations and organic anions from the water. The sol-gel polymer formation approach may, therefore, have a role to play in a wider water remediation context.

## 8. Conclusions

This study has established that a sol gel process can be used to construct metal polymers in saline water. The polymers are demonstrated to remove both  $\text{Na}^+$  and  $\text{Cl}^-$  ions, while reducing the SAR value of the saline water. A model for the ion removal has been proposed where:

- The polymer monomers, once formed, coalesce to form colloidal fluid filled spheres;



- The colloidal fluid filled spheres act as scavenging agents and sequester  $\text{Na}^+$  and  $\text{Cl}^-$  ions from the water within their structure and fluids;
- The colloidal fluid filled spheres coalesce by aggregation and capture to form chains, net structures and colloidal aggregates, with a cellular structure;
- The cellular structured colloidal aggregates restructure to form amorphous structures, and in doing so either release the contents of the fluid filled cells into the water body or aggregate them into dead-end porosity within the amorphous aggregate. Ca based cellular structures may form an outer shell of  $\text{CaCO}_3$  or  $\text{CaSO}_4$  crystals.

This model appears to work for the removal of both  $\text{Na}^+$  and  $\text{Cl}^-$  ions, and may work for the removal of other ion types. It is expected that other cations contained within the water, with an oxidation number of  $>1$  will be incorporated, within the colloid structure.

This study has focussed on demonstrating  $\text{Na}^+$  ion and  $\text{Cl}^-$  ion removal, in 2.3 L reactors, operated as a static water body, where the dominant interaction between the sol-gel metal polymer and water body is by diffusion. There is a reasonable expectation that this process will operate in water tanks with capacities within the range 10 to 5000  $\text{m}^3$ . Consequently, the process has potential applications for the desalination of irrigation water, saline ground water, mining impoundments, associated water produced during oil and gas extraction and flowback water associated with shale oil/shale gas impoundments.

The application examples have demonstrated that the polymers could potentially reduce to salinity of saline irrigation water to increase the expected crop yields. The examples have also demonstrated that they could potentially reduce the salinity of shale gas flowback water sufficiently to allow its reuse as an irrigation water.

**Funding:** This research received no external funding.

**Supplementary Materials:** The following supporting information can be downloaded at: <https://www.mdpi.com/article/10.3390/w14203224/s1>, Figure S1: Entrained polymer placed in seawater at a concentration of  $0.2 \text{ g Fe L}^{-1}$ ; Figure S2: Water salinity desalination polymer quality control check; Figure S3: Test trials illustrating the suitability of the entrained n-Fe@blue crop polymer; Figure S4: High water salinity desalination  $\text{C}^0$ :n-Fe@blue crop polymer pellet quality control check; Figure S5: Medium water salinity desalination pellet quality control check; Figure S6: Estuarine water salinity desalination pellet quality control check; Figure S7: Medium water salinity desalination polymer quality control check; Figure S8: Water salinity desalination polymer quality control check; Figure S9: Water salinity desalination polymer quality control check; Figure S10: Water salinity desalination polymer quality control check; Figure S11: Water salinity desalination polymer quality control check; Figure S12: Water salinity desalination polymer quality control check; Figure S13: Water salinity desalination polymer quality control check; Figure S14: Water salinity desalination polymer quality control check; Figure S15: Water salinity desalination polymer quality control check; Figure S16: Water salinity desalination polymer quality control check; Figure S17: Water salinity desalination polymer quality control check; Figure S18: Water salinity desalination polymer quality control check; Figure S19: Water salinity desalination polymer quality control check; Figure S20: Water salinity desalination polymer quality control check; Figure S21: Water salinity desalination polymer quality control check; Figure S22: Water salinity desalination polymer quality control check; Figure S23: Water salinity desalination polymer quality control check; Figure S24: Water salinity desalination polymer quality control check; Table S1: Regressed ( $C_{t=n}/C_{t=0}$ ) ion concentration for chloride as a function of reaction time (hours); Table S2: Regressed ( $C_{t=n}/C_{t=0}$ ) ion concentration for sodium as a function of reaction time (hours).

**Data Availability Statement:** The data used in this study are placed in the figures and tables contained within the paper, the Appendices A and B and the Supplementary Information File.

**Acknowledgments:** The editorial team and the two reviewers are thanked for their very helpful and constructive comments on the draft of this paper.

**Conflicts of Interest:** The author declares no conflict of interest.

## Appendix A. Example Sol-Gel Formulations and Desalination Outcomes

For ease of access, most graphed ion concentrations versus reaction time graphs generated in this study have been placed in the Supplementary Information File, Figures S1–S24.

Most remediation reactions are first-order or higher-order reactions. For example, for a first order reaction [16,17,39,40]:

$$\ln(C_{t=n}) = -k_{ins} a_s P_w t_r + \ln(C_{t=0}) = -k_{ins2} N_T \eta t_r + \ln(C_{t=0}) = -k_{obs} t_r + \ln(C_{t=0}) = -k_{obs} t_r + [A], \quad (A1)$$

A zero-order reaction [16,17,39,40] replaces the term,  $[t_r]$  (reaction time), with  $[\ln(t_r)]$ . A simple modification of  $k_{ins}$ , may have the same effect as increasing  $a_s$  (surface area), or increasing  $P_w$  (concentration of the colloid in the water). This modification may result in a decrease in  $\ln(C_{t=n})$ . Commonly,  $[A]$  is assumed to be  $[\ln(C_{t=0})]$ . However, in many n-Fe<sup>0</sup> and colloid trials,  $[A] < [\ln(C_{t=0})]$ . The economics of water remediation (desalination) is maximised by minimising  $[A]$ , and maximising  $k_{obs}$ . Minimisation of  $[A]$  maximises the instantaneous reduction in salinity.

### Appendix A.1. Manufacture of n-Fe(b)@Ca@Mn@formate Polymer

The sol-gel process forms an almost instantaneous precipitate, which settles, by gravity differentiation, to form a concentrated hydrated gel (Figure A1). Placement of this precipitate in saline water, and results in a gradual desalination (Supplementary Information, Figure S1), where Na<sup>+</sup> ions and Cl<sup>−</sup> ions can be removed at different rates. Cl<sup>−</sup> removal equates to a first-order reaction, where  $[A] < \ln(C_{t=0})$ .

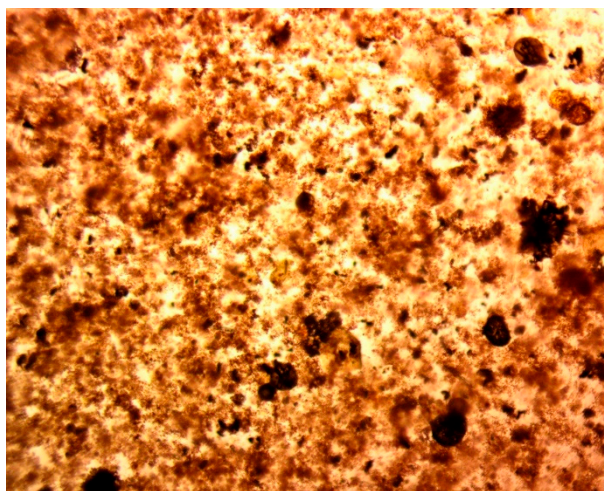


**Figure A1.** Settled entrained hydrated polymer formed by the sol-gel approach (Example A1a); Transmitted light, Field of view 1 mm.

#### Appendix A.1.1. Fe(b)@Ca(a)@Mn(a)@HCOOH Polymer

Two examples of this polymer were trialled (Examples A1a; A1b), where the polymer was constructed within the feed water. The principal difference between the two examples was the amount of CaO used to construct the gel.

- Example A1a: An entrained Fe(b)@Ca(a)@Mn(a)@HCOOH polymer was constructed by mixing 1g FeSO<sub>4</sub> + 1.67 g CaO + 2.52 g MnO<sub>2</sub> + 1 cm<sup>3</sup> (40%) HCOOH L<sup>−1</sup> with 2.3 L of feed water (Cl<sup>−</sup> = 26.55 g L<sup>−1</sup>; Na<sup>+</sup> = 17.21 g L<sup>−1</sup> (sea water)). The water was allowed to rest for 241 h at a temperature of 4.8 to 7.0 °C. The product water contained Cl<sup>−</sup> = 1.35 g L<sup>−1</sup>; Na<sup>+</sup> = 0.78 g L<sup>−1</sup>; Removal: Cl<sup>−</sup> = 94.91%; Na<sup>+</sup> = 95.46%.
- Example A1b: This trial constructed the polymer from 1g FeSO<sub>4</sub> + 3.34 g CaO + 2.52 g MnO<sub>2</sub> + 1 cm<sup>3</sup> (40%) HCOOH L<sup>−1</sup> with the feed water (Cl<sup>−</sup> = 26.55 g L<sup>−1</sup>;

$\text{Na}^+ = 17.21 \text{ g L}^{-1}$  (seawater)). The water (2.3 L) was allowed to rest for 241 h at a temperature of 4.8 to 7.0 °C. The product water contained  $\text{Cl}^- = 9.64 \text{ g L}^{-1}$ ;  $\text{Na}^+ = 2.50 \text{ g L}^{-1}$ ; Removal:  $\text{Cl}^- = 63.19\%$ ;  $\text{Na}^+ = 85.47\%$ .

These polymers produced a high level of desalination. The bulk of the gel settled to form a hydrated gel precipitate (Figure A1). Examination of the product water established that the presence of polymer spheres, which appear to be formed by the coalescence and agglomeration of smaller fluid filled polymer spheres (Figure A2) to provide a cellular construction. The polymer spheres, were typically constructed from Fe(a,b,c) polymers. A few of the larger polymer spheres had aggregated around  $\text{MnO}_2$  particles. Evaporation of the water demonstrated the presence of  $\text{CaSO}_4$  precipitates, indicating that both  $\text{Ca}^{2+}$  and  $\text{SO}_4^{2-}$  ions are present in the product water.

Colloidal Fe will remove pollutants using a zero-order reaction [52]. The inclusion of  $\text{MnO}_2$  colloids has the effect of increasing  $k_{\text{obs}}$ , and can switch the remediation reaction (for some pollutants) from a zero-order reaction to a second-order reaction [52].

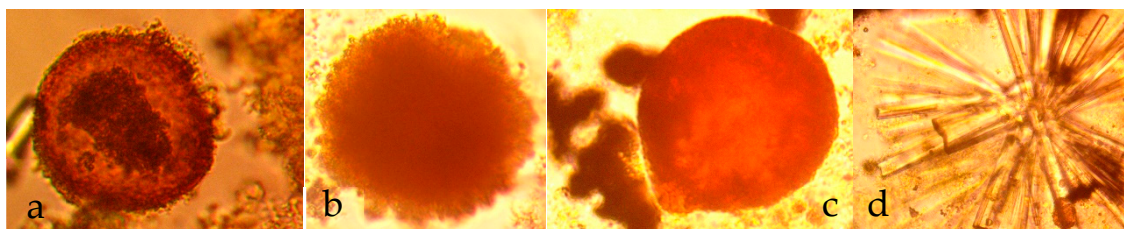


**Figure A2.** Examples of the polymer spheres in transmitted light: (a) Example A1a: Fe(b)Mn(a) polymer where Fe(b) polymer surround a Mn core; Field of view = 0.12 mm; (b) Example A1b: Fe(b) polymer; Field of view = 0.11 mm; (c) Example A1b: Fe(b) polymer; Field of view = 0.16 mm; (d) Example A1b: gypsum flower ( $\text{CaSO}_4$ ) in the evaporated water product; Field of view = 0.27 mm.

#### Appendix A.1.2. Fe(b)@Ca(a)@Mn(a)@K@HCOOH Polymer

The impact of  $\text{KHCO}_3$  and  $\text{C}_x\text{H}_y\text{O}_z$  on the gel formation was evaluated in Examples A2a to A2d.

- Example A2a: An entrained Fe(b)@Ca(a)@Mn(a)@K@HCOOH polymer was constructed by mixing 1g  $\text{FeSO}_4$  + 1.67 g  $\text{CaO}$  + 2.52 g  $\text{MnO}_2$  + 1.22 g  $\text{K}_2\text{CO}_3$  + 1 cm<sup>3</sup> (40%)  $\text{HCOOH L}^{-1}$  with the feed water ( $\text{Cl}^- = 26.55 \text{ g L}^{-1}$ ;  $\text{Na}^+ = 17.21 \text{ g L}^{-1}$ ; (seawater)). The water (2.3 L) was allowed to rest for 241 h at a temperature of 4.8 to 7.0 °C. The product water contained  $\text{Cl}^- = 5.66 \text{ g L}^{-1}$ ;  $\text{Na}^+ = 2.97 \text{ g L}^{-1}$ . Removal:  $\text{Cl}^- = 78.68\%$ ;  $\text{Na}^+ = 82.74\%$ .
- Example A2b: The entrained polymer was constructed from 1g  $\text{FeSO}_4$  + 3.34 g  $\text{CaO}$  + 2.52 g  $\text{MnO}_2$  + 1.22 g  $\text{K}_2\text{CO}_3$  + 1.36 g  $\text{CaCO}_3$  + 0.9 g  $\text{C}_4\text{H}_6\text{O}_6$  + 1 cm<sup>3</sup> (40%)  $\text{HCOOH L}^{-1}$  + feed water ( $\text{Cl}^- = 22.11 \text{ g L}^{-1}$ ;  $\text{Na}^+ = 14.43 \text{ g L}^{-1}$ ; (seawater)). The water (2.3 L) was allowed to rest for 216 h at a temperature of 4.0 to 7.1 °C. The product water contained  $\text{Cl}^- = 1.04 \text{ g L}^{-1}$ ;  $\text{Na}^+ = 5.93 \text{ g L}^{-1}$ . Removal:  $\text{Cl}^- = 95.29\%$ ;  $\text{Na}^+ = 58.90\%$ .
- Example A2c: The entrained polymer was constructed from 1g  $\text{FeSO}_4$  + 1.67 g  $\text{CaO}$  + 2.52 g  $\text{MnO}_2$  + 1.22 g  $\text{K}_2\text{CO}_3$  + 2.72 g  $\text{CaCO}_3$  + 0.8 g  $\text{C}_4\text{H}_6\text{O}_5$  + 1 cm<sup>3</sup> (40%)  $\text{HCOOH L}^{-1}$  + feed water ( $\text{Cl}^- = 22.11 \text{ g L}^{-1}$ ;  $\text{Na}^+ = 14.43 \text{ g L}^{-1}$ ). The water (2.3 L) was allowed to rest for 216 h at a temperature of 4.6 to 7.1 °C. The product water contained  $\text{Cl}^- = 1.00 \text{ g L}^{-1}$ ;  $\text{Na}^+ = 3.25 \text{ g L}^{-1}$ . Removal:  $\text{Cl}^- = 95.47\%$ ;  $\text{Na}^+ = 77.48\%$ .
- Example A2d: The entrained polymer was constructed from 1g  $\text{FeSO}_4$  + 1.67 g  $\text{CaO}$  + 2.52 g  $\text{MnO}_2$  + 1.22 g  $\text{K}_2\text{CO}_3$  + 4.07 g  $\text{CaCO}_3$  + 0.83 g  $\text{C}_6\text{H}_8\text{O}_7$  + 0.83 g  $\text{C}_6\text{H}_8\text{O}_7$  + 1 cm<sup>3</sup> (40%)  $\text{HCOOH L}^{-1}$  + feed water ( $\text{Cl}^- = 22.11 \text{ g L}^{-1}$ ;  $\text{Na}^+ = 14.43 \text{ g L}^{-1}$ ). The water (2.3 L) was allowed to rest for 216 h at a temperature of 4.6 to 7.1 °C. The product water contained  $\text{Cl}^- = 1.99 \text{ g L}^{-1}$ ;  $\text{Na}^+ = 3.18 \text{ g L}^{-1}$ . Removal:  $\text{Cl}^- = 90.99\%$ ;  $\text{Na}^+ = 77.96\%$ .

These examples demonstrated, by reference to the control (Example A2a) that the addition of  $C_xH_yO_z$  can increase  $k_{obs}$  for  $Cl^-$  removal, relative to  $k_{obs}$  for  $Na^+$  removal.

#### Appendix A.1.3. Fe(b)@Ca(a)@Mn(a)@Mg(a)@HCOOH Polymer

An entrained Fe(b)@Ca(a)@Mn(a)@Mg(a)@HCOOH polymer was constructed by mixing 1 g  $FeSO_4$  + 1.67 g  $CaO$  + 2.52 g  $MnO_2$  + 2.96 g  $MgCO_3$  + 1 cm<sup>3</sup> (40%)  $HCOOH$  L<sup>-1</sup> with the feed water ( $Cl^-$  = 26.55 g L<sup>-1</sup>;  $Na^+$  = 17.21 g L<sup>-1</sup>). The water (2.3 L) was allowed to rest for 241 h at a temperature of 4.8 to 7.0 °C. The product water contained  $Cl^-$  = 1.55 g L<sup>-1</sup>;  $Na^+$  = 8.75 g L<sup>-1</sup>. Removal:  $Cl^-$  = 94.16%;  $Na^+$  = 49.15%.

#### Appendix A.1.4. Fe(b)@Ca(a)@Mn(a)@Mg(a)@Zn(a)@HCOOH Polymer

An entrained Fe(b)@Ca(a)@Mn(a)@Mg(a)@Zn(a)@HCOOH polymer was constructed by mixing 2 g  $FeSO_4$  + 3.34 g  $CaO$  + 2.52 g  $MnO_2$  + 1.48 g  $MgCO_3$  + 5.61 g  $ZnO$  + 2 cm<sup>3</sup> (40%)  $HCOOH$  L<sup>-1</sup> with the feed water ( $Cl^-$  = 25.45 g L<sup>-1</sup>;  $Na^+$  = 23.95 g L<sup>-1</sup>). The water (2.3 L) was allowed to rest for 24 h at a temperature of 8.7 to 10.7 °C. The product water contained  $Cl^-$  = 25.18 g L<sup>-1</sup>;  $Na^+$  = 9.00 g L<sup>-1</sup>. Removal:  $Cl^-$  = 1.06%;  $Na^+$  = 62.45%. This polymer demonstrated a high selectivity for  $Na^+$  ion removal.

#### Appendix A.1.5. Fe(b)@Ca(a)@Zn(a)@HCOOH Polymer

An entrained Fe(b)@Ca(a)@Zn(a)@HCOOH polymer was constructed by mixing 2 g  $FeSO_4$  + 3.34 g  $CaO$  + 5.61 g  $ZnO$  + 1 cm<sup>3</sup> (40%)  $HCOOH$  L<sup>-1</sup> with the feed water ( $Cl^-$  = 10.44 g L<sup>-1</sup>;  $Na^+$  = 6.33 g L<sup>-1</sup>). The water (2.3 L) was allowed to rest for 24 h at a temperature of 4.1 to 8.2 °C. The product water contained  $Cl^-$  = 4.51 g L<sup>-1</sup>;  $Na^+$  = 4.91 g L<sup>-1</sup>. Removal:  $Cl^-$  = 56.80%;  $Na^+$  = 22.43%. The decline in ion concentration with time could be accounted for by a first-order reaction (Supplementary Information Figure S2a).

### Appendix A.2. Manufacture of @C<sub>4</sub>H<sub>6</sub>O<sub>6</sub> Polymers

#### Appendix A.2.1. Fe(b)@C<sub>4</sub>H<sub>6</sub>O<sub>6</sub> Polymer

An entrained Fe(b)@C<sub>4</sub>H<sub>6</sub>O<sub>6</sub> polymer was constructed by mixing 1 g  $FeSO_4$  + 0.9 g  $C_4H_6O_6$  L<sup>-1</sup> with the feed water ( $Cl^-$  = 21.11 g L<sup>-1</sup>;  $Na^+$  = 14.43 g L<sup>-1</sup>). The water (2.3 L) was allowed to rest for 0.1 h at a temperature of 3.8 to 4.0 °C. The product water contained  $Cl^-$  = 1.51 g L<sup>-1</sup>;  $Na^+$  = 14.43 g L<sup>-1</sup>. Removal:  $Cl^-$  = 92.84%;  $Na^+$  = 0.00%. The polymer has a high almost instant,  $Cl^-$  ion removal selectivity and appears to be ineffective for the removal of  $Na^+$  ions.

#### Appendix A.2.2. Fe(b)@Ca(a)@K@C<sub>4</sub>H<sub>6</sub>O<sub>6</sub> Polymer

An entrained Fe(b)@Ca(a)@K@C<sub>4</sub>H<sub>6</sub>O<sub>6</sub> polymer was constructed by mixing 1 g  $FeSO_4$  + 1.67 g  $CaO$  + 1.22 g  $K_2CO_3$  + 1.36 g  $CaCO_3$  + 0.9 g  $C_4H_6O_6$  L<sup>-1</sup> with the feed water ( $Cl^-$  = 21.11 g L<sup>-1</sup>;  $Na^+$  = 14.43 g L<sup>-1</sup>). The water (2.3 L) was allowed to rest for 0.1 h at a temperature of 4.0 to 4.3 °C. The product water contained  $Cl^-$  = 1.93 g L<sup>-1</sup>;  $Na^+$  = 12.07 g L<sup>-1</sup>. Removal:  $Cl^-$  = 90.85%;  $Na^+$  = 16.35%. The polymer has a high  $Cl^-$  ion removal selectivity and appears to be less effective for the removal of  $Na^+$  ions.

#### Appendix A.2.3. Fe(b)@Ca(a)@Mn(a)@K@C<sub>4</sub>H<sub>6</sub>O<sub>6</sub> Polymer

An entrained Fe(b)@Ca(a)@Mn(a)@K@C<sub>4</sub>H<sub>6</sub>O<sub>6</sub> polymer was constructed by mixing 1 g  $FeSO_4$  + 1.67 g  $CaO$  + 2.52 g  $MnO_2$  + 1.22 g  $K_2CO_3$  + 1.36 g  $CaCO_3$  + 0.9 g  $C_4H_6O_6$  + 0.8 g  $C_4H_6O_5$  + 0.83 g  $C_6H_8O_7$  L<sup>-1</sup> with the feed water ( $Cl^-$  = 23.22 g L<sup>-1</sup>;  $Na^+$  = 19.83 g L<sup>-1</sup>). The water (2.3 L) was allowed to rest for 24 h at a temperature of 5.2 °C. The product water contained  $Cl^-$  = 0.97 g L<sup>-1</sup>;  $Na^+$  = 3.22 g L<sup>-1</sup>. Removal:  $Cl^-$  = 95.82%;  $Na^+$  = 83.76%.

#### Appendix A.2.4. Fe(b)@Ca(a)@Zn(a)@C<sub>4</sub>H<sub>6</sub>O<sub>6</sub> Polymer

An entrained Fe(b)@Ca(a)@Mn(a)@K@C<sub>4</sub>H<sub>6</sub>O<sub>6</sub> polymer was constructed by mixing 2 g  $FeSO_4$  + 3.34 g  $CaO$  + 11.22 g  $ZnO$  + 0.9 g  $C_4H_6O_6$  L<sup>-1</sup> with the feed water ( $Cl^-$  = 21.11 g L<sup>-1</sup>;

$\text{Na}^+ = 14.43 \text{ g L}^{-1}$ ). The water (2.3 L) was allowed to rest for 96 h at a temperature of 3.8 to 4.6 °C. The product water contained  $\text{Cl}^- = 3.76 \text{ g L}^{-1}$ ;  $\text{Na}^+ = 3.77 \text{ g L}^{-1}$ . Removal:  $\text{Cl}^- = 82.19\%$ ;  $\text{Na}^+ = 73.87\%$ .

A second trial constructed the entrained polymer from 2 g  $\text{FeSO}_4 + 3.34 \text{ g CaO} + 5.61 \text{ ZnO} + 0.9 \text{ g C}_6\text{H}_8\text{O}_7 \text{ L}^{-1}$  + feed water ( $\text{Cl}^- = 26.11 \text{ g L}^{-1}$ ;  $\text{Na}^+ = 19.57 \text{ g L}^{-1}$ ). The water (2.3 L) was allowed to rest for 48 h at a temperature of 8.8 to 10.9 °C. The product water contained  $\text{Cl}^- = 18.10 \text{ g L}^{-1}$ ;  $\text{Na}^+ = 3.75 \text{ g L}^{-1}$ . Removal:  $\text{Cl}^- = 30.67\%$ ;  $\text{Na}^+ = 81.22\%$ . This example demonstrated that the Cl:Na removal selectivity was a function of the ZnO content of the gel.

### Appendix A.3. Manufacture of $\text{M}@\text{C}_6\text{H}_8\text{O}_7$ Polymers

#### Appendix A.3.1. $\text{Fe(b)}@\text{C}_6\text{H}_8\text{O}_7$ polymer

An entrained  $\text{Fe(b)}@\text{C}_6\text{H}_8\text{O}_7$  polymer was constructed by mixing 1 g  $\text{FeSO}_4 + 0.83 \text{ g C}_6\text{H}_8\text{O}_7 \text{ L}^{-1}$  with the feed water ( $\text{Cl}^- = 21.11 \text{ g L}^{-1}$ ;  $\text{Na}^+ = 14.43 \text{ g L}^{-1}$ ). The water (2.3 L) was allowed to rest for 0.1 h at a temperature of 5.1 °C. The product water contained  $\text{Cl}^- = 1.33 \text{ g L}^{-1}$ ;  $\text{Na}^+ = 14.33 \text{ g L}^{-1}$ . Removal:  $\text{Cl}^- = 93.70\%$ ;  $\text{Na}^+ = 0.00\%$ .

#### Appendix A.3.2. $\text{Fe(b)}@\text{Ca(a)}@\text{K}@\text{C}_6\text{H}_8\text{O}_7$ Polymer

An entrained  $\text{Fe(b)}@\text{Ca}@\text{K}@\text{C}_6\text{H}_8\text{O}_7$  polymer was constructed by mixing 1 g  $\text{FeSO}_4 + 1.67 \text{ g CaO} + 1.33 \text{ g CaCO}_3 + 1.22 \text{ g K}_2\text{CO}_3 + 0.83 \text{ g C}_6\text{H}_8\text{O}_7 \text{ L}^{-1}$  with the feed water ( $\text{Cl}^- = 21.11 \text{ g L}^{-1}$ ;  $\text{Na}^+ = 14.43 \text{ g L}^{-1}$ ). The water (2.3 L) was allowed to rest for 0.1 h at a temperature of 5.5 °C. The product water contained  $\text{Cl}^- = 1.29 \text{ g L}^{-1}$ ;  $\text{Na}^+ = 12.82 \text{ g L}^{-1}$ . Removal:  $\text{Cl}^- = 93.89\%$ ;  $\text{Na}^+ = 11.16\%$ .

#### Appendix A.3.3. $\text{Fe(b)}@\text{Ca(a)}@\text{Zn(a)}@\text{C}_6\text{H}_8\text{O}_7$ Polymer

An entrained  $\text{Fe(b)}@\text{Ca(a)}@\text{Zn(a)}@\text{C}_6\text{H}_8\text{O}_7$  polymer was constructed by mixing 2 g  $\text{FeSO}_4 + 3.34 \text{ g CaO} + 11.22 \text{ g ZnO} + 1.60 \text{ g C}_6\text{H}_8\text{O}_7 \text{ L}^{-1}$  with the feed water ( $\text{Cl}^- = 26.40 \text{ g L}^{-1}$ ;  $\text{Na}^+ = 15.83 \text{ g L}^{-1}$ ). The water (2.3 L) was allowed to rest for 24 h at a temperature of 6.4 °C. The product water contained  $\text{Cl}^- = 3.03 \text{ g L}^{-1}$ ;  $\text{Na}^+ = 1.09 \text{ g L}^{-1}$ . Removal:  $\text{Cl}^- = 88.52\%$ ;  $\text{Na}^+ = 93.11\%$ .

A second trial constructed the entrained polymer from 2 g  $\text{FeSO}_4 + 3.34 \text{ g CaO} + 5.60 \text{ g ZnO} + 0.83 \text{ g C}_6\text{H}_8\text{O}_7 \text{ L}^{-1}$  + feed water ( $\text{Cl}^- = 19.94 \text{ g L}^{-1}$ ;  $\text{Na}^+ = 8.47 \text{ g L}^{-1}$ ). The water (2.3 L) was allowed to rest for 24 h at a temperature of 4.8 to 8.2 °C. The product water contained  $\text{Cl}^- = 6.01 \text{ g L}^{-1}$ ;  $\text{Na}^+ = 5.57 \text{ g L}^{-1}$ . Removal:  $\text{Cl}^- = 69.86\%$ ;  $\text{Na}^+ = 34.24\%$ . The removal of both  $\text{Cl}^-$  and  $\text{Na}^+$  ions appear to follow a first-order reaction (Supplementary Information Figure S2b).

#### Appendix A.3.4. $\text{Fe(b)}@\text{Ca(a)}@\text{Mn(a)}@\text{Mg(a)}@\text{Zn(a)}@\text{C}_6\text{H}_8\text{O}_7$ Polymer

An entrained  $\text{Fe(b)}@\text{Ca(a)}@\text{Mn(a)}@\text{Mg(a)}@\text{Zn(a)}@\text{C}_6\text{H}_8\text{O}_7$  polymer was constructed by mixing 2 g  $\text{FeSO}_4 + 3.34 \text{ g CaO} + 2.52 \text{ g MnO}_2 + 5.61 \text{ g ZnO} + 1.48 \text{ g MgCO}_3 + 1.60 \text{ g C}_6\text{H}_8\text{O}_7 \text{ L}^{-1}$  with the feed water ( $\text{Cl}^- = 101.48 \text{ g L}^{-1}$ ;  $\text{Na}^+ = 10.51 \text{ g L}^{-1}$ ). The water (2.3 L) was allowed to rest for 24 h at a temperature of 8.8–10.9 °C. The product water contained  $\text{Cl}^- = 7.27 \text{ g L}^{-1}$ ;  $\text{Na}^+ = 6.46 \text{ g L}^{-1}$ . Removal:  $\text{Cl}^- = 92.83\%$ ;  $\text{Na}^+ = 38.53\%$ .

### Appendix A.4. Manufacture of $@\text{C}_6\text{H}_8\text{O}_7$ Polymers

#### Appendix A.4.1. $\text{Fe(b)}@\text{Ca(a)}@\text{Zn(a)}@\text{C}_2\text{H}_4\text{O}_2$ Polymer

An entrained  $\text{Fe(b)}@\text{Ca(a)}@\text{Zn(a)}@\text{C}_2\text{H}_4\text{O}_2$  polymer was constructed by mixing 2 g  $\text{FeSO}_4 + 3.34 \text{ g CaO} + 5.61 \text{ g ZnO} + 2 \text{ cm}^3 \text{ C}_2\text{H}_4\text{O}_2 \text{ L}^{-1}$  with the feed water ( $\text{Cl}^- = 3.49 \text{ g L}^{-1}$ ;  $\text{Na}^+ = 1.85 \text{ g L}^{-1}$ ). The water (2.3 L) was allowed to rest for 24 h at a temperature of 7.4–8.6 °C. The product water contained  $\text{Cl}^- = 1.39 \text{ g L}^{-1}$ ;  $\text{Na}^+ = 1.60 \text{ g L}^{-1}$ . Removal:  $\text{Cl}^- = 60.17\%$ ;  $\text{Na}^+ = 13.51\%$ .



#### Appendix A.4.2. Fe(b)@C<sub>4</sub>H<sub>6</sub>O<sub>5</sub> Polymer

An entrained Fe(b)@C<sub>4</sub>H<sub>6</sub>O<sub>5</sub> polymer was constructed by mixing 1 g FeSO<sub>4</sub> + 0.8 g C<sub>4</sub>H<sub>6</sub>O<sub>5</sub> L<sup>-1</sup> with the feed water (Cl<sup>-</sup> = 22.11 g L<sup>-1</sup>; Na<sup>+</sup> = 14.43 g L<sup>-1</sup>). The water (2.3 L) was allowed to rest for 0.1 h at a temperature of 4.5 °C. The product water contained Cl<sup>-</sup> = 11.67 g L<sup>-1</sup>; Na<sup>+</sup> = 14.43 g L<sup>-1</sup>. Removal: Cl<sup>-</sup> = 47.21%; Na<sup>+</sup> = 0.00%.

#### Appendix A.4.3. Fe(b)@Ca(a)@K@C<sub>4</sub>H<sub>6</sub>O<sub>5</sub> Polymer

An entrained Fe(b)@Ca(a)@K@C<sub>4</sub>H<sub>6</sub>O<sub>5</sub> polymer was constructed by mixing 1 g FeSO<sub>4</sub> + 1.67 g CaO + 1.22 g K<sub>2</sub>CO<sub>3</sub> + 1.36 g CaCO<sub>3</sub> + 0.8 g C<sub>4</sub>H<sub>6</sub>O<sub>5</sub> L<sup>-1</sup> with the feed water (Cl<sup>-</sup> = 22.11 g L<sup>-1</sup>; Na<sup>+</sup> = 14.43 g L<sup>-1</sup>). The water (2.3 L) was allowed to rest for 0.1 h at a temperature of 4.6 °C. The product water contained Cl<sup>-</sup> = 6.61 g L<sup>-1</sup>; Na<sup>+</sup> = 7.84 g L<sup>-1</sup>. Removal: Cl<sup>-</sup> = 72.41%; Na<sup>+</sup> = 45.68%.

#### Appendix A.4.4. Fe(b)@Ca(a)@Mn(a)@K@C<sub>4</sub>H<sub>6</sub>O<sub>5</sub> Polymer

An entrained Fe(b)@Ca(a)@Mn(a)@K@C<sub>4</sub>H<sub>6</sub>O<sub>5</sub> polymer was constructed by mixing 1 g FeSO<sub>4</sub> + 1.67 g CaO + 2.52 g MnO<sub>2</sub> + 1.22 g K<sub>2</sub>CO<sub>3</sub> + 1.36 g CaCO<sub>3</sub> + 0.8 g C<sub>4</sub>H<sub>6</sub>O<sub>5</sub> L<sup>-1</sup> with the feed water (Cl<sup>-</sup> = 22.11 g L<sup>-1</sup>; Na<sup>+</sup> = 14.43 g L<sup>-1</sup>). The water (2.3 L) was allowed to rest for 96 h at a temperature of 3.8–4.6 °C. The product water contained Cl<sup>-</sup> = 3.76 g L<sup>-1</sup>; Na<sup>+</sup> = 3.77 g L<sup>-1</sup>. Removal: Cl<sup>-</sup> = 82.99%; Na<sup>+</sup> = 73.87%.

#### Appendix A.4.5. Fe(b)@Ca(a)@Zn(a)@C<sub>4</sub>H<sub>6</sub>O<sub>5</sub> Polymer

An entrained Fe(b)@Ca(a)@Zn(a)@C<sub>4</sub>H<sub>6</sub>O<sub>5</sub> polymer was constructed by mixing 1 g FeSO<sub>4</sub> + 3.34 g CaO + 11.22 g ZnO + 0.8 g C<sub>4</sub>H<sub>6</sub>O<sub>5</sub> L<sup>-1</sup> with the feed water (Cl<sup>-</sup> = 19.52 g L<sup>-1</sup>; Na<sup>+</sup> = 13.36 g L<sup>-1</sup>). The water (2.3 L) was allowed to rest for 24 h at a temperature of 6.1 °C. The product water contained Cl<sup>-</sup> = 6.12 g L<sup>-1</sup>; Na<sup>+</sup> = 3.46 g L<sup>-1</sup>. Removal: Cl<sup>-</sup> = 68.45%; Na<sup>+</sup> = 74.10%.

A second trial constructed the entrained polymer from 1 g FeSO<sub>4</sub> + 3.34 g CaO + 5.61 g ZnO + 0.8 g C<sub>4</sub>H<sub>6</sub>O<sub>5</sub> L<sup>-1</sup> with the feed water (Cl<sup>-</sup> = 2.76 g L<sup>-1</sup>; Na<sup>+</sup> = 1.23 g L<sup>-1</sup>). The water (2.3 L) was allowed to rest for 24 h at a temperature of 6.0–6.3 °C. The product water contained Cl<sup>-</sup> = 0.8 g L<sup>-1</sup>; Na<sup>+</sup> = 1.23 g L<sup>-1</sup>. Removal: Cl<sup>-</sup> = 71.01%; Na<sup>+</sup> = 0.00%.

#### Appendix A.5. Manufacture of n-Fe(b)@bluecrop Polyphenol Polymer

Blueberries have previously been used to manufacture nano-scale iron, iron oxides and iron hydroxides, using FeCl<sub>3</sub> as an iron source, which have been used to remediate arsenic [53]. The study observed a reaction process where some of the Fe<sup>3+</sup> ions were reduced to form n-Fe<sup>0</sup> [53].

In this study, the polymer is constructed by mixing crushed blueberry (variety blue crop) juice (with separate extracts constructed from the berries, leaves and stems) with FeSO<sub>4</sub> to produce a polymer (Figure A3). This type of nano-polymer, tends to form as fluid filled, spherical nano-polymer aggregates, which coalesce to form colloidal masses (Figure A3). The central part of the polymer sphere is fluid filled, and may contain hydrogen. The presence of hydrogen may indicate the presence of some n-Fe<sup>0</sup> within the colloids.

Following polymer manufacture, a number of validation tests were undertaken in a static water body (Supplementary Information, Figure S3). These demonstrated three different reaction events:

- An initial first-order desalination reaction, over the initial 10 to 20 h, which removed Na<sup>+</sup> and Cl<sup>-</sup> ions at a slow rate.  $[A] = \ln(C_{t=0})$  or  $[A] < \ln(C_{t=0})$ .
- A first-order desalination reaction, over the period [10 to 300 h], which removed Na<sup>+</sup> and Cl<sup>-</sup> ions at a relatively fast rate.  $[A] > \ln(C_{t=0})$ .
- After 300 h:
  - Berry juice polyphenol: A first-order desalination reaction, over the period [ $>300$  h], which removed Na<sup>+</sup> and Cl<sup>-</sup> ions at a relatively slow rate.  $[A] < \ln(C_{t=0})$ .

- Leaf or stem polyphenol: A first-order desalination reaction, over the period [ $>300$  h], which added  $\text{Na}^+$  and  $\text{Cl}^-$  ions at a relatively slow rate.  $[A] < \ln(C_{t=0})$ .

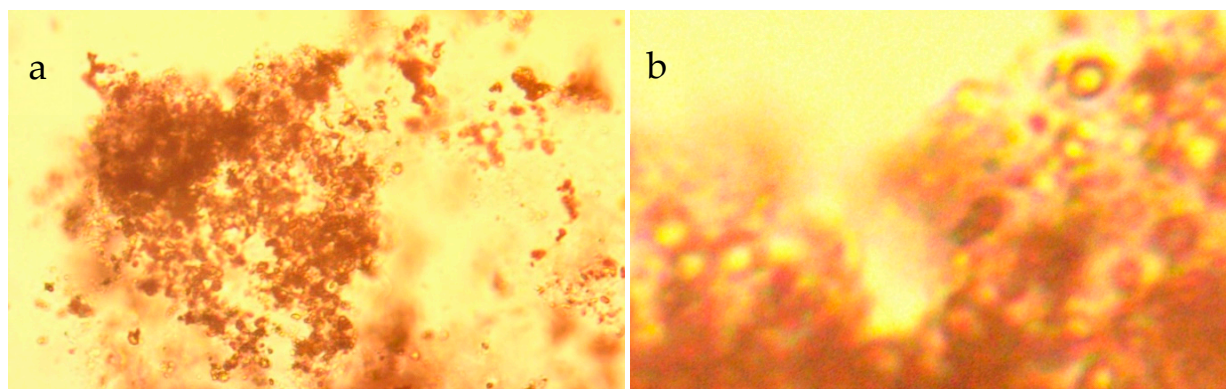


**Figure A3.** n-Fe(b)@bluecrop polyphenol polymer. (a), Agglomerated gel, showing a cellular structure where the gel forms from the aggregation of colloidal spheres. Transmitted light, field of view = 0.26 mm. Manufacture ratio = 1 g  $\text{FeSO}_4$ : 20  $\text{cm}^3$  blueberry (variety: Blue Crop) juice/extract; (b), Enlargement of Agglomerated gel, showing construction from the agglomeration fluid filled polymer spheres. Transmitted light, field of view = 0.04 mm. Individual (pre-aggregation) colloidal sphere sizes: Average = 1.39 microns; standard deviation = 0.50; 1st quartile = 1.07 microns; median = 1.33 microns; 3rd quartile = 1.60 microns;.

#### Appendix A.5.1. n-Fe(b)@bluecrop Polyphenol Polymer Supported on Activated Carbon Pellets

The carbon pellets covered by a supported polymer were constructed by mixing a ratio of: 1 g  $\text{FeSO}_4$ : 20  $\text{cm}^3$  blueberry (variety: Blue Crop) juice/extract: 80  $\text{cm}^3$  water; 50  $\text{cm}^3$  activated carbon pellets. The mixture was left for 7 days, at a temperature of between 3 and 15 °C. The pellets were drained and then air dried, to allow for storage prior to use. The pellets have a high structural porosity (Figure A4). Quality control checks were undertaken for high water salinities (hypersaline, brine) (Supplementary Information Figure S4), medium (seawater range) water salinity (Supplementary Information Figure S5) and low medium (estuarine water range) water salinity (Supplementary Information Figure S6).

These analyses (Supplementary Information Figures S4–S6) demonstrate a number of common features:

- Initially no desalination, or a low level of desalination occurs. Desalination, when present can be described using a first-order reaction where  $[A] = \ln(C_{t=0})$  or  $[A] < \ln(C_{t=0})$ ;
- After a critical time period,  $T_c$ , the pellets start to desalinate the water. The desalination process appears to be a faster first-order reaction where  $[A] > \ln(C_{t=0})$ ;
  - $T_c$  increases with decreasing water salinity;
  - The desalination rate constant decreases with decreasing water salinity;
- After a critical time period,  $T_d$ , the pellets cease desalinating the water.

A number of alternative methods exist for placing n- $\text{Fe}^0$  on a carbon support, using plant (e.g., green tea) derived polyphenols including patents CN109277078A, or unsupported nano-particles (including patents CN104857934B

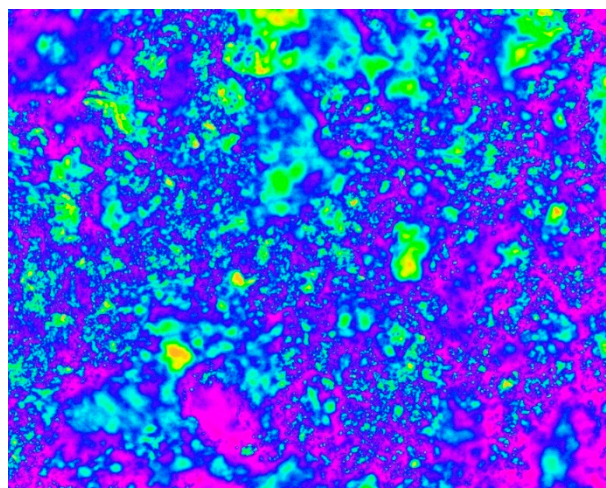


**Figure A4.** Activated carbon pellet (0.5 cm × 1 cm). Polished section, reflected light. Field of view = 1.3 mm, showing activated carbon (purple) separated by porosity (blue, yellow, green).

#### Appendix A.5.2. Comparison of n-Fe(b)@bluecrop Polyphenol Polymer Pellets with m-Fe<sup>0</sup>:n-Fe(b)@n-C<sup>0</sup> Pellets

The cost of manufacturing the n-Fe(b)@bluecrop polyphenol@C<sup>0</sup> polymer desalination pellets, is a fraction of the cost of manufacture of m-Fe<sup>0</sup>:n-Fe(b)@n-C<sup>0</sup> desalination pellets [17]. They appear to offer a faster desalination route, than the m-Fe<sup>0</sup>:n-Fe(b)@n-C<sup>0</sup> polymers [17] (Figure A5).

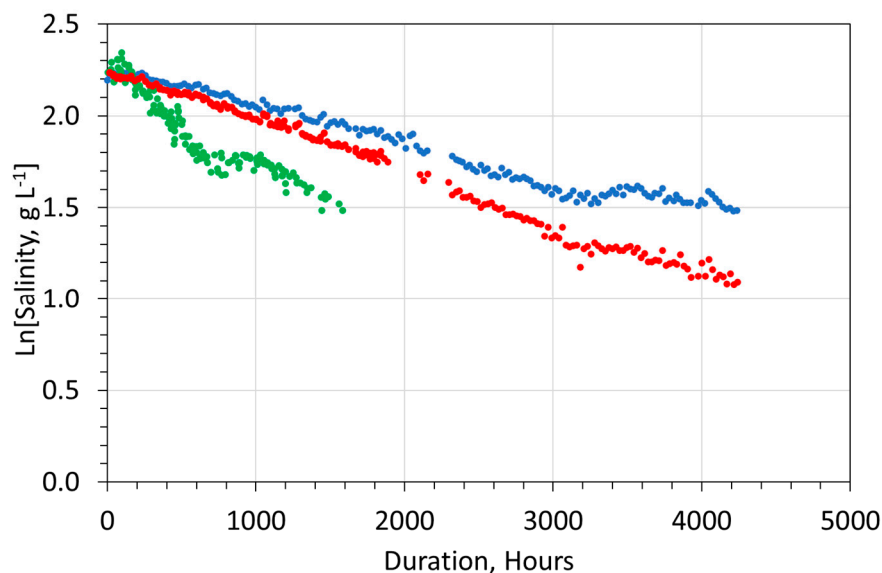


**Figure A5.** Comparison of three different types of desalination pellet: Red markers = m-Fe<sup>0</sup>:n-Fe(b)@n-C<sup>0</sup> polymer, where the n-C<sup>0</sup> is created within the ZVI Reactor during manufacture (Approach A); blue markers = m-Fe<sup>0</sup>:n-Fe(b)@n-C<sup>0</sup> polymer, where the n-C<sup>0</sup> is added to a ZVI Reactor during manufacture (Approach B); green markers = n-Fe(b)@bluecrop polyphenol@C<sup>0</sup> polymer pellets created in this study.

#### Appendix A.6. n-Fe(b)@tomato Polyphenol Polymer

The entrained polymer was constructed by mixing a ratio of: 1 g FeSO<sub>4</sub>: 20 cm<sup>3</sup> tomato leaf extract: 80 cm<sup>3</sup> water;

The analyses demonstrate a number of features:

- Initially no desalination, or a low level of desalination occurs (Supplementary Information, Figure S7);
- After a critical time period,  $T_c$ , the pellets start to desalinate the water.  $T_c$  is about 200 h. The desalination process appears to be a first-order reaction (Supplementary Information Figure S7).

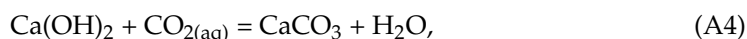
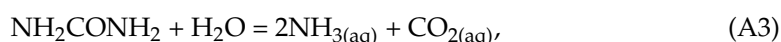
#### Appendix A.7. *n*-Fe(b)@urea Polymers

##### Appendix A.7.1. Activated *n*-Fe(b)@urea@Ca(b) Polymer

Previous CPSAD reactor trials have applied an inactivated *n*-Fe(b)@urea polymer, coating to a steel wool, or quartz support. The polymer is activated during reactor operation by increasing the water pH and oscillating the water pressure applied to the polymer. An activated *n*-Fe(b)@urea@Ca(b) polymer is constructed by mixing  $\text{FeSO}_4$ , urea and  $\text{CaO}$ . An example is provided in Supplementary Information, Figure S8. Both  $\text{Cl}^-$  and  $\text{Na}^+$  ions are removed by a first-order reaction.

##### Appendix A.7.2. Activated *n*-Ca(b)@urea Polymer

An entrained activated *n*-Ca(b)@urea polymer is constructed by mixing urea and  $\text{CaO}$ , and adding the mixture to the saline water. An example is provided in Supplementary Information, Figure S9. The polymer removes both  $\text{Na}^+$  and  $\text{Cl}^-$  ions using a first-order reaction. The polymer forms as framboidal spheres (Figure A6a) constructed from rhombohedral calcite plates (Figure A6b). The framboids aggregate and coalesce to form a network, indicating that they are polar structures (Figure A6a,c). The framboid coatings may form as:



Amorphous (and crystalline) calcium carbonate colloids (ACC) have previously been developed for medicinal purposes [Japanese patent JP7026964B2]. Calcium carbonate colloids can have a trihedral structure (S-PCC), rhombohedral structure (R-PCC), hexagonal column (H-PCC), amorphous colloid (C-PCC), cubic structure (Cu-PCC) or prismatic structure (P-PCC) [Japanese patent JP5866440B2]. Conventionally, calcium carbonate colloids are produced commercially using Equation (A4), where  $\text{CO}_2$  enters the reaction environments as a gas, e.g., [Japanese patent JP5866440B2].

#### Appendix A.8. *n*-Al(b) Polymers

##### Appendix A.8.1. *n*-Al(b)@Mg(a) Polymer

A *n*-Al(b)@Mg(a) polymer was constructed and trialed. It demonstrated, either no reduction in  $\text{Na}^+$  ions, or an initial instant reduction in  $\text{Na}^+$  ions followed by no further reduction, or a first-order reduction in  $\text{Na}^+$  ion concentrations (Supplementary Information, Figures S10 and S11). The  $\text{Cl}^-$  ions consistently demonstrated removal using a first-order reaction (Supplementary Information, Figures S10 and S11).

##### Appendix A.8.2. *n*-Ca(a)@Mn(a)@Al(b) Polymer

An entrained *n*-Ca(a)@Mn(a)@Al(b) polymer was constructed (Supplementary Information, Figure S12). It demonstrated removal of  $\text{Cl}^-$  ions, and minor removal of  $\text{Na}^+$  ions, using a first-order reaction (Supplementary Information, Figure S12).

##### Appendix A.8.3. *n*-Ca(a)@Al(b) Polymer

An entrained *n*-Ca(a)@Al(b) polymer was constructed (Supplementary Information Figure S13a). It demonstrated no removal of  $\text{Na}^+$  ions, and removal of  $\text{Cl}^-$  ions using a first-order reaction (Supplementary Information, Figure S13a).



#### Appendix A.8.4. n-Ca(a)@Zn(a)@Al(b) Polymer

An entrained n-Ca(a)@Zn(a)@Al(b) polymer was constructed (Supplementary Information, Figure S13b–d). It demonstrated an initial drop in  $\text{Na}^+$  and  $\text{Cl}^-$  ion concentrations (Supplementary information, Figure S13b–d), followed by a gradual rise in  $\text{Na}^+$  and  $\text{Cl}^-$  ion concentrations. The reaction order was not defined.

#### Appendix A.8.5. n-Ca(a)@Mg(a)@Al(b) Polymer

An entrained n-Ca(a)@Mg(a)@Al(b) polymer was constructed (Supplementary Information, Figures S14a–c and S15a–c). The polymer indicated that the  $\text{Cl}^-$  ion removal could follow a first-order reaction (Supplementary Information, Figures S14a and S15a,c), or could show an initial high decline, followed by an increase in  $\text{Cl}^-$  ion concentration in the water (Supplementary Information, Figure S14b,c). The  $\text{Na}^+$  ions show either no effective removal, or removal following a first-order reaction (Supplementary Information, Figures S14a–c and S15a–c).

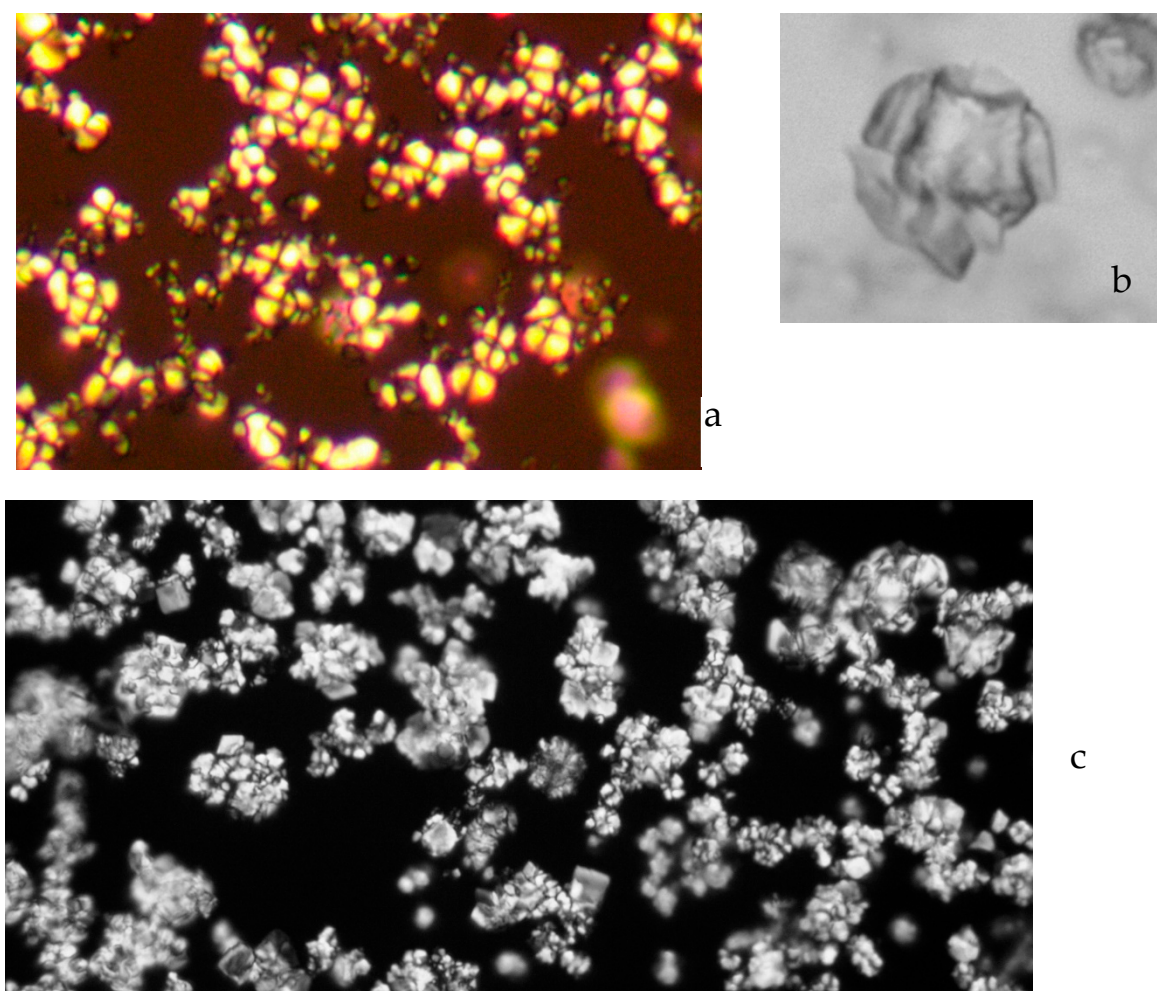


**Figure A6.** Ca(b)@urea polymer colloids with  $\text{CaCO}_3$  or  $\text{CaSO}_4$  outer casing. (a) Framboidal network. Operating conditions: After 48 h: Feed water salinity =  $11.92 \text{ g Cl}^- \text{ L}^{-1} + 5.41 \text{ g Na}^+ \text{ L}^{-1}$ ; Product water salinity =  $4.86 \text{ g Cl}^- \text{ L}^{-1} + 4.27 \text{ g Na}^+ \text{ L}^{-1}$ ; Temperature range:  $14.5$  to  $16.9$  °C; Circular polarised light. Field of view =  $0.1 \text{ mm}$ ; (b) Example polymer framboid. Transmitted light. Field of view =  $0.037 \text{ mm}$ . (c) Framboidal network, operating conditions: After 48 h: Feed water salinity =  $3.07 \text{ g Cl}^- \text{ L}^{-1} + 1.41 \text{ g Na}^+ \text{ L}^{-1}$ ; Product water salinity =  $1.5 \text{ g Cl}^- \text{ L}^{-1} + 1.13 \text{ g Na}^+ \text{ L}^{-1}$ ; Temperature range:  $13.7$  to  $16.2$  °C; Transmitted light. Field of view =  $0.25 \text{ mm}$ .



#### Appendix A.8.6. Mg(a)@K@Al(b) Polymer

An entrained Mg(a)@K@Al(b) polymer was constructed (Supplementary Information, Figures S14d and S15d). It demonstrated a first-order reaction for  $\text{Cl}^-$  removal, coupled with an initial almost instant decline in  $\text{Na}^+$  concentrations.

#### Appendix A.8.7. Mn(a)@Zn(a)@Al(b) Polymer

An entrained Mn(a)@Zn(a)@Al(b) polymer was constructed (Supplementary Information, Figure S16a).  $\text{Cl}^-$  ions were removed preferentially relative to  $\text{Na}^+$  ions. Both ion types were removed by first-order reactions (Supplementary Information, Figure S16a).

#### Appendix A.8.8. Mg(a)@Mn(a)@K@Al(b) Polymer

An entrained Mg(a)@Mn(a)@K@Al(b) polymer was constructed (Supplementary Information, Figure S16b).  $\text{Cl}^-$  ions were removed preferentially relative to  $\text{Na}^+$  ions.  $\text{Na}^+$  ions were removed by a first-order reaction (Supplementary Information, Figure S16b). An almost instantaneous removal of 39% of  $\text{Cl}^-$  ions was followed by a gradual increase in  $\text{Cl}^-$  ion concentration (Supplementary Information, Figure S16b).

#### Appendix A.8.9. Mg(a)@Mn(a)@Al(b) Polymer

An entrained Mg(a)@Mn(a)@Al(b) polymer was constructed (Supplementary information, Figure S16c).  $\text{Cl}^-$  ions were removed preferentially relative to  $\text{Na}^+$  ions.  $\text{Na}^+$  ions were not removed (Supplementary Information, Figure S16c). An almost instantaneous removal of  $\text{Cl}^-$  ions was followed by a gradual increase in  $\text{Cl}^-$  ion concentration (Supplementary Information, Figure S16c).

#### Appendix A.8.10. Zn(a)@Al(b) Polymer

An entrained Zn(a)@Al(b) polymer was constructed (Supplementary Information, Figure S17a–c).  $\text{Cl}^-$  ions were removed preferentially relative to  $\text{Na}^+$  ions. An almost instantaneous removal of  $\text{Na}^+$  and  $\text{Cl}^-$  ions was followed by a gradual increase in  $\text{Na}^+$  and  $\text{Cl}^-$  ion concentration (Supplementary Information, Figure S17a,b). No effective ion removal occurred if the polymer was constructed from ZnO and  $\text{Al}(\text{OH})_3$  (Supplementary Information, Figure S17c).

### Appendix A.9. Fe(b) Polymers

#### Appendix A.9.1. Fe(b)@Ca(a)@Zn(a)@Al(b) Polymer

An entrained Zn(a)Ca(a)@Zn(a)@Al(b) polymer was constructed (Supplementary Information, Figure S17d).  $\text{Cl}^-$  ions were removed preferentially relative to  $\text{Na}^+$  ions. An almost instantaneous removal of  $\text{Cl}^-$  ions was followed by a gradual increase in  $\text{Cl}^-$  ion concentration (Supplementary Information, Figure S17d). No effective  $\text{Na}^+$  ion removal occurred (Supplementary Information, Figure S17d).

#### Appendix A.9.2. Fe(b)@Mg(a)@K@Al(b) Polymer

An entrained Fe(b)@Mg(a)@K@Al(b) polymer was constructed (Supplementary Information, Figure S18a,b). Ion removal follows a first-order removal reaction (Supplementary Information, Figure S18a,b). Increasing the K, results in a decrease in  $\text{Cl}^-$  ion removal (Supplementary Information, Figure S18b), and a preferential removal of  $\text{Na}^+$  ions.

#### Appendix A.9.3. Fe(b)@Mg(a)@Al(b) Polymer

An entrained Fe(b)@Mg(a)@Al(b) polymer was constructed (Supplementary Information, Figure S19a–c). Ion removal follows a first-order removal reaction for  $\text{Na}^+$  ions (Supplementary Information, Figure S19a–c). No  $\text{Cl}^-$  ion removal may occur (Supplementary Information, Figure S19b).

#### Appendix A.9.4. Fe(b)@Mg(a)@Zn(a)@Al(b) Polymer

An entrained Fe(b)@Mg(a)@Zn(a)@Al(b) polymer was constructed (Supplementary Information, Figure S19d). Ion removal follows a first-order removal reaction for Na<sup>+</sup> ions and Cl<sup>−</sup> ions, though Cl<sup>−</sup> ions are removed at a faster rate than Na<sup>+</sup> ions (Supplementary Information, Figure S19d).

#### Appendix A.9.5. Fe(b)@Mg(a)@Ca(a)@Mn(a)@Zn(a)@Al(b) Polymer

An entrained Fe(b)@Mg(a)@Ca(a)@Zn(a)@Al(b) polymer was constructed (Supplementary Information, Figure S20a–c). Ion removal follows a first-order removal reaction for Cl<sup>−</sup> and Na<sup>+</sup> ions (Supplementary Information, Figure S20a–c). No Cl<sup>−</sup> ion removal may occur (Supplementary Information, Figure S20c). The initial ion removal may be almost instantaneous (Supplementary Information, Figure S20a,b).

#### Appendix A.9.6. Fe(b)@Mg(a)@Ca(a)@Al(b) Polymer

An entrained Fe(b)@Mg(a)@Ca(a)@Al(b) polymer was constructed (Supplementary Information, Figure S20d). Ion removal follows a first-order removal reaction for Cl<sup>−</sup> and Na<sup>+</sup> ions (Supplementary Information, Figure S20d).

#### Appendix A.9.7. Fe(b)@Mg(a)@Urea Polymer

An entrained Fe(b)@Mg(a)@Urea polymer was constructed (Supplementary Information, Figure S21a). Ion removal follows a first-order removal reaction for Cl<sup>−</sup> and Na<sup>+</sup> ions (Supplementary Information, Figure S21a).

#### Appendix A.9.8. Fe(b)@Mg(a)@K@Urea Polymer

An entrained Fe(b)@Mg(a)@K@Urea polymer was constructed (Supplementary Information, Figure S21b). Ion removal follows a first-order removal reaction for Cl<sup>−</sup> and Na<sup>+</sup> ions (Supplementary Information, Figure S21b).

#### Appendix A.9.9. Fe(b)@Mg(a) Polymer

An entrained Fe(b)@Mg(a) polymer was constructed (Supplementary Information, Figure S21c). Ion removal follows a first-order removal reaction for Cl<sup>−</sup> and Na<sup>+</sup> ions (Supplementary Information, Figure S21c).

#### Appendix A.9.10. Fe(b) Polymer

An entrained Fe(b) polymer was constructed (Supplementary Information, Figure S21d). Ion removal follows a first-order removal reaction for Cl<sup>−</sup> and Na<sup>+</sup> ions (Supplementary Information, Figure S21d).

#### Appendix A.9.11. Fe(b)@Mg(a)@Ca(a)@K feldspar Polymer

An entrained Fe(b) polymer was constructed (Supplementary Information, Figure S22a). Ion removal follows a first-order removal reaction for Cl<sup>−</sup> and Na<sup>+</sup> ions (Supplementary Information, Figure S22a).

#### Appendix A.9.12. Fe(b)@Mg(a)@Ca(a) Polymer

An entrained Fe(b) polymer was constructed (Supplementary Information, Figure S22b). Ion removal follows a first-order removal reaction for Cl<sup>−</sup> (Supplementary Information, Figure S22b). No effective removal of Na<sup>+</sup> ions was observed.

#### Appendix A.9.13. Fe(b)@Mg(a)@Ca(a)@Zn(a) Polymer

An entrained Fe(b)@Mg(a)@Ca(a)@Zn(a) polymer was constructed (Supplementary Information, Figure S22c). Ion removal follows a first-order removal reaction for Cl<sup>−</sup> and Na<sup>+</sup> ions (Supplementary Information, Figure S22c).

#### Appendix A.9.14. Fe(b)@Mg(a)@Ca(a)@K@Zn(a) Polymer

An entrained Fe(b)@Mg(a)@Ca(a)@K@Zn(a) polymer was constructed (Supplementary Information, Figure S22d). Ion removal follows a first-order removal reaction for  $\text{Cl}^-$  and  $\text{Na}^+$  ions (Supplementary Information, Figure S22d).

#### Appendix A.9.15. Fe(b)@Zn(a) Polymer

An entrained Fe(b)@Zn(a) polymer was constructed (Supplementary Information, Figure S23a,b). Ion removal follows a first-order removal reaction for  $\text{Cl}^-$  ions (Supplementary Information, Figure S23a) and  $\text{Na}^+$  ions (Supplementary Information, Figure S23a,b). At a high  $\text{Cl}^-:\text{Na}^+$  feed water molar ratio,  $\text{Na}^+$  ions are removed and  $\text{Cl}^-$  ions are initially removed before being desorbed back into the water (Supplementary Information, Figure S23b).

#### Appendix A.9.16. Fe(b)@Ca(a)@Al<sup>0</sup>@Zn(a) Polymer

An entrained Fe(b)@Ca(a)@Al<sup>0</sup>@Zn(a) polymer was constructed (Supplementary Information, Figure S23c). Ion removal follows a first-order removal reaction (Supplementary Information, Figure S23c).

#### Appendix A.10. Fe(b)@Ca(a)@gallic Acid Polymers

An entrained Fe(b)@Ca(a)@gallic acid polymer was constructed (Supplementary Information, Figure S24a–c). Ion removal follows a first-order removal reaction (Supplementary Information, Figure S24a–c). Replicate analysis show a similar trend, but with a relatively high outcome variability

### Appendix B. Polymer Manufacture and Operation Tables

**Table A1.** Feed water composition for polymer trials.

Trial	hrs	pH	Eh, mV	T, °C	$\text{Cl}^-$ , g/L	$\text{Na}^+$ , g/L	NaCl, g/L
1	0	8.31	372	4.8	26.55	17.21	43.76
2	0	8.31	372	4.8	26.55	17.21	43.76
3	0	8.31	372	4.8	26.55	17.21	43.76
4	0	8.31	372	4.8	26.55	17.21	43.76
5	0	8.69	39	4.0	22.11	14.43	36.54
6	0	8.69	39	4.0	22.11	14.43	36.54
7	0	8.69	39	4.0	22.11	14.43	36.54
8	0	8.69	39	4.5	22.11	14.43	36.54
9	0	8.69	39	4.6	22.11	14.43	36.54
10	0	8.69	39	4.6	22.11	14.43	36.54
11	0	8.69	39	5.1	22.11	14.43	36.54
12	0	8.69	39	5.5	22.11	14.43	36.54
13	0	8.69	39	4.6	22.11	14.43	36.54
14	0	8.69	39	4.6	22.11	14.43	36.54
15	0	8.57	249	5.2	23.22	19.83	43.05
16	0	8.75	246	6.1	19.52	13.36	32.88
17	0	8.70	233	6.4	26.40	15.83	42.23
18	0	9.33	177	10.6	26.11	19.57	45.68
19	0	9.49	154	10.9	101.48	10.51	111.99
20	0	9.37	265	10.0	47.76	21.49	69.25
21	0	9.17	229	8.7	25.47	23.95	49.42
22	0	9.58	173	7.8	17.40	18.73	36.13
23	0	9.54	228	7.4	19.94	8.47	28.41
24	0	9.51	181	6.9	10.44	6.33	16.77
25	0	9.78	152	6.3	2.76	1.23	3.99
26	0	9.76	144	7.4	3.49	1.85	5.34
27	0	9.54	162	7.6	4.40	1.79	6.19
28	0	9.06	196	12.0	9.40	4.98	14.38

Table A1. Cont.

Trial	hrs	pH	Eh, mV	T, °C	Cl <sup>−</sup> , g/L	Na <sup>+</sup> , g/L	NaCl, g/L
29	0	9.05	215	9.1	12.14	3.13	15.27
30	0	8.69	255	9.2	22.11	14.33	36.44
31	0	8.69	255	9.2	22.11	14.33	36.44
32	0	8.69	255	9.2	22.11	14.33	36.44
33	0	8.81	344	12.5	30.14	18.38	48.52
34	0	8.81	344	12.5	30.14	18.38	48.52
35	0	8.81	344	12.5	30.14	18.38	48.52
36	0	10.35	84	15.0	11.92	5.41	17.33
37	0	10.42	74	13.7	3.07	1.41	4.48
38	0	9.07	159	11.6	8.14	4.31	12.45
39	0	8.56	289	13.8	30.47	10.30	40.77
40	0	8.56	289	13.8	30.47	10.30	40.77
41	0	8.55	259	13.8	25.36	16.44	41.80
42	0	10.31	81	13.8	14.50	9.99	24.49
43	0	10.17	85	13.8	14.50	9.99	24.49
44	0	9.13	155	14.1	1.22	1.52	2.74
45	0	9.86	187	13.9	10.57	10.10	20.67
46	0	8.64	303	13.7	57.04	45.57	102.61
47	0	11.35	36	18.4	2.19	7.01	9.20
48	0	12.06	−301	18.1	33.17	19.96	53.13
49	0	12.68	−474	16.3	11.54	16.77	28.31
50	0	12.68	−474	16.3	11.54	16.77	28.31
51	0	9.78	172	16.8	24.72	19.50	44.22
52	0	10.67	72	17.2	1.48	0.70	2.18
53	0	9.91	166	18.2	2.06	1.53	3.59
54	0	9.96	201	17.3	19.50	14.75	34.25
55	0	9.96	201	17.3	19.50	14.75	34.25
56	0	9.53	226	17.5	57.26	44.14	101.40
57	0	9.53	226	17.5	57.26	44.14	101.40
58	0	8.86	274	14.5	19.17	9.76	28.93
59	0	8.86	274	15.5	19.17	9.76	28.93
60	0	8.29	326	16.3	1.24	0.82	2.06
61	0	8.29	326	16.3	1.24	0.82	2.06
62	0	8.49	360	14.6	24.67	13.23	37.90
63	0	8.49	360	14.6	24.67	13.23	37.90
64	0	8.13	405	15.2	19.30	11.18	30.48
65	0	8.13	405	15.2	19.30	11.18	30.48
66	0	9.80	194	14.2	49.31	15.40	64.71
67	0	9.80	194	14.2	49.31	15.40	64.71
68	0	8.84	317	15.2	21.87	17.74	39.61
69	0	8.84	317	15.2	21.87	17.74	39.61
70	0	8.72	321	17.2	14.50	16.04	30.54
71	0	8.72	321	17.2	14.50	16.04	30.54
72	0	8.68	308	14.2	28.10	14.73	42.83
73	0	8.68	308	14.2	28.10	14.73	42.83
74	0	9.60	230	15.2	10.92	7.57	18.49
75	0	9.60	230	15.2	10.92	7.57	18.49
76	0	8.96	297	14.9	6.41	3.96	10.37
77	0	8.96	297	14.9	6.41	3.96	10.37
78	0	8.92	343	15.7	10.59	9.47	20.06
79	0	8.92	343	15.7	10.59	9.47	20.06
80	0	9.06	423	15.6	11.48	15.61	27.09
81	0	9.06	423	15.6	11.48	15.61	27.09
82	0	9.79	360	16.0	9.60	7.54	17.14
83	0	9.79	360	16.0	9.60	7.54	17.14
84	0	9.67	361	17.9	9.68	9.50	19.18
85	0	9.67	361	17.9	9.68	9.50	19.18
86	0	9.80	347	16.8	7.96	7.74	15.70
87	0	9.80	347	16.8	7.96	7.74	15.70

**Table A2.** Product water composition for polymer trials.

Trial	hrs	pH	Eh, mV	T, °C	Product			Removed		
					Cl <sup>−</sup> , g/L	Na <sup>+</sup> , g/L	NaCl, g/L	Cl <sup>−</sup>	Na <sup>+</sup>	NaCl
1	241	11.85	−45	7.0	1.35	0.78	2.13	94.92%	95.47%	95.13%
2	241	12.23	−74	7.0	5.66	2.97	8.63	78.68%	82.74%	80.28%
3	241	9.31	193	7.0	1.55	8.75	10.30	94.16%	49.16%	76.46%
4	241	12.54	−98	7.0	9.64	2.50	12.14	63.69%	85.47%	72.26%
5	0.1	2.9	868	3.8	1.51	14.43	15.94	93.17%	0.00%	56.38%
6	0.1	6.2	24	4.3	1.93	12.07	14.00	91.27%	16.35%	61.69%
7	216	9.37	172	7.1	1.04	5.93	6.97	95.30%	58.91%	80.93%
8	0.1	3.42	805	4.5	11.67	14.43	26.10	47.22%	0.00%	28.57%
9	0.1	6.91	29	4.6	6.61	7.84	14.45	70.10%	45.67%	60.45%
10	216	10.11	61	7.1	1.00	3.25	4.25	95.48%	77.48%	88.37%
11	0.1	3.83	723	5.1	1.33	14.33	15.66	93.98%	0.69%	57.14%
12	0.1	6.57	117	5.5	1.29	12.82	14.11	94.17%	11.16%	61.38%
13	216	10.34	37	7.1	1.99	3.18	5.17	91.00%	77.96%	85.85%
14	96	11.18	26	3.8	3.76	3.77	7.53	82.99%	73.87%	79.39%
15	24	12.28	−103	5.2	0.97	3.32	4.29	95.82%	83.26%	90.03%
16	24	12.16	−98	6.1	6.12	3.46	9.58	68.65%	74.10%	70.86%
17	24	12.15	−345	6.4	3.03	1.09	4.12	88.52%	93.11%	90.24%
18	48	11.96	−26	7.8	18.10	3.75	21.85	30.68%	80.84%	52.17%
19	24	9.91	284	8.8	7.27	6.46	13.73	92.84%	38.53%	87.74%
20	24	12.33	−45	8.4	9.15	9.42	18.57	80.84%	56.17%	73.18%
21	24	11.72	−35	10.7	25.18	9.00	34.18	1.14%	62.42%	30.84%
22	24	11.22	63	6.1	8.71	9.37	18.08	49.94%	49.97%	49.96%
23	24	13.1	−81	4.8	6.01	5.57	11.58	69.86%	34.24%	59.24%
24	24	11.87	−4	4.1	4.51	4.91	9.42	56.80%	22.43%	43.83%
25	24	13.08	−80	6.0	0.80	1.23	2.03	71.01%	0.00%	49.12%
26	24	12.42	−37	8.6	1.39	1.60	2.99	60.17%	13.51%	44.01%
27	24	12.51	−23	8.3	2.32	1.74	4.06	47.27%	2.79%	34.41%
28	24	12.82	−77	11.1	5.86	3.30	9.16	37.66%	33.73%	36.30%
29	24	12.87	−66	9.2	6.50	3.13	9.63	46.46%	0.00%	36.94%
30	1344	7.97	354	6.2	1.34	6.65	7.99	93.94%	53.59%	78.07%
31	1344	8.66	282	6.2	2.32	3.76	6.08	89.51%	73.76%	83.32%
32	1398	9.62	184	6.2	2.93	3.29	6.22	86.75%	77.04%	82.93%
33	0.08	6.19	326	12.3	12.46	18.38	30.84	58.66%	0.00%	36.44%
34	0.08	6.61	170	12.3	24.67	11.38	36.05	18.15%	38.08%	25.70%
35	72	12.96	−131	16.4	9.43	11.22	20.65	68.71%	38.96%	57.44%
36	48	13.07	−139	14.5	4.86	4.27	9.13	59.23%	21.07%	47.32%
37	48	12.36	−104	14.2	1.50	1.13	2.63	51.14%	19.86%	41.29%
38	48	7.17	153	15.7	5.22	2.06	7.28	35.87%	52.20%	41.53%
39	24	7.34	13	14.3	30.47	6.78	37.25	0.00%	34.17%	8.63%
40	24	7.35	88	14.3	23.49	6.58	30.07	22.91%	36.12%	26.24%
41	96	11.98	−71	15.0	13.35	13.95	27.30	47.36%	15.15%	34.69%
42	96	12.75	−111.6	15.0	7.36	8.65	16.01	49.24%	13.41%	34.63%
43	24	12.78	−108.6	14.2	7.34	9.36	16.70	49.38%	6.31%	31.81%
44	24	10.49	126.8	15.1	0.64	0.92	1.56	47.54%	39.47%	43.07%
45	72	11.35	36.3	18.4	2.19	7.01	9.20	79.28%	30.59%	55.49%
46	72	12.06	−301.3	18.1	33.17	19.96	53.13	41.85%	56.20%	48.22%
47	48	6.77	158.1	18.1	0.23	5.48	5.71	89.50%	21.83%	37.93%
48	24	6.51	175.2	16.3	13.38	11.78	25.16	59.66%	40.98%	52.64%
49	24	9.23	236.6	17.2	10.36	15.29	25.65	10.23%	8.83%	9.40%
50	24	10.58	107.9	17.5	9.13	14.28	23.41	20.88%	14.85%	17.31%
51	72	12.41	−71.3	18.6	0.21	13.99	14.20	99.15%	28.26%	67.89%
52	24	11.47	35.5	19.5	0.17	0.68	0.85	88.51%	2.86%	61.01%
53	24	10.31	187.6	19.3	1.35	1.19	2.54	34.47%	22.22%	29.25%
54	24	9.58	211.6	17.6	10.97	11.31	22.28	43.74%	23.32%	34.95%
55	24	10.13	158.5	17.8	12.16	8.35	20.51	37.64%	43.39%	40.12%
56	24	6.11	593.4	15.6	26.66	37.97	64.63	53.44%	13.98%	36.26%



Table A2. Cont.

Trial	hrs	pH	Eh, mV	T, °C	Product			Removed		
					Cl <sup>−</sup> , g/L	Na <sup>+</sup> , g/L	NaCl, g/L	Cl <sup>−</sup>	Na <sup>+</sup>	NaCl
57	24	12.55	−30.5	15.7	41.19	26.95	68.14	28.06%	38.94%	32.80%
58	24	5.51	655.8	15.4	11.61	5.19	16.80	39.44%	46.82%	41.93%
59	24	6.55	555.6	15.7	7.87	4.34	12.21	58.95%	55.53%	57.79%
60	24	8.12	368.5	14.2	0.76	0.26	1.02	38.71%	68.29%	50.49%
61	24	9.1	294.1	13.3	0.67	0.23	0.90	45.97%	71.95%	56.31%
62	48	7.46	469.8	14.2	18.86	11.25	30.11	23.55%	14.97%	20.55%
63	48	7.56	461.2	14.3	22.60	8.56	31.16	8.39%	35.30%	17.78%
64	72	6.68	529	14.4	14.88	9.73	24.61	22.90%	12.97%	19.26%
65	72	12.86	−61.8	14.4	9.60	10.56	20.16	50.26%	5.55%	33.86%
66	24	8.92	329.9	15.3	44.17	15.11	59.28	10.42%	1.88%	8.39%
67	24	8.89	334.9	15.4	47.47	14.85	62.32	3.73%	3.57%	3.69%
68	24	5.42	686.8	16.3	9.33	17.74	27.07	57.34%	0.00%	31.66%
69	24	11.12	186.5	16.4	7.32	14.99	22.31	66.53%	15.50%	43.68%
70	24	5.64	625.3	16.6	10.88	14.22	25.10	24.97%	11.35%	17.81%
71	24	12.68	−8	16.6	7.12	11.95	19.07	50.90%	25.50%	37.56%
72	24	6.34	458.3	15.4	22.86	14.28	37.14	18.65%	3.05%	13.29%
73	24	12.92	−41.7	15.6	19.61	14.12	33.73	30.21%	4.14%	21.25%
74	96	7.12	−67.9	14.6	10.92	5.91	16.83	0.00%	21.93%	8.98%
75	96	12.69	−635.6	14.9	4.58	5.64	10.22	58.06%	25.50%	44.73%
76	24	7.83	415.5	14.4	4.69	3.85	8.54	26.83%	2.78%	17.65%
77	24	12.27	57.9	14.5	2.30	3.68	5.98	64.12%	7.07%	42.33%
78	24	7.43	75.8	14.7	10.59	8.84	19.43	0.00%	6.65%	3.14%
79	24	7.45	162.5	14.8	6.66	7.12	13.78	37.11%	24.82%	31.31%
80	24	7.41	84.1	16.2	10.94	13.70	24.64	4.70%	12.24%	9.04%
81	24	9.69	−3.6	16.5	10.57	9.06	19.63	7.93%	41.96%	27.54%
82	24	9.49	378.5	17.0	7.34	6.86	14.20	23.54%	9.02%	17.15%
83	24	10.37	297.7	17.1	7.19	6.85	14.04	25.10%	9.15%	18.09%
84	24	9.54	364.2	19.0	6.79	8.81	15.60	29.86%	7.26%	18.67%
85	24	10.26	280.9	19.0	6.85	8.80	15.65	29.24%	7.37%	18.40%
86	24	9.13	385.1	17.5	5.66	7.43	13.09	28.89%	4.01%	16.62%
87	24	10.53	239.2	17.5	5.39	7.74	13.13	32.29%	0.00%	16.37%

**Table A3.** Inorganic polymer ingredients: Inorganic solutes, g/L; 1 = FeSO<sub>4</sub>; 2 = MgSO<sub>4</sub>; 3 = Al<sup>0</sup>; 4 = CaO; 5 = MnO<sub>2</sub>; 6 = MgCO<sub>3</sub>; 7 = K<sub>2</sub>CO<sub>3</sub>; 8 = CaCO<sub>3</sub>; 9 = ZnO; 10 = Al<sub>2</sub>O<sub>3</sub>; 11 = K-Feldspar; 12 = Al<sub>2</sub>(SO<sub>4</sub>)<sub>3</sub>; 13 = Al(OH)<sub>3</sub>.

Trial	1	2	3	4	5	6	7	8	9	10	11	12	13
1	1			1.67	2.52								
2	1			1.67	2.52		1.22						
3	1			1.67	2.52	2.96							
4	1			3.34	2.52								
5	1												
6	1			1.67			1.22	1.36					
7	1			3.34	2.52		1.22	1.36					
8	1												
9	1			1.67			1.22	1.36					
10	1			1.67	2.52		1.22	2.71					
11	1												
12	1			1.67			1.22	1.36					
13	1			1.67	2.52		1.22	4.07					
14	1			1.67	2.52		1.22	1.36					
15	2			3.34					11.22				
16	2			3.34					11.22				
17	2			3.34					11.22				

Table A3. Cont.

Trial	1	2	3	4	5	6	7	8	9	10	11	12	13
18	2			3.34					5.61				
19	2			3.34					5.61				
20	2			3.34				2.71	5.61				
21	2			3.34	2.52	1.48		2.71	2.81				
22	2			3.34	2.52	1.48		2.71	5.61				
23	2			3.34					5.61				
24	2			3.34					5.61				
25	2			3.34					5.61				
26	2			3.34					5.61				
27	2			3.34					5.61				
28	2			3.34									
29	1			1.67									
30	0.69			3.34	2.52	1.48	0.61						
31	0.8			3.34	2.52								
32	0.8			3.34				2.71					
33	1.42			3.34									
34	1.42			1.67									
35	1.42			3.34									
36				3.34									
37				3.34									
38	1.42								5.61				
39	1.42								5.61				
40	1.42		1.36	3.34					8.42				
41				1.67	2.52					1.99			
42				1.67	2.52					1.99			
43				1.67						1.99			
44		1.51					1.22			1.99			
45	1.42	1.51		1.67					2.81	1.99			
46	1.42	0.76		1.67			1.22		2.81				
47	1.42												
48	1.42												
49	1.42	1.51											
50	1.42	1.51					1.22						
51	2.84	1.51		3.34				2.71			2.5		
52	5.68	1.51		1.67									
53		1.51											1.2
54		3.02											2.4
55		3.02		1.67									3.6
56		1.51										1.34	1.2
57		1.51		1.67								1.34	1.2
58		3.02										1.34	2.4
59		3.02		1.67								1.34	2.4
60	1.42	3.02		1.67	2.52			1.36	2.81			1.34	3.6
61	1.42	3.02		3.34	2.52			1.36	2.81			1.34	3.6
62									2.81			1.34	1.2
63				1.67					2.81			1.34	1.2
64									4.22			2	1.8
65				3.34					4.22			2	1.8
66				1.67				1.36	2.81			1.34	1.2
67									2.81			0	1.2
68		1.51										1.34	1.2
69		1.51		1.67								1.34	1.2
70		1.51										1.34	1.2
71		1.51		1.67								1.34	1.2
72		1.51										1.34	1.2
73		1.51		1.67								1.34	1.2
74	1.42	1.51										0	1.2
75	1.42	1.51		1.67								0	1.2

Table A3. Cont.

Trial	1	2	3	4	5	6	7	8	9	10	11	12	13
76	1.42	1.51							2.81			1.34	0
77	1.42	1.51		1.67				1.36	2.81			1.34	1.2
78	1.42	1.51											1.2
79	1.42	1.51					1.22						1.2
80	1.42	1.51											1.2
81	1.42	1.51					3.66						1.2
82		2.27											1.2
83		2.27					1.22						1.2
84		1.51			2.52								1.2
85		1.51			2.52		3.66						1.2
86					2.52				2.81			1.34	
87	1.42			1.67					2.81			1.34	

Table A4. Organic Polymer Ingredients: powders = g L<sup>-1</sup>; Formic acid = 40%, cm<sup>3</sup> L<sup>-1</sup>; Acetic acid = glacial cm<sup>3</sup> L<sup>-1</sup>; Tea = polyphenol extract from black tea, g L<sup>-1</sup>

Trial	Formic Acid	Acetic Acid	Malic Acid	Citric Acid	Tartaric Acid	Tea (Gallic Acid)	Urea
1	1						
2	1						
3	1						
4	1						
5					0.9		
6					0.9		
7	1				0.9		
8			0.8				
9			0.8				
10	1		0.8				
11				0.83			
12				0.83			
13	1			0.83			
14			0.8	0.83	0.9		
15					0.9		
16			0.8				
17				1.67			
18					1.79		
19				0.83			
20							
21	2						
22							
23				0.83			
24	1						
25			0.8				
26		2					
27							
28							
29							
30						0.94	
31						0.94	
32						0.94	
33							1.32
34							1.32
35							1.32
36							1.32
37							1.32
38							
39							

Table A4. Cont.

Trial	Formic Acid	Acetic Acid	Malic Acid	Citric Acid	Tartaric Acid	Tea (Gallic Acid)	Urea
40							
41							
42							
43							
44							
45							
46							
47							
48							1.32
49							
50							1.32

**Table A5.** Measured values of [a], [b], and  $R^2$  associated with ion removal in Trials 1 to 87, Table A1, Table A2, Table A3, and Table A4. Values calculated from a regression plot of  $k_{obs}$  vs. reaction time (hours). ( $t = n$ ) = time spent in the reaction environment, seconds. n/a = not applicable; PPC = Pearson correlation coefficient.

Trial	Cl <sup>−</sup>				Na <sup>+</sup>			
	[a]	[b]	$R^2$	PPC	[a]	[b]	$R^2$	PPC
1	0.00004980	−0.4236	0.918	0.958	0.00023480	−1.05551	0.842	0.918
2	0.00003149	−0.4312	0.732	0.856	0.00015187	−0.92883	0.906	0.952
3	0.00017958	−0.7637	0.990	0.995	0.00014111	−0.94756	0.996	0.998
4	0.00013545	−0.7804	0.975	0.987	0.00021644	−0.88604	0.955	0.977
5	n/a	n/a	n/a	n/a	n/a	n/a	n/a	n/a
6	n/a	n/a	n/a	n/a	n/a	n/a	n/a	n/a
7	0.00065307	−0.9610	0.985	0.992	0.00018974	−0.96922	0.999	0.999
8	n/a	n/a	n/a	n/a	n/a	n/a	n/a	n/a
9	n/a	n/a	n/a	n/a	n/a	n/a	n/a	n/a
10	0.00062608	−0.9715	0.996	0.998	0.00008924	−0.85519	0.968	0.984
11	n/a	n/a	n/a	n/a	n/a	n/a	n/a	n/a
12	n/a	n/a	n/a	n/a	n/a	n/a	n/a	n/a
13	0.00100064	−1.0372	0.998	0.999	0.00013866	−0.85425	0.971	0.985
14	0.00008985	−0.7902	0.935	0.967	0.00020695	−0.86526	1.000	1.000
15	0.00028994	−0.7276	0.963	0.981	0.00037814	−0.86185	0.988	0.994
16	0.00004954	−0.6694	0.665	0.816	0.00036220	−0.92115	0.982	0.991
17	0.00042454	−0.8737	0.999	0.999	0.00060368	−0.91001	0.997	0.998
18	0.00011063	−1.0061	1.000	1.000	0.00022458	−0.91708	0.982	0.991
19	0.00014622	−0.5851	0.876	0.936	0.00013026	−0.88899	0.933	0.966
20	0.00011476	−0.5061	0.931	0.965	0.00020437	−0.94213	0.997	0.998
21	0.00004542	−0.4884	0.862	0.928	0.00028932	−0.92967	0.974	0.987
22	0.00003102	−0.3341	0.463	0.680	0.00012206	−0.89222	0.997	0.998
23	0.00023506	−0.8838	0.962	0.981	0.00005493	−0.87502	0.964	0.982
24	0.00028050	−0.8072	0.970	0.985	0.00003633	−0.33088	0.718	0.847
25	0.00021541	−0.7717	0.969	0.985	0.00000998	−1.69972	1.000	1.000
26	0.00022242	−0.9562	0.999	0.999	0.00004715	−0.93281	0.920	0.959
27	0.00008986	−0.7856	1.000	1.000	n/a	n/a	n/a	n/a
28	0.00012054	−0.9842	0.999	1.000	0.00008506	−0.92801	0.997	0.998
29	0.00016821	−0.9867	0.999	0.999	0.00000387	−1.61133	1.000	1.000
30	0.00004453	−0.6028	1.000	1.000	0.00287146	−1.36095	1.000	1.000
31	0.00000022	0.1043	1.000	1.000	n/a	n/a	n/a	n/a
32	0.00002082	−0.5451	1.000	1.000	n/a	n/a	n/a	n/a
33	n/a	n/a	n/a	n/a	n/a	n/a	n/a	n/a
34	n/a	n/a	n/a	n/a	n/a	n/a	n/a	n/a
35	0.00027845	−0.9542	0.954	0.977	0.00013306	−1.01025	1.000	1.000
36	0.00016647	−0.8917	1.000	1.000	0.00000137	−0.15570	1.000	1.000

Table A5. Cont.

Cl <sup>−</sup>					Na <sup>+</sup>			
Trial	[a]	[b]	R <sup>2</sup>	PPC	[a]	[b]	R <sup>2</sup>	PPC
37	0.00013302	−0.8999	0.999	0.999	0.00001813	−0.69694	0.999	0.999
38	0.00006524	−0.8094	0.990	0.995	0.00012418	−0.88951	0.999	0.999
39	0.00002758	−1.1817	1.000	1.000	0.00007301	−0.86425	0.999	0.999
40	0.00012969	−1.1434	0.994	0.997	0.00009155	−0.93490	0.995	0.997
41	0.00012274	−0.8943	0.996	0.998	0.00001469	−0.75229	1.000	1.000
42	0.00011897	−0.8951	0.999	1.000	0.00000002	0.61712	1.000	1.000
43	0.00012533	−0.8612	0.999	1.000	n/a	n/a	n/a	n/a
44	0.00000394	0.2002	1.000	1.000	0.00014470	−1.00597	1.000	1.000
45	0.00035246	−0.9451	1.000	1.000	0.00012584	−1.03805	0.999	0.999
46	0.00017440	−0.9769	0.995	0.997	0.00016058	−0.96516	0.996	0.998
47	0.00030808	−0.9051	0.987	0.994	0.00002837	−0.86593	0.985	0.992
48	0.00018884	−0.8827	0.996	0.998	0.00003072	−0.46577	0.962	0.981
49	n/a	n/a	n/a	n/a	0.00002289	−0.96488	1.000	1.000
50	0.00006452	−0.9979	1.000	1.000	0.00004202	−0.98071	1.000	1.000
51	0.00021200	−0.7400	0.778	0.882	0.00002835	−0.76823	0.984	0.992
52	0.00031988	−0.7421	0.967	0.983	0.00007991	−1.71288	1.000	1.000
53	0.00010941	−0.9289	0.987	0.993	0.00010748	−1.11038	0.998	0.999
54	0.00010665	−0.8374	0.992	0.996	0.00005539	−0.90984	1.000	1.000
55	0.00011384	−0.9658	0.999	1.000	0.00010375	−0.89297	0.996	0.998
56	0.00013233	−0.8722	0.997	0.999	0.00001208	−0.61099	1.000	1.000
57	0.00013563	−1.0919	0.996	0.998	0.00010545	−0.97158	0.986	0.993
58	0.00021719	−1.1093	0.997	0.998	n/a	n/a	n/a	n/a
59	0.00020969	−0.9204	0.996	0.998	0.00009402	−0.72548	1.000	1.000
60	0.00014835	−1.0751	0.992	0.996	0.00026394	−0.93524	1.000	1.000
61	0.00018920	−1.0488	0.999	0.999	0.00032635	−0.97755	1.000	1.000
62	0.00010253	−1.4081	0.905	0.952	0.00007970	−1.14889	1.000	1.000
63	0.00011499	−1.2897	0.989	0.994	0.00011197	−1.05830	0.991	0.995
64	0.00008288	−0.8907	0.959	0.979	0.00003477	−1.06312	0.945	0.972
65	0.00026005	−1.0435	0.999	1.000	0.00001502	−0.84279	0.922	0.960
66	0.00004073	−1.3033	0.888	0.942	0.00002833	−1.41765	0.972	0.986
67	0.00000697	−1.0130	0.914	0.956	0.00003494	−1.29302	0.974	0.987
68	0.00012969	−0.7576	0.977	0.988	n/a	n/a	n/a	n/a
69	0.00018281	−0.7875	0.979	0.990	0.00006728	−1.10058	0.999	0.999
70	0.00010252	−1.0152	0.982	0.991	0.00004124	−1.07313	1.000	1.000
71	0.00021541	−1.0602	0.995	0.998	0.00002797	−0.50468	0.682	0.826
72	0.00005290	−0.9648	1.000	1.000	0.00001498	−1.17100	1.000	1.000
73	0.00013789	−1.1211	0.999	0.999	0.00000739	−1.00488	0.899	0.948
74	0.00008728	−1.0597	0.998	0.999	0.00000864	−0.54435	1.000	1.000
75	0.00025650	−1.0282	1.000	1.000	0.00000211	−0.17304	0.872	0.934
76	0.00001435	−0.4328	1.000	1.000	n/a	n/a	n/a	n/a
77	0.00023930	−0.9511	1.000	1.000	n/a	n/a	n/a	n/a
78	n/a	n/a	n/a		0.00002120	−0.99668	0.994	0.997
79	0.00013118	−1.0060	1.000	1.000	0.00007453	−0.97234	1.000	1.000
80	0.00002086	−0.9102	0.760	0.872	0.00001505	−0.72404	1.000	1.000
81	0.00003655	−1.1122	0.995	0.998	0.00013304	−0.96749	1.000	1.000
82	0.00003131	−0.7526	0.995	0.997	0.00002059	−0.91397	0.999	0.999
83	0.00003074	−0.7632	0.966	0.983	0.00005497	−1.18850	0.995	0.997
84	0.00011783	−1.0472	1.000	1.000	0.00001430	−0.87934	1.000	1.000
85	0.00011954	−1.0602	1.000	1.000	0.00000510	−0.50974	0.972	0.986
86	0.00006956	−0.9105	1.000	1.000	n/a	n/a	n/a	n/a
87	0.00011565	−1.0153	1.000	1.000	0.00000258	−0.79701	1.000	1.000



**Table A6.** Example Water Analyses for Fe(a,b,c)@Ca@HCOOH Polymers which showed no effective desalination after 24 h.

Trial	hrs	pH	Eh, mV	T °C	Cl <sup>-</sup> , g/L	Na <sup>+</sup> g/L	hrs	pH	Eh, mV	T °C	Cl <sup>-</sup> , g/L	Na <sup>+</sup> g/L
1	0	8.69	255	9.2	22.11	14.43	2880	7.94	362	14.8	12.16	3.67
2	0	8.69	255	9.2	22.11	14.43	2880	6.62	461	14.2	20.54	6.18
3	0	8.69	255	9.2	22.11	14.43	2880	7.58	406	14.3	22.11	8.68
4	0	8.69	255	9.2	22.11	14.43	2880	8.01	376	14.2	2.28	0.67
5	0	8.69	255	9.2	22.11	14.43	2880	8.99	285	14.2	7.36	3.50
6	0	8.69	255	9.2	22.11	14.43	2880	8.21	341	14.2	22.11	7.05
7	0	8.69	255	9.2	22.11	14.43	2880	8.15	361	14.9	22.11	7.75
8	0	8.69	255	9.2	22.11	14.43	2880	8.11	366	15.3	21.80	13.84
9	0	8.69	255	9.2	22.11	14.43	2880	7.98	382	14.9	22.11	11.78

**Table A7.** Impact of dilution with fresh water on the stored water described in Table A6. Dilution is 1-part stored water + 5-parts fresh water. Product water analyses made 24 h after dilution. Percentages indicate the total ion removal, relative to diluted seawater.

Trial	hrs	Cl <sup>-</sup> , g/L	Na <sup>+</sup> g/L	hrs	pH	Eh, mV	T °C	Cl <sup>-</sup> , g/L	Na <sup>+</sup> g/L	Cl <sup>-</sup>	Na <sup>+</sup>
1	2880	2.03	0.61	2904	8.33	359	13.1	0.82	0.49	77.8%	79.7%
2	2880	3.42	1.03	2904	8.32	357	13.2	1.57	0.73	57.4%	69.6%
3	2880	3.69	1.45	2904	8.34	355	13.4	2.03	1.06	44.8%	55.9%
4	2880	0.38	0.11	2904	8.63	339	13.4	0.19	0.11	95.0%	95.4%
5	2880	1.23	0.58	2904	8.76	326	13.6	0.66	0.53	82.0%	78.0%
6	2880	3.69	1.18	2904	8.43	353	13.4	1.99	1.18	46.0%	50.9%
7	2880	3.69	1.29	2904	8.55	348	13.6	2.30	0.83	37.6%	65.4%
8	2880	3.63	2.31	2904	8.44	365	13.8	2.03	0.83	44.8%	65.4%
9	2880	3.69	1.96	2904	8.36	371	13.9	3.10	1.20	16.0%	49.9%

**Table A8.** Ion decline parameters following dilution.  $k_{obs} = [a](t = n \text{ in hrs})[b]$ .

Trial	Cl <sup>-</sup>			Na <sup>+</sup>		
	[a]	[b]	R <sup>2</sup>	[a]	[b]	R <sup>2</sup>
1	0.000159	-0.846301	0.999879	0.000100	-1.149606	0.999996
2	0.000150	-0.889702	0.999968	0.000119	-1.110224	0.999616
3	0.000094	-0.862291	0.998579	0.000143	-1.140650	0.999858
4	0.000122	-0.873837	0.999197	0.000031	-1.400760	0.991862
5	0.000139	-0.974937	0.999223	0.000071	-1.302737	0.999987
6	0.000137	-0.934201	0.999987	n/a	n/a	n/a
7	0.000102	-0.901164	0.999373	0.000154	-1.068848	0.999994
8	0.000138	-0.947561	0.999991	0.000334	-1.040462	0.999927
9	n/a	n/a	n/a	0.000176	-1.065346	0.999834

**Table A9.** Product water, polymer slurry, following >700 h storage for 20 different polymers.

Trial	hrs	pH	Eh, mV	T °C	Cl <sup>-</sup> , g/L	Na <sup>+</sup> g/L	hrs	pH	Eh, mV	T °C	Cl <sup>-</sup> , g/L	Na <sup>+</sup> g/L
1	0	9.06	423	15.6	11.48	15.61	768	8.32	428	18.1	11.48	14.49
2	0	9.06	423	15.6	11.48	15.61	768	12.54	-15	18.4	10.77	14.82
3	0	8.72	321	17.2	14.50	16.04	744	4.92	716	17.7	12.03	14.89
4	0	8.72	321	17.2	14.50	16.04	744	12.71	14	16.8	7.65	11.98
5	0	8.68	308	14.2	28.10	14.73	720	5.76	570	17.6	12.76	14.73
6	0	8.68	308	14.2	28.10	14.73	720	12.64	2	17.4	14.26	14.18
7	0	9.60	230	15.2	10.92	7.57	792	5.64	249	17.7	9.62	7.57
8	0	9.60	230	15.2	10.92	7.57	792	12.33	-22	17.5	5.11	6.21

Table A9. Cont.

Trial	hrs	pH	Eh, mV	T °C	Cl <sup>−</sup> , g/L	Na <sup>+</sup> g/L	hrs	pH	Eh, mV	T °C	Cl <sup>−</sup> , g/L	Na <sup>+</sup> g/L
9	0	8.49	360	14.6	24.67	13.23	744	7.03	73	16.0	14.53	10.95
10	0	8.49	360	14.6	24.67	13.23	744	7.65	433	15.2	13.24	6.98
11	0	8.84	317	15.2	21.87	17.74	720	5.70	589	15.8	16.18	17.40
12	0	8.84	317	15.2	21.87	17.74	720	11.91	−18	15.7	11.10	15.09
13	0	9.53	226	17.5	57.26	44.14	720	6.85	382	15.7	11.67	14.57
14	0	9.53	226	17.5	57.26	44.14	720	11.73	10	15.8	15.96	16.90
15	0	9.67	361	17.9	9.68	9.50	720	6.12	221	15.3	9.68	9.04
16	0	9.67	361	17.9	9.68	9.50	720	6.90	268	15.5	9.68	7.01
17	0	9.67	361	17.9	9.68	9.50	720	9.18	344	14.0	7.56	5.60
18	0	9.67	361	17.9	9.68	9.50	720	9.54	292	14.0	9.68	6.03
19	0	9.80	347	16.8	7.96	7.74	720	7.90	465	13.9	7.94	7.34
20	0	9.80	347	16.8	7.96	7.74	720	7.92	458	13.9	7.96	7.34

**Table A10.** Product water composition immediately following dilution and at 24 to 72 h following dilution. Dilution Ratio = (Product water volume)/(Product water volume + Feed water volume). Percentages indicate total ion removal relative to the feed water (Table A9).

Trial	hrs	Cl <sup>−</sup> g/L	Na <sup>+</sup> g/L	hrs	pH	Eh, mV	T °C	Cl <sup>−</sup> g/L	Na <sup>+</sup> g/L	Cl <sup>−</sup>	Na <sup>+</sup>	Dilution Ratio
1	768	3.34	4.21	24	9.57	287	17.5	2.45	2.29	26.6%	49.5%	0.29
2	768	1.36	1.88	24	11.76	104	17.5	0.77	1.25	47.0%	36.8%	0.13
3	744	2.01	2.48	48	7.79	356	17.6	1.24	0.97	48.7%	63.7%	0.17
4	744	0.94	1.47	48	11.90	77	17.6	0.88	1.22	50.6%	38.1%	0.12
5	720	2.98	3.44	72	7.59	363	15.8	5.90	2.24	10.2%	34.9%	0.23
6	720	2.23	2.21	72	12.53	−35	15.9	1.26	2.19	71.3%	4.8%	0.16
7	792	2.51	1.98	72	7.52	186	15.9	2.14	1.19	24.9%	39.7%	0.26
8	792	1.63	1.99	72	12.13	−5	15.9	1.28	2.21	63.3%	8.7%	0.32
9	744	4.84	3.65	24	7.02	367	14.9	3.96	2.57	51.8%	41.7%	0.33
10	744	2.56	1.35	24	7.45	457	14.8	1.66	0.96	65.2%	62.5%	0.19
11	720	7.66	8.24	24	6.32	521	14.9	9.66	7.95	6.8%	5.4%	0.47
12	720	1.61	2.19	24	10.48	206	14.8	0.88	1.03	72.3%	60.0%	0.15
13	720	1.61	2.01	24	7.97	377	14.7	1.11	0.67	85.9%	89.0%	0.14
14	720	3.54	3.75	24	9.53	308	14.8	2.30	2.32	81.9%	76.3%	0.22
15	720	2.86	2.67	24	7.28	225	14.0	2.50	2.06	12.7%	26.7%	0.30
16	720	2.67	1.93	24	7.37	264	14.8	2.10	1.45	21.2%	44.6%	0.28
17	720	0.96	0.71	24	10.10	209	13.7	0.55	0.47	55.1%	60.9%	0.13
18	720	1.81	1.13	24	10.00	216	13.8	0.93	0.77	48.6%	56.7%	0.19
19	720	1.10	1.01	24	9.96	210	13.7	0.71	0.47	35.3%	56.0%	0.14
20	720	2.31	2.13	24	9.69	234	13.6	1.53	1.36	33.9%	39.6%	0.29

## References

- Potapov, P.; Turubanova, S.; Hansen, M.C.; Tyukavina, A.; Zalles, V.; Khan, A.; Song, X.-P.; Pickens, A.; Shen, Q.; Cortez, J. Global maps of cropland extent and change show accelerated cropland expansion in the twenty-first century. *Nat. Food* **2022**, *3*, 19–28. [\[CrossRef\]](#)
- Liu, S.; Wang, Y.; Zhang, G.J.; Wei, L.; Wang, B.; Yu, L. Contrasting influences of biogeophysical and biogeochemical impacts of historical land use on global economic inequality. *Nat. Commun.* **2022**, *13*, 2479. [\[CrossRef\]](#) [\[PubMed\]](#)
- Siebert, S.; Burke, J.; Faures, J.-M.; Frenken, K.; Hoogeveen, J.; Döll, P.; Portmann, F.T. Groundwater use for irrigation—a global inventory. *Hydrol. Earth Syst. Sci.* **2010**, *14*, 1863–1880. [\[CrossRef\]](#)
- Zhao, H.; Di, L.; Sun, Z. WaterSmart-GIS: A Web Application of a Data Assimilation Model to Support Irrigation Research and Decision Making. *ISPRS Int. J. Geo-Inf.* **2022**, *11*, 271. [\[CrossRef\]](#)
- Arboleda, P.; Ducharme, A.; Yin, Z.; Ciais, P. Tuning an improved irrigation scheme inside ORCHIDEE land surface model and assessing its sensitivity over land surface hydrology and energy budget. In Proceedings of the EGU General Assembly 2022, Vienna, Austria, 23–27 May 2022. EGU22-1984. [\[CrossRef\]](#)
- Jehan, S.; Iqbal, M.; Samreen, T.; Liaquat, M.; Kanwal, S.; Naseem, M. Effect of Deficit Irrigation Practice on Nitrogen Mineralization and Nitrate Nitrogen Leaching under Semi-Arid Conditions. *J. Water Resour. Prot.* **2022**, *14*, 385–394. [\[CrossRef\]](#)

7. Wang, X. Managing Land Carrying Capacity: Key to Achieving Sustainable Production Systems for Food Security. *Land* **2022**, *11*, 484. [\[CrossRef\]](#)
8. Rosa, L. Adapting agriculture to climate change via sustainable irrigation: Biophysical potentials and feedbacks. *Environ. Res. Lett.* **2022**, *17*, 063008. [\[CrossRef\]](#)
9. Negacz, K.; Malek, Z.; Vos, A.; Vellinga, P. Saline soils worldwide: Identifying the most promising areas for saline agriculture. *J. Arid Environ.* **2022**, *203*, 104775. [\[CrossRef\]](#)
10. Machado, R.M.A.; Serralheiro, R.P. Soil Salinity: Effect on Vegetable Crop Growth. Management Practices to Prevent and Mitigate Soil Salinization. *Horticulturae* **2017**, *3*, 30. [\[CrossRef\]](#)
11. Ayers, R.S.; Westcot, D.W. *Water Quality for Agriculture*; Fao Irrigation and Drainage Paper; Food and Agriculture Organization of the United Nations: Rome, Italy, 1985; Volume 29.
12. Wei, C.; Li, F.; Yang, P.; Ren, S.; Wang, S.; Wang, Y.; Xu, Z.; Xu, Y.; Wei, R.; Zhang, Y. Effects of Irrigation Water Salinity on Soil Properties, N<sub>2</sub>O Emission and Yield of Spring Maize under Mulched Drip Irrigation. *Water* **2019**, *11*, 1548. [\[CrossRef\]](#)
13. Amer, R. Spatial Relationship between Irrigation Water Salinity, Waterlogging, and Cropland Degradation in the Arid and Semi-Arid Environments. *Remote Sens.* **2021**, *13*, 1047. [\[CrossRef\]](#)
14. Slater, Y.; Reznik, A.; Finkelshtain, I.; Kan, I. Blending Irrigation Water Sources with Different Salinities and the Economic Damage of Salinity: The Case of Israel. *Water* **2022**, *14*, 917. [\[CrossRef\]](#)
15. Silber, A.; Israeli, Y.; Elingold, I.; Levi, M.; Levkovitch, I.; Russo, D.; Assouline, S. Irrigation with desalinated water: A step toward increasing water saving and crop yields. *Water Resour. Res.* **2015**, *51*, 450–464. [\[CrossRef\]](#)
16. Antia, D.D.J. Desalination of Water Using ZVI (Fe<sup>0</sup>). *Water* **2015**, *7*, 3671–3831. [\[CrossRef\]](#)
17. Antia, D.D.J. Purification of Saline Water Using Desalination Pellets. *Water* **2022**, *14*, 2639. [\[CrossRef\]](#)
18. Antia, D.D.J. Provision of Desalinated Irrigation Water by the Desalination of Groundwater Abstracted from a Saline Aquifer. *Hydrology* **2022**, *9*, 128. [\[CrossRef\]](#)
19. Antia, D.D.J. Catalytic Partial Desalination of Saline Water. *Water* **2022**, *14*, 2893. [\[CrossRef\]](#)
20. Antia, D.D.J. Water Treatment and Desalination Using the Eco-materials n-Fe<sup>0</sup> (ZVI), n-Fe<sub>3</sub>O<sub>4</sub>, n-Fe<sub>x</sub>O<sub>y</sub>H<sub>z</sub>[mH<sub>2</sub>O], and n-Fe<sub>x</sub>[Cation]<sub>n</sub>O<sub>y</sub>H<sub>z</sub>[Anion]<sub>m</sub> [rH<sub>2</sub>O]. In *Handbook of Nanomaterials and Nanocomposites for Energy and Environmental Applications*, 1st ed.; Kharissova, O.V., Torres-Martínez, L.M., Kharisov, B.I., Eds.; Springer: Berlin/Heidelberg, Germany, 2021; pp. 3159–3242.
21. Antia, D.D.J. Remediation of Saline Wastewater Producing a Fuel Gas Containing Alkanes and Hydrogen Using Zero Valent Iron (Fe<sup>0</sup>). *Water* **2022**, *14*, 1926. [\[CrossRef\]](#)
22. Konadu-Amoah, B.; Hu, R.; Cao, V.; Tao, R.; Yang, H.; Ndé-Tchoupé, A.I.; Gwenzi, W.; Ruppert, H.; Noubactep, C. Realizing the potential of metallic iron for the mitigation of toxics: Flee or adapt? *Appl. Water Sci.* **2022**, *12*, 1–11. [\[CrossRef\]](#)
23. Xiao, M.; Hu, R.; Ndé-Tchoupé, A.I.; Gwenzi, W.; Noubactep, C. Metallic Iron for Water Remediation: Plenty of Room for Collaboration and Convergence to Advance the Science. *Water* **2022**, *14*, 1492. [\[CrossRef\]](#)
24. Hu, R.; Gwenzi, W.; Sipowo-Tala, V.R.; Noubactep, C. Water Treatment Using Metallic Iron: A Tutorial Review. *Processes* **2019**, *7*, 622. [\[CrossRef\]](#)
25. Noubactep, C. Should the term ‘metallic iron’ appear in the title of a research paper? *Chemosphere* **2022**, *287*, 132314. [\[CrossRef\]](#)
26. Hu, R.; Ndé-Tchoupé, A.I.; Cao, V.; Gwenzi, W.; Noubactep, C. Metallic iron for environmental remediation: The fallacy of the electron efficiency concept. *Front. Environ. Chem.* **2021**, *2*, 677813. [\[CrossRef\]](#)
27. Hu, R.; Noubactep, C. Iron Corrosion: Scientific Heritage in Jeopardy. *Sustainability* **2018**, *10*, 4138. [\[CrossRef\]](#)
28. British Standards Institute. Quality management systems, BSI Handbook 25. In *Statistical Interpretation of Data*; British Standards Institute: London, UK, 1985; p. 318. ISBN 0580150712/9780580150715.
29. Schober, P.; Boer, C.; Schwarte, L.A. Correlation Coefficients: Appropriate Use and Interpretation. *Anesth. Analg.* **2018**, *126*, 1763–1768. [\[CrossRef\]](#)
30. Taylor, R. Interpretation of the Correlation Coefficient: A Basic Review. *J. Diagn. Med. Sonogr.* **1990**, *6*, 35–39. [\[CrossRef\]](#)
31. Bottero, J.Y.; Manceau, A.; Villieras, F.; Tchoubar, D. Structure and mechanisms of formation of iron oxide hydroxide (chloride) polymers. *Langmuir* **1994**, *10*, 316–319. [\[CrossRef\]](#)
32. Spiro, T.G.; Allerton, S.E.; Renner, J.; Terzis, A.; Bils, R.; Saltman, P. The Hydrolytic Polymerization of Iron(III). *J. Am. Chem. Soc.* **1966**, *88*, 2721–2726. [\[CrossRef\]](#)
33. Dong, H.; Gao, B.; Yue, Q.; Sun, S.; Wang, Y.; Li, Q. Floc properties and membrane fouling of different monomer and polymer Fe coagulants in coagulation–ultrafiltration process: The role of Fe (III) species. *Chem. Eng. J.* **2014**, *258*, 442–449. [\[CrossRef\]](#)
34. Chen, D.-W.; Liu, C.; Lu, J.; Mehmood, T.; Ren, Y.-Y. Enhanced phycoerythrin and DON removal by the synergism of H<sub>2</sub>O<sub>2</sub> and micro-sized ZVI: Optimization, performance, and mechanisms. *Sci. Total Environ.* **2020**, *738*, 140134. [\[CrossRef\]](#)
35. Ward, D.A.; Ko, E.I. Preparing catalytic materials by the sol-gel method. *Ind. Eng. Chem. Res.* **1995**, *34*, 421–433. [\[CrossRef\]](#)
36. Sakka, S.; Kozuka, H. *Handbook of Sol-Gel Science and Technology 1. Sol-Gel Processing*; Springer Science & Business Media: Berlin/Heidelberg, Germany, 2005; Volume 1.
37. Hench, L.L.; West, J.K. The sol-gel process. *Chem. Rev.* **1990**, *90*, 33–72. [\[CrossRef\]](#)
38. Klein, L.; Aparicio, M.; Jitianu, A. (Eds.) *Handbook of Sol-Gel Science and Technology*; Springer International Publishing: Berlin/Heidelberg, Germany, 2016.
39. Ebbing, D.D.; Gammon, S.D. *General Chemistry*, 8th ed.; Houghton Mifflin Company: New York, NY, USA, 2005; ISBN 0618399429.

40. Pilling, M.J.; Seakins, P.W. *Reaction Kinetics*; Oxford Science Publications; Oxford University Press: Oxford, UK, 1995; Volume 305, ISBN 019855527X.
41. Castellan, G.W. *Physical Chemistry*, 3rd ed.; Addison Wesley: Boston, MA, USA, 2004; ISBN 0201103850.
42. Shiyan, L.N.; Tropina, E.A.; Machekhina, K.I.; Gryaznova, E.N.; An, V.V. Colloid stability of iron compounds in groundwater of Western Siberia. *Springerplus* **2014**, *22*, 260. [[CrossRef](#)] [[PubMed](#)]
43. Hwang, Y.; Kim, D.; Shin, H.-S. Inhibition of nitrate reduction by NaCl adsorption on a nano-zero valent iron surface during concentrate treatment for water reuse. *Environ. Technol.* **2015**, *36*, 1178–1187. [[CrossRef](#)]
44. Antia, D.D.J. Desalination of groundwater and impoundments using Nano-Zero Valent Iron, n-Fe<sup>0</sup>. *Meteorol. Hydrol. Water Management. Res. Oper. Appl.* **2015**, *3*, 21–38. [[CrossRef](#)]
45. Fronczyk, J.; Pawluk, K.; Michniak, M. Application of permeable reactive barriers near roads for chloride ions removal. *Ann. Wars. Univ. Life Sci.-SGGW Land Reclam.* **2010**, *42*, 249–259. [[CrossRef](#)]
46. Kovalchuk, N.M.; Starov, V.M. Aggregation in colloidal suspensions: Effect of colloidal forces and hydrodynamic interactions. *Adv. Colloid Interface Sci.* **2012**, *179*, 99–106. [[CrossRef](#)]
47. Pourbaix, M. *Atlas of Electrochemical Equilibria in Aqueous Solutions*, 2nd ed.; Library of Congress Catalog Card No 65-11670; Franklin, J.A., Translator; NACE International: Houston, TX, USA, 1974; p. 644.
48. Misstear, B.; Banks, D.; Clark, L. *Water Wells and Boreholes*; John Wiley & Sons: Hoboken, NY, USA, 2006; ISBN 978-0-470-84989-7.
49. Oetjen, K.; Chan, K.E.; Gulmark, K.; Christensen, J.H.; Blotevogel, J.; Borch, T.; Spear, J.R.; Cath, T.Y.; Higgins, C.P. Temporal characterization and statistical analysis of flowback and produced waters and their potential for reuse. *Sci. Total Environ.* **2018**, *619*, 654–664. [[CrossRef](#)]
50. Owen, J.; Bustin, R.M.; Bustin, A.M.M. Insights from mixing calculations and geochemical modeling of Montney Formation post hydraulic fracturing flowback water chemistry. *J. Pet. Sci. Eng.* **2020**, *195*, 107589. [[CrossRef](#)]
51. Golding, L.A.; Kumar, A.; Adams, M.S.; Binet, M.T.; Gregg, A.; King, J.; McKnight, K.S.; Nidumolu, B.; Spadaro, D.A.; Kirby, J.K. The influence of salinity on the chronic toxicity of shale gas flowback wastewater to freshwater organisms. *J. Hazard. Mater.* **2022**, *428*, 128219. [[CrossRef](#)]
52. Luo, M.; Zhang, H.; Zhou, P.; Xiong, Z.; Huang, B.; Peng, J.; Liu, R.; Liu, W.; Lai, B. Efficient activation of ferrate (VI) by colloid manganese dioxide: Comprehensive elucidation of the surface-promoted mechanism. *Water Res.* **2022**, *215*, 118243. [[CrossRef](#)]
53. Manquían-Cerda, K.; Cruces, E.; Rubio, M.A.; Reyes, C.; Arancibia-Miranda, N. Preparation of nanoscale iron (oxide, oxyhydroxides and zero-valent) particles derived from blueberries: Reactivity, characterization and removal mechanism of arsenate. *Ecotoxicol. Environ. Saf.* **2017**, *145*, 69–77. [[CrossRef](#)] [[PubMed](#)]